Reflection-asymmetric rotor model of odd $A \sim 219-229$ nuclei

G. A. Leander
UNISOR, Oak Ridge Associated Universities, Oak Ridge, Tennessee 37831

Y. S. Chen*
Joint Institute for Heavy Ion Research, Oak Ridge, Tennessee 37831
(Received 16 March 1988)

The low-energy spectroscopy of odd-A nuclei in the mass region $A \sim 219-229$ is modeled by coupling states of a deformed shell model including octupole deformation to a reflection-asymmetric rotor core. Theory and experiment are compared for the nuclei in which data are available: ^{219,221,223,225}Rn, ^{221,223,225,227}Fr, ^{219,221,223,225,227}Ra, ^{219,223,225,227,229}Ac, ^{221,223,225,227,229}Th, and ^{229}Pa. Overall agreement requires an octupole deformation $\beta_3 \sim 0.1$. The results throughout the region are synthesized to evaluate the model.

I. INTRODUCTION

The issue that underlies the present investigation is whether some nuclei can be characterized as having intrinsic mean fields with spontaneously broken reflection symmetry. This possibility was first considered[1] in the 1950's, following the observation of low-lying $K^p=0^-$ bands in doubly even radium nuclei.[2] In the 1980's, a flurry of experimental and theoretical discoveries (reviewed, e.g., in Ref. 3) have provided new indications of reflection-asymmetric octupole deformation in this region of nuclei. Among other things, it was predicted that an octupole component of the mean field deformation would affect some single-particle orbitals in ways that should be clearly manifested by the spectroscopy of odd-A nuclei.[4] Subsequent comparisons between octupole-deformed orbitals and largely new data revealed good agreement on some counts,[5-8] but mostly it appeared that the limit of strong coupling to octupole deformation was approached but not reached. This could imply that the octupole deformation component is not stable enough to make the reflection-asymmetric mean field a useful starting point for spectroscopic modeling, an interpretation that has been endorsed by some authors.[9,10] There exist alternative models of odd-A nuclei that use single-particle basis states obtained from a reflection *symmetric* mean field, with dynamical octupole correlations introduced either on a fully fermionic level,[11,12] or by coupling to a core with collective dynamics.[8,13] A limitation of the fully fermionic models[11,12] is that they assume strong coupling to a symmetry axis of the deformed mean field.

A different reason for the discrepancies between experiment and the octupole-deformed model was suggested in Ref. 8, namely that they arise largely from the nonadiabaticity of the odd-particle motion. A model was formulated in which the reflection-asymmetric deformation is taken to be completely rigid, and the decoupling of odd-particle orbits from the octupole deformation is treated on the same footing as the familiar Coriolis decoupling from aspherical deformation in general. (A precursor model based on reflection-asymmetric deformation that contains both kinds of decoupling can be found in the earlier literature.[14]) The familiar Coriolis decoupling from rotational asymmetry occurs because of the nonzero energy splitting between the states in the core rotational band, reflecting a finite moment of inertia. Similarly, "parity decoupling" from reflection asymmetry occurs because of the nonzero energy splitting between the $K^p=0^+$ and $K^p=0^-$ bands of the core, reflecting the finite energy needed to achieve a parity inversion. In both cases, the energy splitting can be regarded as a model parameter given, for example, by the spectroscopy of the neighboring even-even nuclei. A first realistic application of this rigid reflection-asymmetric rotor model, to the nucleus ^{227}Ac, showed that the main discrepancies between experiment and the octupole-deformed strong-coupled theory were indeed removed or significantly reduced by taking nonadiabaticity into account.[15]

In this paper, the model calculations are extended and compared with the available low-energy spectroscopic data throughout the relevant mass region, $A=219-229$, where reflection-asymmetric equilibrium shapes have been derived from mean field theory (e.g., Refs. 16-19) and are suggested by experimental data (e.g., Ref. 20). These calculations create a broader base for evaluating the model, set a standard for other models, and also provide a first theoretical interpretation of some experimental data.

The model is described in Sec. II. Detailed calculations for 24 nuclei are made feasible by taking the parameters largely from theory, *a priori* prescriptions, or smooth trends. Further parameter fitting for individual nuclei has been undertaken as needed to obtain a meaningful description of specific items of data. The prescriptions and adopted parameter values are given in Sec. III A. The adiabatic single-particle levels are shown as a function of deformation in Sec. III B. The correspondence between calculated spectra and experimental level schemes is established, nucleus by nucleus, in Secs. III C and III D. On the basis of this correspondence, results and data from the whole mass region are compiled and compared in Sec. IV. General conclusions are summarized and discussed in Sec. V.

II. THE MODEL

A. The Hamiltonian

The reflection-asymmetric model described below is similar in many ways to the familiar, cylindrically symmetric rotor-plus-particle model.[21] The important differences are that (i) the core has an additional set of states $R^P=1^-,3^-,5^-,\ldots$, and (ii) the adiabatic single-particle orbits in a reflection-asymmetric potential have mixed parity.

Empirically, the negative-parity rotational states in doubly even nuclei are displaced upward in energy relative to the positive-parity states. Therefore the negative-parity states of the model core are displaced upward, by an amount denoted $E(0^-)$ because it can be viewed as the excitation energy for $K^P=0^-$. The physical mechanisms that determine this displacement are only partly understood.[22] Whatever its cause, its effect is to break the degeneracy of parity doublets that would otherwise occur in the strong-coupled limit of the core-particle system. The core Hamiltonian is written as

$$\hat{H}_{\rm core}=\frac{\hbar^2}{2J}(\hat{R}_1^2+\hat{R}_2^2)+\tfrac{1}{2}E(0^-)(1-\hat{P}) , \tag{2.1}$$

where $\hat{R}_{1,2}$ are the core angular momentum components perpendicular to the symmetry axis and $\hat{P}$ is the core parity operator.

The adiabatic single-particle orbits available to the odd particle are obtained from a standard single-particle potential[23,24] with an axially symmetric, reflection asymmetric shape that is parametrized by the usual coefficients of the multipole expansion of the radius:[21] β_2, β_3, β_4, β_5, and β_6. The coordinate frame in single-particle space is adjusted so that the origin lies at the center of gravity of the potential. The basis of the particle-core coupling calculation needs to span only a limited number of single-particle states around the Fermi level, since the adiabatic model is a useful leading-order approximation in deformed nuclei. The single-particle states, χ^ν_Ω, are characterized by energy, $e_{\nu\Omega}$, and by the angular momentum projection along the symmetry axis, Ω. Explicit formulas are available in the literature[25] for the evaluation of intrinsic single-particle matrix elements in the basis used by Ref. 23. Also available[25] are formulas for matrix elements of the type $\langle\chi^{\nu'}_{\Omega=1/2}|\hat{0}|\hat{R}\chi^\nu_{\Omega=1/2}\rangle$, where $\hat{R}$ rotates χ by an angle π about an axis perpendicular to the symmetry axis. The corresponding matrix elements in the reflection-asymmetric rotor-plus-particle model will turn out to be $\langle\hat{\pi}\chi^{\nu'}_{\Omega=1/2}|\hat{0}|\hat{R}\chi^\nu_{\Omega=1/2}\rangle$, where $\hat{\pi}$ is the single-particle parity operator, and are evaluated in the same way except that the amplitudes of negative-parity basis components of $\chi^{\nu'}_{\Omega=1/2}$ acquire an additional phase factor, -1.

In the rotor plus particle Hamiltonian, the core operators are rewritten as

$$\begin{aligned}\hat{\mathbf{R}}&=\hat{\mathbf{I}}-\hat{\mathbf{j}} ,\\ \hat{P}&=\hat{p}\hat{\pi} ,\end{aligned} \tag{2.2}$$

where $\hat{\mathbf{I}}$ is the angular momentum operator of the total system, $\hat{\mathbf{j}}$ is the single-particle angular momentum operator, and $\hat{p}$ is the total parity operator. Since total parity is good, $\hat{p}$ can be replaced by its eigenvalue, p. The total Hamiltonian can then be written

$$\begin{aligned}\hat{H}=&\frac{\hbar^2}{2J}[\hat{\mathbf{I}}^2-\hat{I}_3^2-(\hat{I}_+\hat{j}_-+\hat{I}_-\hat{j}_+)+\hat{j}_1^2+\hat{j}_2^2]\\ &+\tfrac{1}{2}E(0^-)(1-p\hat{\pi})+\hat{H}_{\rm sp}+\hat{H}_{\rm pair} ,\end{aligned} \tag{2.3}$$

where $\hat{H}_{\rm sp}$ is the deformed single-particle Hamiltonian, and $\hat{H}_{\rm pair}$ the pairing interaction. $\hat{H}_{\rm pair}$ is diagonalized in the BCS approximation by a Bogoliubov transformation to quasiparticle states in the intrinsic frame.[21] This transformation is characterized by the BCS gap parameter, Δ, and the Fermi level, λ. The BCS transformation is taken to be independent of the state of the core and the odd particle, so the pairing energy is state independent and need not be included explicitly, except in that the single-particle energy is replaced by a quasiparticle energy,

$$\bar{e}_{\nu\Omega}=[(e_{\nu\Omega}-\lambda)^2+\Delta^2]^{1/2} . \tag{2.4}$$

The Hamiltonian $\hat{H}$ is diagonalized numerically in the strong-coupled basis. A strong-coupled intrinsic core-quasiparticle wave function is written $\Phi_a\tilde{\chi}^\nu_\Omega$, where Φ_a describes the core with the same orientation in space as the intrinsic single-particle potential, and $\tilde{\chi}^\nu_\Omega$ is the BCS state with the odd particle in the orbit χ^ν_Ω. In the laboratory-frame basis used to diagonalize $\hat{H}$, these states are symmetrized to good parity and angular momentum

$$\psi^\nu_{IM\Omega p}=\frac{1}{2N}(1+\hat{R})D^I_{M\Omega}(1+p\hat{P}\hat{\pi})\Phi_a\tilde{\chi}^\nu_\Omega , \tag{2.5}$$

where N is a normalization constant and $D^I_{M\Omega}$ the rotation matrix.[21]

The first operator in $\hat{H}$, $\hat{\mathbf{I}}^2-\hat{I}_3^2$, is diagonal in this basis, with the eigenvalue $I(I+1)-\Omega^2$ characteristic of a rotor. The next operator, $\hat{I}_+\hat{j}_-+\hat{I}_-\hat{j}_+$, is precisely the familiar "Coriolis" term of the axially symmetric rotor plus particle model. The off-diagonal Coriolis matrix elements for $\Omega\neq\frac{1}{2}$ are formally identical in the reflection symmetric and asymmetric models. The diagonal matrix elements for $\Omega=\frac{1}{2}$ can also be given formally identical expressions in terms of a "decoupling factor," a, if the latter is defined in the asymmetric model as

$$a=-p\langle\hat{\pi}\chi^\nu_{1/2}|\hat{j}_+|\hat{R}\chi^\nu_{1/2}\rangle . \tag{2.6}$$

This coincides with the usual definition if $\chi^\nu_{1/2}$ has good parity. Note that the two strong-coupled bands of opposite parity, p, based on a parity-mixed orbit $\chi^\nu_{1/2}$, have decoupling factors of equal magnitude but opposite sign. The matrix elements of the Coriolis term includes BCS pairing factors $uu'+vv'$, due to the use of BCS states in-

stead of single-particle states in the basis. It is a common experience with rotor-plus-quasiparticle models that Coriolis couplings across the Fermi level must be further attenuated. One phenomenological prescription[26] for doing so is to raise the $uu'+vv'$ factors to an *ad hoc* power n. Empirical values of n range from 1 to 5.

The next operator in $\hat{H}$, $\hat{j}_1^2+\hat{j}_2^2$, is a two-body operator in single-particle space and its matrix elements in the BCS quasiparticle basis are somewhat more complicated:[27]

$$\begin{aligned}\langle\tilde{\alpha}\Omega\,|\,\hat{j}_1^2+\hat{j}_2^2\,|\,\tilde{\beta}\Omega\rangle &= \tfrac{1}{2}\sum_\gamma (u_\Omega^\alpha u_{\Omega-1}^\gamma+v_\Omega^\alpha v_{\Omega-1}^\gamma)\langle\gamma\Omega-1\,|\,\hat{j}_-\,|\,\alpha\Omega\rangle(u_\Omega^\beta u_{\Omega-1}^\gamma+v_\Omega^\beta v_{\Omega-1}^\gamma)\langle\gamma\Omega-1\,|\,\hat{j}_-\,|\,\beta\Omega\rangle \\ &+\tfrac{1}{2}\sum_\gamma (u_\Omega^\alpha u_{\Omega+1}^\gamma+v_\Omega^\alpha v_{\Omega+1}^\gamma)\langle\gamma\Omega+1\,|\,\hat{j}_+\,|\,\alpha\Omega\rangle(u_\Omega^\beta u_{\Omega+1}^\gamma+v_\Omega^\beta v_{\Omega+1}^\gamma)\langle\gamma\Omega+1\,|\,\hat{j}_+\,|\,\beta\Omega\rangle \\ &-\tfrac{1}{2}\sum_\gamma (u_\Omega^\alpha v_{\Omega+1}^\gamma-v_\Omega^\alpha u_{\Omega+1}^\gamma)^2\langle\gamma\Omega+1\,|\,\hat{j}_+\,|\,\alpha\Omega\rangle^2\delta_{\alpha\beta} \\ &-\tfrac{1}{2}\sum_\gamma (u_\Omega^\alpha v_{\Omega-1}^\gamma-v_\Omega^\alpha u_{\Omega-1}^\gamma)^2\langle\gamma\Omega-1\,|\,\hat{j}_-\,|\,\alpha\Omega\rangle^2\delta_{\alpha\beta}\,. \end{aligned} \tag{2.7}$$

Here the symbol χ has been suppressed in the brackets. The index γ runs over a complete set of single-particle states for given Ω, not just the states included in the basis space of the rotor-particle calculation.

The operator $\hat{\pi}$ in $\hat{H}$ plays a role analogous to that of the Coriolis term. In a simple model, where a pair of parity-mixed single-particle orbits results from the mixing of two reflection-symmetric orbits of opposite parity, it can be shown explicitly that the off-diagonal matrix elements of $\hat{\pi}$ tend to "decouple" the particle from the reflection asymmetry and to put it in one of the symmetric, good-parity orbits.[8] The diagonal matrix element of $\hat{\pi}$ determines the energy splitting, $E_{I^-}-E_{I^+}$, within a parity doublet of the odd mass system in the strong coupling limit:

$$E_{I^-}-E_{I^+}=\langle\hat{\pi}\rangle E(0^-)\,. \tag{2.8}$$

Thus $\langle\hat{\pi}\rangle$ can be viewed as the "parity decoupling factor" of a single-particle orbit. Note that since $\langle\hat{\pi}\rangle$ lies between -1 and $+1$, the magnitude of the odd-A parity splitting in strong coupling is always less than or equal to that of the core. The odd-A parity splitting ranges from zero for an equal admixture of parities in the single-particle state to the full core value, $E(0^-)$, for a single-particle state of good parity. In the BCS transformation, it is assumed that $\hat{\pi}$ can be treated as a one-body operator. Since the parity does not change under particle-hole conjugation, the appropriate pairing factor on matrix elements of $\hat{\pi}$ is $uu'+vv'$.

In summary, the nonzero matrix elements of the Hamiltonian $\hat{H}$ between strong-coupled basis states $\psi^\nu_{IM\Omega p}$ are

$$\langle IM\nu\Omega p\,|\,\hat{H}\,|\,IM\nu\Omega p\rangle=\frac{\hbar^2}{2J}[I(I+1)-\Omega^2+\delta_{\Omega=1/2}(-)^{I+(1/2)}(I+\tfrac{1}{2})a+\langle\bar{\nu}\Omega\,|\,\hat{j}_1^2+\hat{j}_2^2\,|\,\bar{\nu}\Omega\rangle] +\tfrac{1}{2}E(0^-)(1-p\langle\nu\Omega\,|\,\hat{\pi}\,|\,\nu\Omega\rangle)+\varepsilon_{\nu\Omega}\,, \tag{2.9}$$

$$\langle IM\nu'\Omega p\,|\,\hat{H}\,|\,IM\nu\Omega p\rangle=\frac{\hbar^2}{2J}[\delta_{\Omega=1/2}(-)^{I+(1/2)}(I+\tfrac{1}{2})(-p)\langle\hat{\pi}\chi^{\nu'}_{1/2}\,|\,\hat{j}_+\,|\,\hat{R}\chi^\nu_{1/2}\rangle(uu'+vv')^n+\langle\bar{\nu}'\Omega\,|\,\hat{j}_1^2+\hat{j}_2^2\,|\,\bar{\nu}\Omega\rangle] -\tfrac{1}{2}E(0^-)p\langle\nu'\Omega\,|\,\hat{\pi}\,|\,\nu\Omega\rangle(uu'+vv')\,, \tag{2.10}$$

$$\langle IM\nu'\Omega+1p\,|\,\hat{H}\,|\,IM\nu\Omega p\rangle=-\frac{\hbar^2}{2J}\sqrt{(I-\Omega)(I+\Omega+1)}\langle\nu'\Omega+1\,|\,\hat{j}_+\,|\,\nu\Omega\rangle(uu'+vv')^n\,. \tag{2.11}$$

Numerical diagonalization of $\hat{H}$ gives eigenstates

$$\Psi_{IMp}=\sum_{\nu\Omega}c^\nu_{I\Omega p}\psi^\nu_{IM\Omega p}\,. \tag{2.12}$$

B. Electromagnetic operators

The reduced rate of transitions between the eigenstates Ψ_{IMp}, induced by a spherical tensor operator $\hat{\mathbf{M}}_\lambda$, is[21]

$$B(M\lambda;i\to f)=\frac{1}{2I_i+1}\,|\,\langle I_fp_f\|\hat{\mathbf{M}}_\lambda\|I_ip_i\rangle\,|^2\,, \tag{2.13}$$

where

$$\langle I_f P_f \| \hat{\mathbf{M}}_\lambda \| I_i p_i \rangle = \sum_{\nu_i \Omega_i} \sum_{\nu_f \Omega_f} c^{\nu_i}_{I_i \Omega_i p_i} c^{\nu_f}_{I_f \Omega_f p_f} \langle I_f \nu_f \Omega_f p_f \| \hat{\mathbf{M}}_\lambda \| I_i \nu_i \Omega_i p_i \rangle \ . \tag{2.14}$$

Here the reduced matrix element between the strong-coupled basis states is

$$\langle I_f \nu_f \Omega_f p_f \| \hat{\mathbf{M}}_\lambda \| I_i \nu_i \Omega_i p_i \rangle = \sqrt{2I_i+1} \{ \langle I_i \Omega_i \lambda \Omega_f - \Omega_i \mid I_f \Omega_f \rangle \langle \tilde{\chi}^{\nu_f}_{\Omega_f} \mid \hat{M}_{\lambda \Omega_f - \Omega_i} \mid \tilde{\chi}^{\nu_i}_{\Omega_i} \rangle + (-)^{I_i + K_i} p_f \langle I_i - \Omega_i \lambda \Omega_f + \Omega_i \mid I_f \Omega_f \rangle \langle \hat{\pi} \tilde{\chi}^{\nu_f}_{\Omega_f} \mid \hat{M}_{\lambda \Omega_f + \Omega_i} \mid \hat{R} \tilde{\chi}^{\nu_i}_{\Omega_i} \rangle \} \ , \tag{2.15}$$

where $\hat{M}_{\lambda\Omega}$ on the right-hand side is in the intrinsic frame of reference.

The electromagnetic multipole operators employed in this work are

$$\hat{M}(E1\mu) = e_{\text{eff}} r Y_{1\mu} + \sqrt{3/4\pi}(Q_{10} - e_{\text{eff}} z_0) D^1_{\mu 0} \ , \tag{2.16}$$

$$\hat{M}(M1\mu) = \sqrt{3/4\pi}[g_R \hat{I}_\mu + (g_l - g_R)\hat{l}_\mu + (g_s - g_R)\hat{s}_\mu] \ , \tag{2.17}$$

$$\hat{M}(E\lambda\mu) = \left[\frac{2\lambda+1}{16\pi} \right]^{1/2} Q_{\lambda 0} D^\lambda_{\mu 0}, \quad \lambda \geq 2 \ . \tag{2.18}$$

The integration over the D functions has already been carried out in the expression on the right-hand side of (2.15) for the matrix elements. The evaluation of matrix elements of the intrinsic single-particle angular momenta and spherical harmonics was discussed in the paragraph preceding Eq. (2.2). Having BCS quasiparticle states $\tilde{\chi}$ instead of single-particle states χ in (2.15) implies that the single-particle matrix elements of the one-body terms in the operators $\hat{\mathbf{M}}_\lambda$ are to be multiplied by pairing factors: $u_i u_f + v_i v_f$ for magnetic and $u_i u_f - v_i v_f$ for electric operators.

For the total angular momentum,

$$\langle f \| \hat{\mathbf{I}} \| i \rangle = \delta_{if} \sqrt{I(I+1)(2I+1)} \ . \tag{2.19}$$

The single-particle effective $E1$ charge in (2.16) is[21]

$$e_{\text{eff}} = e \left[\frac{N-Z}{A} - t_3 \right] \left[1 - 0.7 \frac{(\hbar\omega)^2}{(\hbar\omega)^2 - E_\gamma^2} \right] , \tag{2.20}$$

where $t_3 = +\frac{1}{2}$ or $-\frac{1}{2}$ for neutrons or protons, respectively, $\hbar\omega$ is the giant resonance energy, $78 A^{-1/3}$ MeV, and E_γ is the $E1$ transition energy. The constant z_0 is the microscopic center of mass of the single-particle model,

$$z_0 = \frac{1}{A} \sum_{\nu\Omega} \langle \nu\Omega \mid z \mid \nu\Omega \rangle v^2 \ . \tag{2.21}$$

This small correction is important for the single-particle electric dipole matrix elements, which are also small, but is neglected for the other single-particle matrix element. Q_{10} is the intrinsic collective $E1$ moment that results because the proton and neutron centers of mass do not in general coincide in a reflection asymmetric nucleus. The evaluation of this quantity can be based on an expression similar to (2.21), but with the important inclusion of Strutinsky renormalization and screening.[28]

The $M1$ operator (2.17) is standard. For the gyromagnetic factors, we use

$$g_R = \frac{Z}{A}; \quad g_l = \begin{cases} 0 \\ 1; \end{cases} \quad g_s = 0.6 g_s(\text{free}) \ ; \tag{2.22}$$

$$g_s(\text{free}) = \begin{cases} -3.83, & \text{neutrons} \\ 5.56, & \text{protons} \ . \end{cases}$$

The single-particle parts of the $E\lambda$ operators are neglected for $\lambda \geq 2$ because the main contributions are expected to be collective, and the calculated rates are not expected to be accurate down to the level of a single-particle unit. The intrinsic collective moments, $Q_{\lambda 0}$, for $\lambda > 1$ are obtained from the shape of the single-particle potential. It is conventional to parametrize these moments using the leading term in an expansion in deformation coordinates,

$$Q_{\lambda 0} = \frac{3}{\sqrt{(2\lambda+1)\pi}} Z R_0^\lambda \bar{\beta}_\lambda, \quad \lambda \geq 2 \ , \tag{2.23}$$

or, if Nilsson's ϵ_λ coefficients[29] in the multipole expansion of the equipotentials are used to describe the shape,

$$Q_{20} = \tfrac{4}{5} Z R_0^2 \bar{\epsilon}_2 \ , \tag{2.24}$$

$$Q_{\lambda 0} = -\tfrac{6}{7} Z R_0^\lambda \bar{\epsilon}_\lambda, \quad \lambda > 2 \ . \tag{2.25}$$

For a shape containing surface radius multipoles 2 to 6,

$$\bar{\beta}_2 = \beta_2 + \sqrt{5/4\pi} \left[\tfrac{4}{7}\beta_2^2 + \tfrac{8}{15}\beta_3^2 + \tfrac{40}{77}\beta_4^2 + \tfrac{20}{39}\beta_5^2 + \tfrac{196}{386}\beta_6^2 + \frac{24}{7}\frac{1}{\sqrt{5}}\beta_2\beta_4 + \tfrac{40}{21}\sqrt{7/11}\beta_3\beta_5 + \frac{60}{11}\frac{1}{\sqrt{13}}\beta_4\beta_6 \right] , \tag{2.26}$$

$$\bar{\beta}_3 = \beta_3 + \frac{5}{\sqrt{4\pi}} \left[\tfrac{4}{15}\sqrt{5}\beta_2\beta_3 + \tfrac{6}{11}\beta_3\beta_4 + \tfrac{60}{91}\sqrt{7/11}\beta_4\beta_5 + \tfrac{7}{33}\sqrt{77/13}\beta_5\beta_6 + \tfrac{10}{21}\sqrt{35/11}\beta_2\beta_5 + \frac{100}{33}\frac{1}{\sqrt{13}}\beta_3\beta_6 \right] , \tag{2.27}$$

$$\bar{\beta}_4 = \beta_4 + \frac{6}{\sqrt{4\pi}} \left[\tfrac{3}{7}\beta_2^2 + \tfrac{3}{11}\beta_3^2 + \tfrac{243}{1001}\beta_4^2 + \tfrac{3}{13}\beta_5^2 + \tfrac{42}{187}\beta_6^2 + \tfrac{20}{77}\sqrt{5}\beta_2\beta_4 + \tfrac{60}{91}\sqrt{7/11}\beta_3\beta_5 + \frac{20}{11}\frac{1}{\sqrt{13}}\beta_4\beta_6 + \tfrac{15}{11}\sqrt{5/13}\beta_2\beta_6 \right] . \tag{2.28}$$

The $E2/M1$ mixing ratio δ is defined by[21]

$$\delta = yE_\gamma \frac{\langle I_f p_f \| \hat{\mathbf{M}}(E2) \| I_i p_i \rangle}{\langle I_f p_f \| \hat{\mathbf{M}}(M1) \| I_i p_i \rangle} , \tag{2.29}$$

where y is a constant such that δ^2 is the ratio of the $E2$ and $M1$ partial transition rates. If E_γ is in MeV, the $E2$ matrix element in e b, and the $M1$ element in μ_N, y is $\sim\sqrt{0.7}$.

Spectroscopic moments are given by

$$\mu = \sqrt{4\pi/3} \frac{1}{\sqrt{2I+1}} \langle II10 \mid II \rangle \langle Ip \| \hat{\mathbf{M}}(M1) \| Ip \rangle , \tag{2.30}$$

$$Q = \sqrt{16\pi/5} \frac{1}{\sqrt{2I+1}} \langle II20 \mid II \rangle \langle Ip \| \hat{\mathbf{M}}(E2) \| Ip \rangle . \tag{2.31}$$

C. Particle transfer

The cross section for single-particle transfer on a doubly even target to an odd-A state of angular momentum j and parity $(-)^l$, where $l = j \pm \frac{1}{2}$, is written in the formalism of Ref. 30 as

$$\frac{d\sigma}{d\Omega}(\theta) = NS_{lj}\sigma_{lj}(\theta) , \tag{2.32}$$

where N is a normalization constant for the reaction, σ_{lj} is the particle transfer cross section calculated by DWBA to a spherical orbit at the same binding energy with orbital and total angular momenta l and j, and the spectroscopic factor S_{lj} contains the nuclear structure information. The spectroscopic factor is given by

$$S_{lj} = \frac{2}{2j+1} \mid \langle \Psi \| a_{lj}^\dagger \| \tilde{0} \rangle \mid^2 \tag{2.33}$$

for a stripping reaction and

$$S_{lj} = 2 \mid \langle \Psi \| a_{lj} \| \tilde{0} \rangle \mid^2 \tag{2.34}$$

for a pickup reaction. Here $\mid \tilde{0} \rangle$ is the BCS vacuum, and $a_{lj}^\dagger$ creates a particle in a spherical state χ_{lj}. $\mid \Psi \rangle$ in the present application is a rotor-plus-quasiparticle state (2.12) with $I = j$ and $p = (-)^l$, and the reduced matrix elements become

$$\langle Ip \| a_{lj}^\dagger \| \tilde{0} \rangle = \sum_{\nu\Omega} u_\Omega^\nu c_{I\Omega p}^\nu C_{lj\Omega}^\nu , \tag{2.35}$$

$$\langle Ip \| a_{lj} \| \tilde{0} \rangle = \sum_{\nu\Omega} v_\Omega^\nu c_{I\Omega p}^\nu C_{lj\Omega}^\nu , \tag{2.36}$$

where $C_{lj\Omega}^\nu$ is the amplitude of the spherical state χ_{lj} in the deformed state χ_Ω^ν. The squares of the reduced matrix elements (2.35) and (2.36) are called the nuclear structure factors.

For $\sigma_{lj}(0)$, we rely on the DWBA calculations that are presented in most experimental papers together with the measured cross sections, in which each spherical state is obtained from a spherical Woods-Saxon potential with the depth adjusted so that one solution χ_{lj}^n matches the experimental separation energy. We obtain the amplitudes $C_{lj\Omega}^\nu$ in the nuclear structure factors (2.35) and (2.36) in the same approximation, by calculating the overlaps of the deformed Woods-Saxon orbitals χ_Ω^ν with states in a spherical Woods-Saxon potential,

$$C_{lj\Omega}^\nu = \langle \chi_{lj\Omega}^n \mid \chi_\Omega^\nu \rangle . \tag{2.37}$$

The relative phases of spherical substates $\chi_{lj\Omega}^n$ that differ only by Ω is obtained by requiring the j_+ matrix elements between them to be positive. Energy matching is not crucial for the overlaps (2.37) and was done in a crude way: For states χ_{lj}^n that would otherwise be unbound, the depth parameter V_0 of the Woods-Saxon potential was increased by 10 MeV. The value of n is chosen so as to maximize the structure factor (2.35) or (2.36). In some cases, structure factors of comparable magnitude are obtained for two different values of n and the method of Ref. 30 is unreliable. In principle, the spherical states χ_{lj} used in the DWBA calculation, and the coefficients $C_{lj\Omega}^\nu$, should have been obtained from the octupole-deformed single-particle orbitals by angular momentum projection.[31,32] However, the deformed orbitals are presently calculated by diagonalization in an oscillator basis[23] and cannot be used at distances of several fm outside the nuclear surface, where the main contribution to particle transfer is made.

III. CALCULATIONS

A. Model parameters

1. *The deformed shell model*

The adiabatic single-particle states were obtained from a Woods-Saxon deformed shell model[23] with a "universal" set of parameters.[24] This parameter set, originally fitted to ^{208}Pb, has been tested by numerous applications in all mass regions from $A = 56$ to the superheavy elements and appears to be close to optimal (e.g., Ref. 33, and references therein). The A- and Z-dependent parameters were assigned the appropriate values for each individual nucleus in the present work. A basis of 14 stretched harmonic oscillator shells was employed.

Equilibrium deformations have been calculated previously for even-even nuclei in the present mass region, and the β_2 deformation of the odd-mass nuclei considered here was obtained by interpolation in Table II of Ref. 17. For near-spherical nuclei, where this procedure gives β_2 less than 0.1, an effective value of 0.1, or in one case 0.05, was adopted. The values employed for β_2 are listed in Table I. The values employed for β_4 are given by a parametrization of the calculated equilibrium values,

$$\beta_4 = 0.5\beta_2 + 0.01 . \tag{3.1}$$

The spirit of the present investigation is to treat β_3 as a phenomenological parameter to be fitted to the odd-A spectroscopy for each individual case. The adopted values of β_3 are given in Table II. The calculated static equilibrium values of β_3 range from 0 to 0.11, but in the octupole shape transitional cases one may expect that the effective β_3 includes a contribution from dynamical fluc-

TABLE I. The β_2 deformations employed in the calculations.

Z, A	219	221	223	225	227	229
91						0.185
90		0.100	0.120	0.142	0.164	0.184
89	0.050		0.126	0.144	0.168	0.185
88	0.100	0.110	0.129	0.148	0.169	
87		0.100	0.128	0.152	0.172	
86	0.100	0.110	0.131	0.155		

tuations, just as the effective β_2 of quadrupole shape transitional nuclei is typically of the order of 0.1. This may explain why the empirical β_3 values in Table II are close to 0.1 even at the fringes of the octupole deformed region. Enhanced β_3 values were used for the $\Omega=\frac{1}{2}$ single-particle wave functions in four odd-neutron nuclei, namely $\beta_3=0.15$ in ^{223,225}Ra and ^{225}Th and $\beta_3=0.13$ in ^{227}Th. This is discussed in Sec. III D 4.

The liquid drop equilibrium values were used for β_5 and β_6. They are given by[17]

$$\beta_5=\beta_3(0.0089+0.117\beta_2+0.655\beta_4-0.0352\beta_3^2) , \quad (3.2)$$

$$\beta_6=0.1055\beta_3^2+0.2215\beta_4^2+0.1476\beta_2\beta_4-0.0285\beta_2^3 . \quad (3.3)$$

The Strutinsky equilibrium values of β_6 are known to be larger in this region of nuclei,[10,19] but have not yet been evaluated systematically for the present single-particle model.

2. *The reflection-asymmetric rotor core*

The parameters of the core are its moment of inertia, parity splitting, and electric multipole moments. For odd-A nuclei with known rotational bands, the core moment of inertia parameter $\hbar^2/2J$ was adjusted so that the calculation reproduced the overall spacing in the ground band. This established an empirical trend with Z and A that was used to select $\hbar^2/2J$ for the remaining cases. The adopted values are given in Table III. The measured 2^+ energies of even-even nuclei in the region[34] exhibit a similar trend with Z and A, although $\hbar^2/2J=E(2^+)/6$ is systematically larger than for the neighboring odd-A nuclei, especially in the near-spherical region. This is commonly the case in all regions of nuclei.

The core parity splitting was obtained by taking the average experimental 1^- excitation energy in the two neighboring even-even nuclei[34] and subtracting the model core rotational energy for $I=1$,

$$E(0^-)=E(1^-)-\hbar^2/J . \quad (3.4)$$

If the 1^- energy is not known for both even-even neighbors, the $E(1^-)$ value for some nearby odd-A core was used. The adopted values of $E(1^-)$ are given in Table IV.

The reflection-asymmetric rotor model largely accounts for the low-lying levels observed in even-even nuclei of the present mass region. One of the best studied cases experimentally[34] is ^{224}Ra, where one extraneous, unidentified level has been placed at 414 keV in the γ-decay scheme following β decay of ^{224}Fr, and the next extraneous level comes at 832 keV.

The model core spectra in two representative cases, ^{219}Ac and ^{225}Ra, are compared with the experimental level spectra of the even-even neighbors in Figs. 1 and 2. The nucleus ^{219}Ac is near-spherical and its neighbors have "quasivibrational" rather than rotational bands. In the model core, however, there is a rotational stretching of the level spacings with increasing spin (Fig. 1) that will also show up below in the calculated bands of the odd-A nucleus. The even-even neighbors of ^{225}Ra have more rotational-like bands, but the empirical moments of inertia are quite different for positive and negative parity (Fig. 2). The model core moment of inertia, fitted to the empirical band spacings in ^{225}Ra, is similar to that of the negative parity band.

The intrinsic electric dipole moment of the core, Q_{10}, has been determined empirically within the present mod-

TABLE II. The β_3 deformations employed in the calculations.

Z, A	219	221	223	225	227	229
91						0.08
90		0.1	0.1	0.1[a]	0.1[a]	0.07
89	0.05		0.1	0.1	0.1	0.07
88	0.1	0.1	0.1[a]	0.1[a]	0.1	
87		0.14	0.1	0.1	0.1	
86	0.1	0.1	0.1	0.1		

[a]A larger β_3, specified in the text a few lines above (3.2), is used to calculate the $\Omega=\frac{1}{2}$ single-particle wave functions.

TABLE III. The core rotational inertia parameter, $\hbar/2J$ (keV), employed in the calculations.

Z, A	219	221	223	225	227	229
91						7
90		30	11	9.5	8	7
89	30		9	8.5	8	7
88	30	12	8.5	7	8	
87		11	8.5	8	8	
86	15	10	8	8		

el framework for the odd-A nuclei in which data are available. These values of Q_{10} are given in Table V. The intrinsic electric quadrupole, octupole, and hexadecapole moments, Q_{20}, Q_{30}, and Q_{40}, were obtained from the deformation parameters of the single-particle potential (Sec. III A 1) using Eqs. (2.23)–(2.28) and $R_0 = 1.2A^{1/3}$ fm.

The electromagnetic properties of the ^{225}Ra model core are compared with experimental data for the even-even neighbors in Table VI. The average experimental value of $\bar{\beta}_2$ is slightly larger than the theoretical estimate (see Sec. IV B 4), and the experimental $\bar{\beta}_3$ is consistent with the adopted octupole deformation. The experimental $\bar{\beta}_4$ is significantly larger than the value obtained from the Strutinsky equilibrium shape. Only one other $\bar{\beta}_4$ has been measured in the $A = 219$–229 region,[42] for the nucleus ^{229}Th. Its value, 0.25 ± 0.05, is also significantly larger than the theoretical value, 0.15, obtained from the equilibrium shape of ^{229}Th by (2.23) and (2.28). Large discrepancies between measured hexadecapole transition moments and calculated intrinsic moments are also known to occur in several rare earth nuclei for reasons that have not yet been firmly established.[43] As for the measured $E1$ matrix elements in ^{226}Ra, they are consistent with a constant Q_{10} at low spins,[41] while the data for ^{224}Ra deviate[39] from this model assumption. However, the experimental $B(E1)$ branching ratios follow the rotor model "Alaga rules" in both nuclei.

3. *Quasiparticle and coupling parameters*

The quasiparticle parameters are the gap parameter Δ, the Fermi level λ, and empirical corrections $d\tilde{\epsilon}_{\nu\Omega}$ to the quasiparticle energies $\tilde{\epsilon}_{\nu\Omega}$. The core-particle coupling parameters are the Coriolis attenuation and the truncation limits of the quasiparticle space.

The gap parameter, Δ, was set equal to 0.6 MeV for all nuclei considered. The calculations are not very sensitive to this value, which was chosen rather small to reflect the blocking of pairing by the odd quasiparticle and the octupole shell structure. The empirical odd-even mass differences, extracted by the usual four-point formula,[44] do in fact exhibit a local minimum in the region where octupole deformation is predicted, at 0.72 MeV for neutrons in ^{224}Th and 0.84 MeV for protons in ^{226}Th and ^{228}U.

The Fermi level, λ, was usually placed on the orbital that contains the last, odd nucleon in the single-particle scheme. Four exceptions were made to this Hartree-Fock prescription. For ^{219}Ac and ^{229}Pa, the calculated results came closer to the data using the Fermi level obtained by solving the BCS particle number equation. In these nuclei, the BCS Fermi level lies 140 keV below and 310 keV above the Hartree-Fock Fermi level, respectively. For ^{223}Rn and ^{223}Ac, the experimental ground-state properties were reproduced by arbitrarily moving the Fermi level up by 330 keV and 170 keV, respectively, into the gap between the single-particle level prescribed by Hartree-Fock and the next higher level.

The adiabatic quasiparticle spectrum of the present deformed shell model generally reproduces the ordering of the low-lying band heads that are seen experimentally. It is sometimes desirable, however, to make empirical adjustments of the quasiparticle energies in the core-quasiparticle coupling calculations. In some cases, more accurate energy spacings between the bands are required than a single-particle model can provide, in order to make the inclusion of small nonadiabatic couplings meaningful. In other cases, especially in near-spherical

TABLE IV. The core 1^- excitation energy, $E(1^-)$ (keV), employed in the calculations. The underlined values were obtained as the average of the measured 1^- energies in the two even-even neighbors.

Z, A	219	221	223	225	227	229
91						347
90		327	229	238	279	418
89	327		244	223	290	491
88	327	327	229	235	364	
87		327	229	235	364	
86	327	327	229	235		

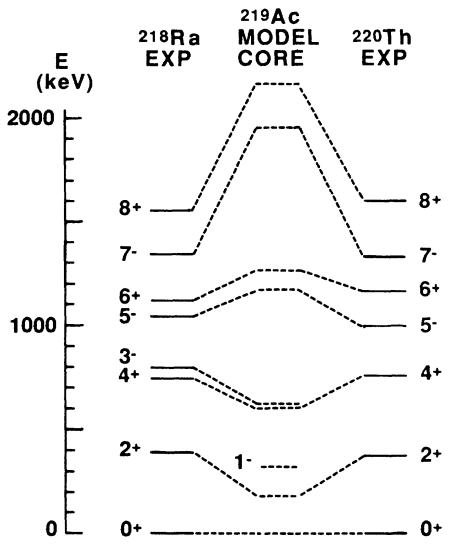

FIG. 1. The spectrum of the reflection-asymmetric rotor model core used for ^{219}Ac is compared with the experimentally known levels up to the first 8^+ in the doubly even neighbors. The ^{218}Ra levels are from Refs. 35 and 36, and the ^{220}Th levels from Ref. 37.

nuclei, large nonadiabatic and recoil effects sometimes cause unphysical rearrangements of the band head energies and the original ordering needs to be restored. For odd-Z nuclei, no such adjustments of the quasiparticle energies were made in the present work. For odd-N nuclei, however, the corrections listed in Table VII were applied. The largest corrections, made in the near-spherical nucleus ^{219}Rn, essentially compensate for rearrangements relative to the adiabatic scheme. The systematic lowering

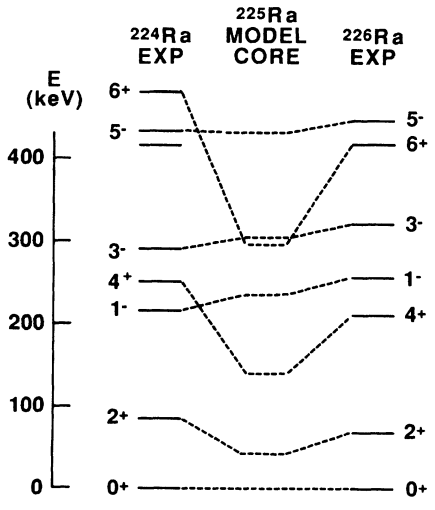

FIG. 2. The spectrum of the reflection-asymmetric rotor model core used for ^{225}Ra is compared with the experimentally known levels up to the first 5^- or 6^+ in the doubly even neighbors. The experimental levels are from Ref. 34.

TABLE V. Intrinsic electric dipole moments for odd-A nuclei in which experimental data are available (see Sec. IV B 1). The first column of numbers gives the adopted empirical values in this work, and the last columns give theoretical values from Ref. 28 for the neighboring even-even nuclei.

	Q_{10} (e fm)		
	Empirical,	Theory,	
Nucleus	odd A	$A-1$	$A+1$
^{223}Ra	0.13	0.18	0.12
^{225}Ra	0.14	0.12	0.05
^{219}Ac	$\sim$0.2	−0.07	0.20
^{225}Ac	$>$0.18	0.12	0.29
^{227}Ac	0.03	0.05	0.10
^{223}Th	0.32	0.32	0.33
^{229}Pa	0.6	0.10	?

of the $2\nu=134$, $\Omega=\frac{5}{2}$ orbital by about 100 keV in six weakly deformed nuclei also tends to restore the adiabatic band-head spacings. The other corrections are mostly smaller and not systematic.

The single-particle space available to the odd nucleon was truncated to 16 levels χ^{ν}_{Ω}, eight above and eight on or below the Hartree-Fock Fermi level. Increasing the size of the single-particle space did not have a significant effect on particle-rotor bands starting below about 1 MeV, but an enlarged basis space would be required for higher-lying bands.

Attenuation of the Coriolis interaction can be achieved by assigning a value greater than unity to the parameter n appearing in Eqs. (2.10) and (2.11). The adopted empirical values are listed in Table VIII and discussed in Sec. IV A 3.

B. Single-particle levels

Nilsson diagrams at fixed octupole deformation corresponding to $\beta_3\sim0.1$ have been presented in Ref. 8 for the folded Yukawa single-particle potential employed in that work. The levels were labeled by the single-particle matrix elements $\langle\hat{\pi}\rangle$, $\langle\hat{s}_z\rangle$, and $\langle\hat{\pi}\chi\,|\,-\hat{j}_+\,|\,\hat{R}\chi\rangle$ that govern the odd-A spectroscopy in the strong-coupling approximation. These diagrams are by themselves a powerful tool for interpreting the spectroscopy of odd-A nuclei in the $A\sim219$–229 region. The corresponding octupole-deformed Nilsson diagrams for protons and neutrons in the present Woods-Saxon potential are provided in the right-hand parts of Figs. 3 and 4, respectively. Figures 3 and 4 also show the single-particle levels for spherical shape, the usual Nilsson diagrams for reflection-symmetric prolate shapes, and single-particle levels as a function of octupole deformation. The spherical single-particle energies of the present Woods-Saxon potential are somewhat different from those of the folded Yukawa model with the FYII parameter set,[45] but the level spectra become quite similar for the two models in the presence of both quadrupole and octupole deformation.

TABLE VI. The electromagnetic properties of the model core for ^{225}Ra are related to measurements (Refs. 38–41) in the neighboring doubly even nuclei. The experimental $\bar{\beta}_\lambda$ values are defined as $4\pi[B(E\lambda;0^+\rightarrow\lambda)]^{1/2}/(3ZR_0^\lambda)$, where $R_0=1.2A^{1/3}$ fm, the experimental Q_{10} is defined as $[4\pi(2I+1)B(E1;I\rightarrow I-1)/(3I)]^{1/2}$, and the model $B(E1)$ ratios are given by $\langle I010\,|\,I-10\rangle^2/\langle I010\,|\,I+10\rangle^2$.

Quantity	Transition	^{224}Ra Expt.	^{225}Ra Model core	^{226}Ra Expt.
$\bar{\beta}_2$	$0^+\rightarrow2^+$	0.179	0.175	0.202
$\bar{\beta}_3$	$0^+\rightarrow3^-$		0.122	0.128
$\bar{\beta}_4$	$0^+\rightarrow4^+$		0.12	0.17
Q_{10} (e fm)	$3^-\rightarrow2^+$	0.05	0.14	0.11
Q_{10} (e fm)	$5^-\rightarrow4^+$	0.15	0.14	0.09
Q_{10} (e fm)	$7^-\rightarrow6^+$		0.14	0.12
$\frac{B(E1;I\rightarrow I-1)}{B(E1;I\rightarrow I+1)}$	$1^-\rightarrow0^+/1^-\rightarrow2^+$	0.44	0.50	0.48
$\frac{B(E1;I\rightarrow I-1)}{B(E1;I\rightarrow I+1)}$	$3^-\rightarrow2^+/3^-\rightarrow4^+$		0.75	0.69

The details of how Figs. 3 and 4 were constructed are as follows. The levels were obtained with the "universal" parameter set,[24] with Z and A corresponding to ^{225}Ra. β_4, β_5, and β_6 deformations were included for $\beta_2>0.1$ according to the prescriptions (3.1)–(3.3). For β_2 between 0 and 0.1, the single-particle levels are indicated schematically by straight dashed lines since the prescription (3.1) cannot be used to approach spherical shape. At zero deformation the orbitals are labeled by the spherical quantum numbers lj. At $\beta_2>0.1$, the reflection symmetric orbitals are labeled by the cylindrical stretched oscillator component, $Nn_z\Lambda\Omega$, that becomes dominant in the dia-

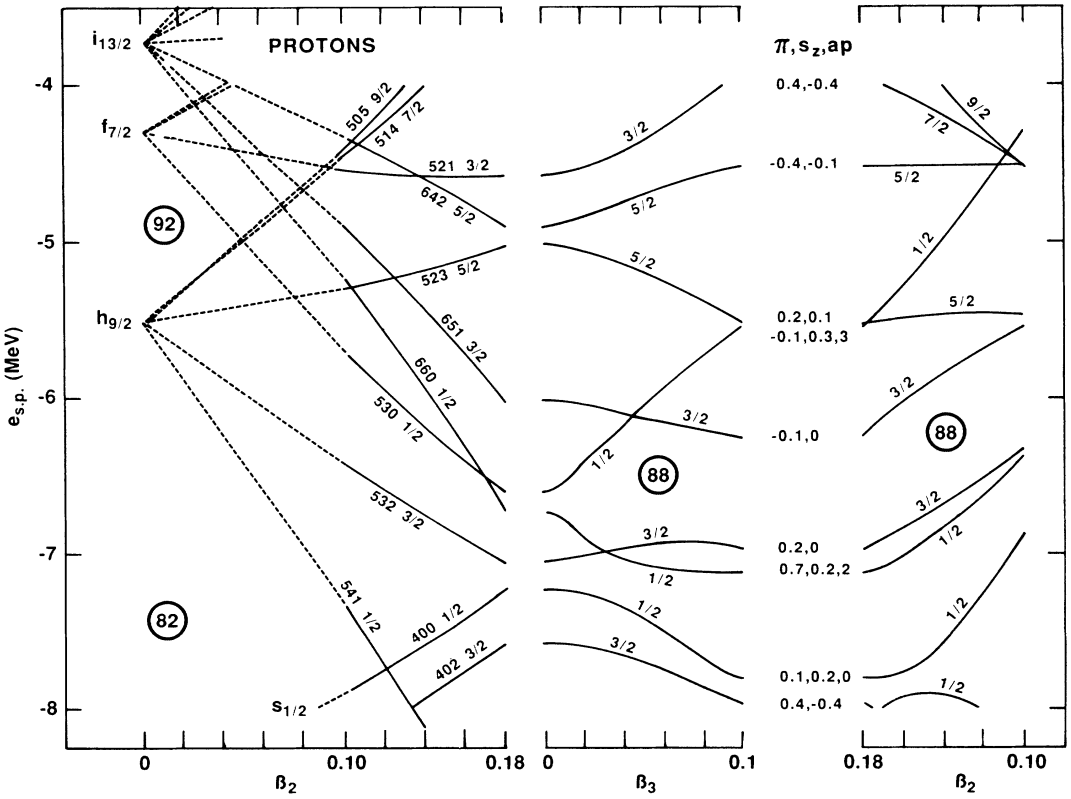

FIG. 3. Proton single-particle levels in the present Woods-Saxon potential for $\beta_2=0$–0.18 with $\beta_3=0$, for $\beta_3=0$–0.1 with $\beta_2=0.18$, and for $\beta_2=0.18$–0.10 with $\beta_3=0.1$. See Sec. III B for details.

TABLE VII. Empirical increments $d\bar{e}_{\nu\Omega}$ to the quasiparticle energies $\bar{e}_{\nu\Omega}$ for odd-neutron nuclei. No such corrections were made for odd-proton nuclei. The quasiparticle states are labeled by the usual angular momentum projection Ω on the symmetry axis and by the counting number ν of the corresponding single-particle level (2ν is the number of neutrons that would fill the single-particle states up to and including this level).

Nucleus	$2\nu,\Omega$	$d\bar{e}_{\nu\Omega}$ (keV)
$N=131$		
^{219}Ra	$134,\frac{5}{2}$	−120
^{221}Th	$134,\frac{5}{2}$	−120
$N=133$		
^{219}Rn	$132,\frac{1}{2}$	220
	$134,\frac{5}{2}$	−90
	$136,\frac{3}{2}$	100
^{221}Ra	$134,\frac{5}{2}$	−90
^{223}Th	$134,\frac{5}{2}$	−90
$N=135$		
^{221}Rn	$134,\frac{5}{2}$	−95
	$136,\frac{3}{2}$	95
^{223}Ra	$136,\frac{3}{2}$	−125
	$138,\frac{1}{2}$	40
^{225}Th		
$N=137$		
^{223}Rn		
^{225}Ra	$136,\frac{3}{2}$	40
	$138,\frac{1}{2}$	−105
^{227}Th	$136,\frac{3}{2}$	80
$N=139$		
^{225}Rn	$142,\frac{7}{2}$	25
	$144,\frac{5}{2}$	100
^{227}Ra	$140,\frac{3}{2}$	−75
	$146,\frac{1}{2}$	80
^{229}Th	$140,\frac{3}{2}$	70

batic continuation to large elongation. At $\beta_2=0.18$, the single-particle levels are shown as a function of β_3. This helps to reveal the composition of the reflection-asymmetric orbitals in terms of reflection-symmetric ones. The reflection-asymmetric orbitals are labeled by their only good quantum number, Ω. The single-particle matrix elements mentioned above, $\pi\equiv\langle\hat{\pi}\rangle$, $s_z\equiv\langle\hat{s}_z\rangle$, and $ap=\langle\hat{\pi}\chi\,|\,-\hat{j}_+\,|\,\hat{R}\chi\rangle$, are given at $\beta_2=0.18$, $\beta_3=0.1$. The reflection-asymmetric levels at $\beta_3=0.1$ are plotted from $\beta_2=0.18$ back to 0.10 in the right-hand part of each figure.

C. Odd-Z nuclei

1. *The isotopes ^{221,223,225,227}Fr*

The ground-state spins and electromagnetic moments of these four francium isotopes have been established by laser measurements[46] and are listed in Table IX. Excited states of ^{221,223}Fr are known from decay studies.[34,47] The laser measurements showed that the structure of the ground state changes between $N=134$ and 136, and again between $N=138$ and 140. All the ground-state spins, and also the moments for the $K\neq\frac{1}{2}$ cases ^{223,225}Fr, could be understood on the basis of changing quadrupole deformation in the octupole-deformed single-particle diagram that had been published previously in Ref. 8. In the experimental paper it was pointed out, however, that the magnetic moment of ^{227}Fr would be consistent with a reflection-*symmetric* 400 $\frac{1}{2}$ assignment. The present work will show that the octupole-deformed particle-rotor model reproduces both the ground-state spins and moments of all four isotopes, and furthermore that a reflection-*asymmetric* interpretation is more or less strongly preferred in all four cases.

In the calculations, the low-energy structure is governed by the $\Omega=\frac{1}{2}$ and $\frac{3}{2}$ Nilsson orbits near the $N=87$ Fermi level in the right-hand part of Fig. 3. The $\Omega=\frac{1}{2}$ orbital is seen to have more curvature as a function of β_2, and in the Nilsson diagram of Ref. 8 these two orbitals cross twice, corresponding to the two changes of ground-state structure that are evidenced by the laser measurements. In Fig. 3, the $\Omega=\frac{1}{2}$ orbital stays below the $\frac{3}{2}$ orbital, but the two changes of the ground-state structure are nevertheless obtained after the inclusion of

TABLE VIII. Adopted values of the parameter n in (2.10) and (2.11). Values greater than unity lead to attenuation of the Coriolis interaction (Ref. 26).

Z,A	219	221	223	225	227	229
91						1
90		5	5	2	2	2.5
89	5		2	2	1	1
88	5	5	2	3	1	
87		2	2	1	1	
86	5	1	2	1		

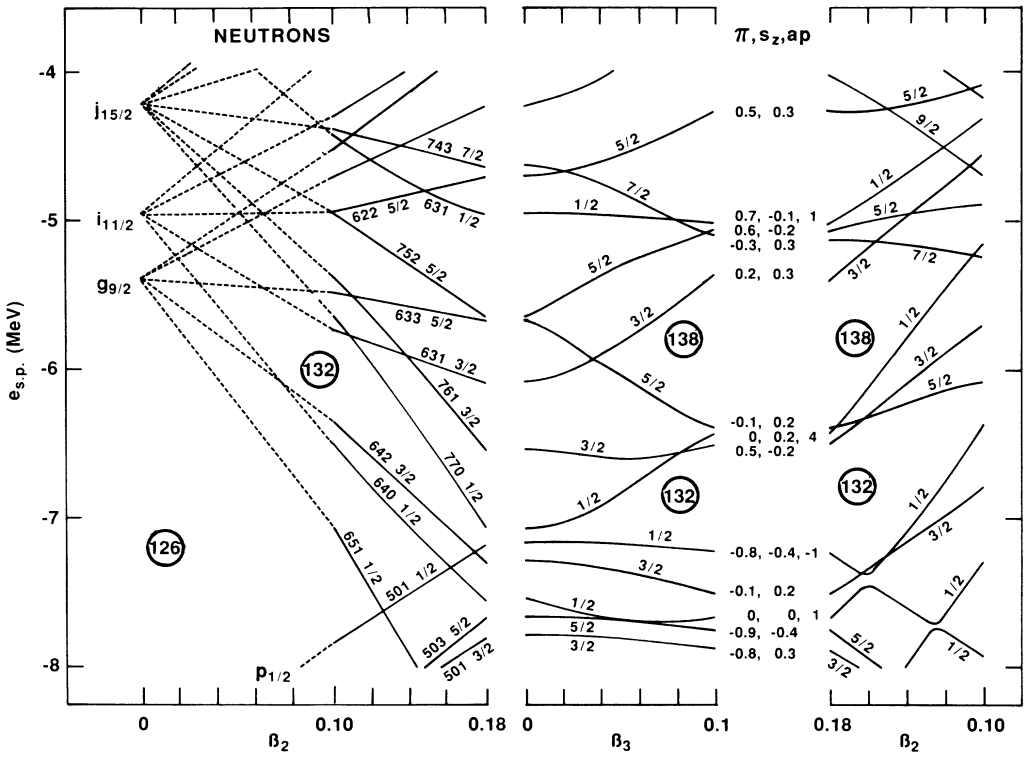

FIG. 4. Similar to Fig. 3, but for neutrons.

nonadiabatic couplings.

In ^{221}Fr, all the experimental levels up to 272 keV can be assigned[47] to $K=\frac{1}{2}$ and $\frac{3}{2}$ parity doublet bands (Fig. 5). The $K^p=\frac{1}{2}^-$ ground-state band has a decoupled $h_{9/2}$-like character. Experimentally, the decoupled nature of the $I=\frac{5}{2}$ ground state is confirmed by a negative value of the spectroscopic quadrupole moment (Table IX), and its magnetic moment of 1.6 μ_N is consistent with the measured magnetic moments of decoupled $h_{9/2}$ $\frac{5}{2}^-$ proton states in other regions of nuclei, which range from 1.4 to 2.6 μ_N.[48] Low-lying positive-parity states that are connected to the ground band by $E1$ transitions are also observed. The corresponding positive-parity states from the calculation arise through parity doubling caused by the octupole deformation. The experimental positive-parity states also fit the description of a $K^p=\frac{1}{2}^+$ band

TABLE IX. Experimental versus calculated ground-state spins, parities, spectroscopic magnetic dipole and electric quadrupole moments for the odd-Z nuclei considered in this work. Experimental data are from Refs. 34 and 46.

	Experiment			Theory		
Nucleus	I^p ($\hbar$)	μ (μ_N)	Q (b)	I^p ($\hbar$)	μ (μ_N)	Q (b)
^{221}Fr	$\frac{5}{2}^{(-)}$	1.58	−1.00	$\frac{5}{2}^-$	1.76	−1.08
^{223}Fr	$\frac{3}{2}$	1.17	1.17	$\frac{3}{2}^-$	1.22	1.00
^{225}Fr	$\frac{3}{2}$	1.07	1.32	$\frac{3}{2}^-$	1.13	1.23
^{227}Fr	$\frac{1}{2}$	1.50		$\frac{1}{2}^+$	1.42	
^{219}Ac	$\frac{9}{2}^-$			$\frac{9}{2}^-$	3.50	0.00
^{223}Ac	$(\frac{5}{2}^-)$			$\frac{5}{2}^-$	1.93	1.83
^{225}Ac	$(\frac{3}{2}^-)$			$\frac{3}{2}^-$	1.20	1.21
^{227}Ac	$\frac{3}{2}^-$	1.1	1.7	$\frac{3}{2}^-$	1.08	1.44
^{229}Ac	$\frac{3}{2}^+$			$\frac{3}{2}^+$	1.73	1.56
^{229}Pa	$\frac{5}{2}^+$			$\frac{5}{2}^+$	2.67	2.86

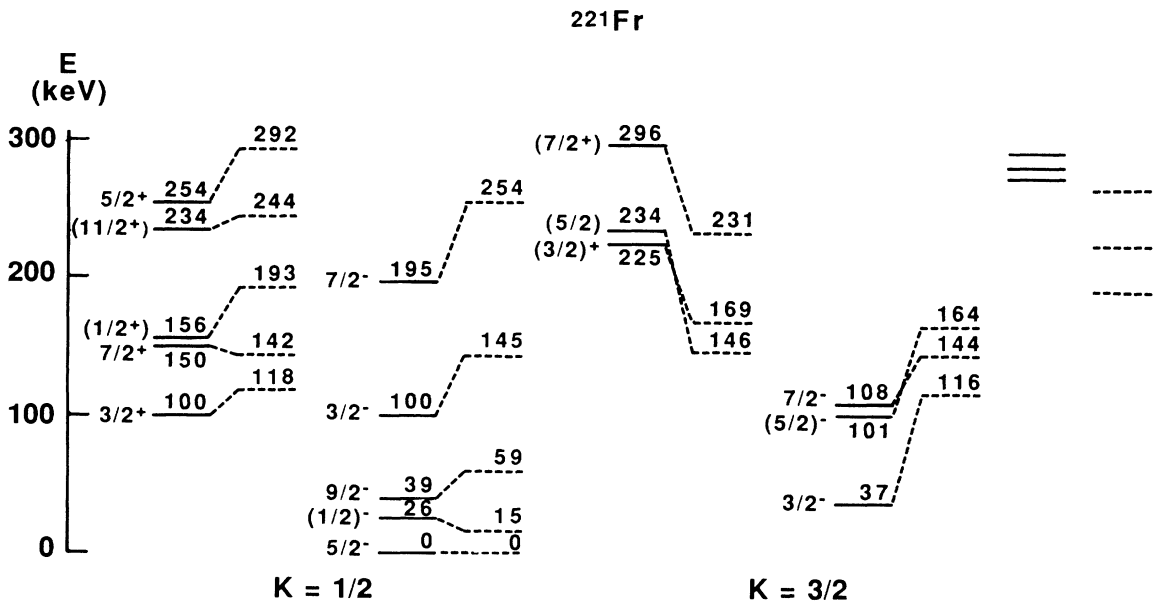

FIG. 5. Experimental levels (Ref. 34) of ^{221}Fr below 300 keV and calculated levels with $I \leq \frac{11}{2}$. The experimental levels are associated with calculated levels according to the I^p, K assignments proposed in Ref. 47, which are partly tentative, especially for $K^p = \frac{3}{2}^+$.

with a decoupling factor of opposite sign from that of the $K^p = \frac{1}{2}^-$ ground band, as would be expected for a parity doublet. An alternative explanation for the positive-parity states might be sought in the low-spin positive-parity orbitals from below the $Z = 82$ gap, but these are not calculated to lie near the Fermi level of ^{221}Fr. Figure 3 shows that a considerably larger quadrupole deformation would be required to account for low-lying positive-parity levels without octupole deformation. Both the $h_{9/2}$-like $K^p = \frac{1}{2}^-$ ground band and a strong-coupled $I^p = \frac{3}{2}^-$ state at low energy are reproduced by the model for a wide range of nonzero β_3 values. The additional requirement that all the low-energy levels be grouped in two parity-doublet bands calls for a larger octupole deformation, with β_3 equal to at least 0.14, than was adopted for most nuclei in this work (Table II). For smaller β_3, parity decoupling would bring out a decoupled $f_{7/2}$-like band in the very low-energy domain of ^{221}Fr.

The $\frac{3}{2}^-$ state mentioned above is calculated to be the ground state in ^{223,225}Fr, in agreement with the measured ground-state spins. The strong-coupled nature of these states is supported experimentally by the large positive values of the spectroscopic quadrupole moments (Table IX), which agree with the strong-coupling formula

$$Q = \{[3K^2 - I(I+1)]/[(I+1)(2I+3)]\} Q_{20} \ . \quad (3.5)$$

With Q_{20} given by (2.23), (2.26), and the deformation parameters of Sec. III A 1, this formula gives Q equal to 1.04 e b and 1.26 e b, respectively, for ^{223,225}Fr. In an alternative interpretation with $\beta_3 = 0$, the 651 $\frac{3}{2}$ and 532 $\frac{3}{2}$ candidates nearest the $Z = 87$ Fermi level originate from the $i_{13/2}$ and $h_{9/2}$ shells (Fig. 3), and Coriolis coupling would be expected to modify both the ground-state spin and quadrupole moment. Furthermore, the measured magnetic moments indicate a wave function with equal admixtures of the reflection-symmetric 532 $\frac{3}{2}$ and 651 $\frac{3}{2}$ orbitals as might be caused by octupole deformation. These two reflection-symmetric orbitals are predominantly spin down and spin up, respectively, with $\langle \hat{s}_z \rangle = -0.26$ and $+0.24$, and the corresponding magnetic moments would be 0.77 and 1.47 μ_N in strong coupling. The measured magnetic moments, however, are consistent with the hybridized value of $\langle \hat{s}_z \rangle$ close to zero that is calculated in the presence of octupole deformation (Table IX).

The other $\Omega = \frac{3}{2}$ orbital resulting from the octupole coupling of 532 $\frac{3}{2}$ and 651 $\frac{3}{2}$ is located just above the $Z = 88$ gap at $\beta_3 = 0.1$ in Fig. 3. Experimental observations are consistent with this description of the two $\Omega = \frac{3}{2}$ orbitals. The upper orbital would give rise to the $\frac{3}{2}^-$ ground states of ^{225,227}Ac (Sec. III C 2). Although the measured ground state magnetic moment of ^{227}Ac is similar to that of ^{223,225}Fr (Table IX), it is clear experimentally that the $\frac{3}{2}^-$ ground states of ^{225,227}Ac arise from a different $\Omega = \frac{3}{2}$ orbital than the $\frac{3}{2}$ ground states of ^{223,225}Fr, because the favored α transitions from the Ac ground states go to excited states in the Fr daughters.[34] The similar ground-state magnetic moments are accounted for by the picture of two $\Omega = \frac{3}{2}$ orbitals, both arising from the hybridization of 532 $\frac{3}{2}$ and 651 $\frac{3}{2}$. The calculated energies of the $\frac{3}{2}^-$ band heads in ^{223,225}Fr due to the upper $\Omega = \frac{3}{2}$ are 563 keV and 535 keV, respectively, in

good agreement with the energies of 553 keV and 518 keV, respectively, of the experimental levels favored by α decay.

In ^{227}Fr the calculated ground-state spin changes to $\frac{1}{2}$, in agreement with the laser measurement. The dominant component of the wave function is 400 $\frac{1}{2}$. The measured magnetic moment is equally consistent with the moment obtained from this calculation at $\beta_3=0.1$ (Table IX) and the value obtained for the 400 $\frac{1}{2}$ orbital assuming $\beta_3=0$. The latter is $\mu=1.62\ \mu_N$ [with the present single-particle model, the g factors (2.22), and strong coupling]. A circumstance that slightly favors octupole deformation is that either octupole deformation or a quadrupole deformation larger than the Strutinsky equilibrium value is required to bring the 400 $\frac{1}{2}$ orbital close to the $Z=87$ Fermi level. The effect of octupole deformation can be seen in the middle part of Fig. 3. At $\beta_3=0$, the $\Omega=\frac{1}{2}$ orbitals near the $Z=87$ Fermi level are 660 $\frac{1}{2}$ and 530 $\frac{1}{2}$, but when β_3 increases, the branch that stays close to the Fermi level exchanges character with the 400 $\frac{1}{2}$ orbital.

2. *The nuclei ^{223,225,227}Ac and ^{229}Pa*

The three actinium isotopes have been studied in α decay, and the two heavier ones also in β decay.[34] States of the nucleus ^{227}Ac have also been populated by one-particle transfer reactions,[49] and its ground-state moments are known from optical spectroscopy.[34] The nucleus ^{229}Pa has been studied by electron capture decay and the (p,t) reaction.[50] $K=\frac{5}{2}$, and in several cases, $K=\frac{1}{2}$ and $\frac{3}{2}$ parity doublet bands have been identified in these nuclei (Figs. 6–9). There have been several earlier theoretical calculations using the strong coupling approximation with octupole correlations introduced either through a static deformation[4,5,8] or diagonalization of fermionic octupole-octupole interaction.[11,12]

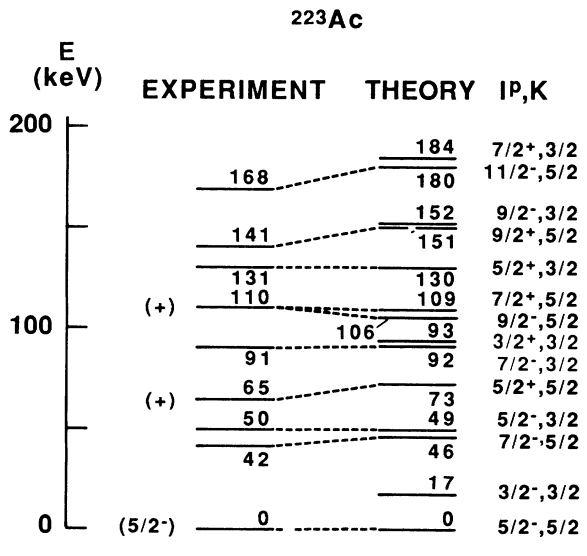

FIG. 6. Experimental levels (Ref. 34) and calculated levels below 200 keV in the nucleus ^{223}Ac. I^p and the predominant K are given for the calculated levels. The assignments indicated by dashed lines are proposed for the experimental levels on the basis of energies and α- and γ-decay properties.

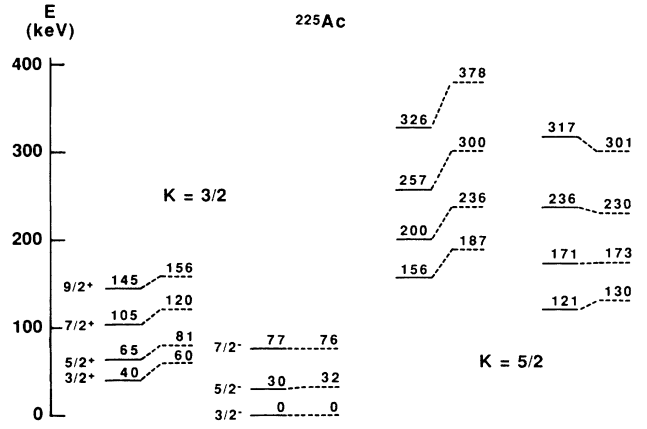

FIG. 7. Experimental levels (Ref. 34) (solid lines) and calculated levels (dashed lines) in the nucleus ^{225}Ac. The experimental I^p,K assignments are valid for the calculated levels as indicated by connecting dashed lines. The calculated bands are only shown up to the highest observed spin. There are no other calculated bands below 400 keV.

The experimental ground-state K^p values are $\frac{5}{2}^-$, $\frac{3}{2}^-$, and $\frac{3}{2}^-$ for ^{223,225,227}Ac, respectively, and $\frac{5}{2}^+$ and $\frac{1}{2}^-$ for ^{229,231}Pa. These values can be understood from the single-particle diagram at $\beta_3=0.1$ (right part of Fig. 3), which gives $K=\frac{3}{2}$, or for small β_2 deformations $\frac{5}{2}$, at the $Z=89$ Fermi level, and $K=\frac{5}{2}$, or for large β_2 deformations $\frac{1}{2}$, at the $Z=91$ Fermi level. The ground-state parity is reproduced in each case by the present calculations. Any major deviations from the adopted β_3 values around 0.1 (see Table II) would lead to a significant deterioration of the overall agreement between the experimental and calculated spectra.

The low-energy spectrum of ^{223}Ac (Fig. 6) might be expected to display the same $K=\frac{3}{2}$ and $\frac{5}{2}$ parity doublet bands that are experimentally well established in ^{225}Ac (Fig. 7). The earlier level assignments for ^{223}Ac in standard compilations[34,51] create two major problems: (i) Although the level at 50 keV has the lowest hindrance factor of all the excited states, no other member of the same band could be assigned, and (ii) the hindrance factor of the $\frac{7}{2}^+$ level at 110 keV was anomalously low relative to the hindrance factor of the other two band members (Table IV of Ref. 52). A new set of level assignments is proposed in Fig. 6. The assignment of a doublet to the observed 110 keV level, which can account for the extra α intensity, is supported by the fact that the α peak is strongly asymmetric.[52] The nonobservation of the low-lying $\frac{3}{2}^-$ level can be understood, since this level cannot obtain a Coriolis admixture from the $K=\frac{5}{2}$ band and thus would have a very large α hindrance factor from an $I=K=\frac{5}{2}$ parent state. The same phenomenon is observed[34] in α decay to ^{225}Ac. Furthermore, in ^{223}Ac none of the populated levels channel a significant fraction of

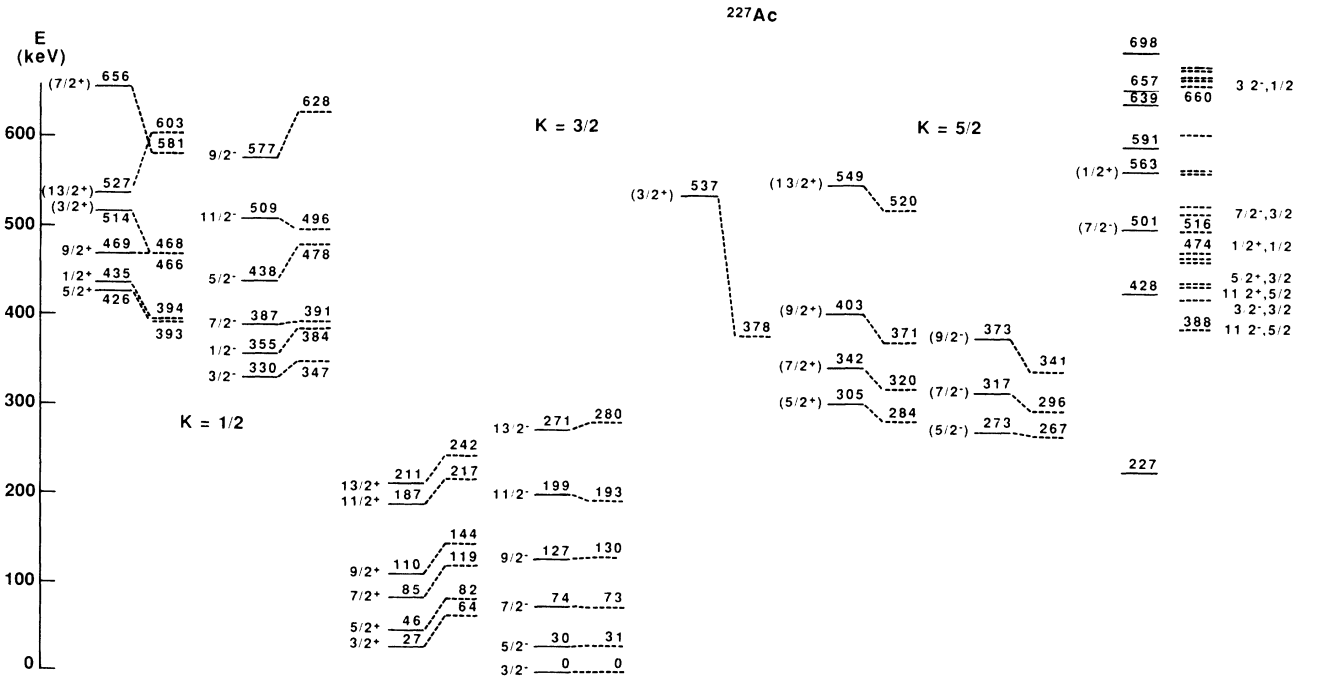

FIG. 8. Experimental levels (Refs. 34 and 49) (solid lines) and calculated levels with $I \leq \frac{13}{2}$ (dashed lines) below 700 keV in the nucleus ^{227}Ac. The level assignments are discussed in Refs. 5 and 49 and this text. The unassigned level at 227 keV is only seen in the particle transfer data.

their γ decay through the $\frac{3}{2}^-$ level according to the present calculation. It should be noted that the calculation does not *predict* the position of the $K^p = \frac{3}{2}^-$ band head, since the Fermi level was prescribed *ad hoc* (Sec. III A 3).

The nucleus ^{227}Ac was the first one considered in the present set of particle-rotor calculations, and some of the results have already been published and discussed in our previous paper, Ref. 15. Since then the calculated nuclear structure factors for particle transfer have been compared with an extended and revised set of experimental structure factors,[49] and the spectrum of assigned levels has been extended (Fig. 8). In the present work, we propose, on the basis of the spectroscopic factors (Sec. IV C), the reassignment of the $(\frac{3}{2}^+)$ level at 537 keV as

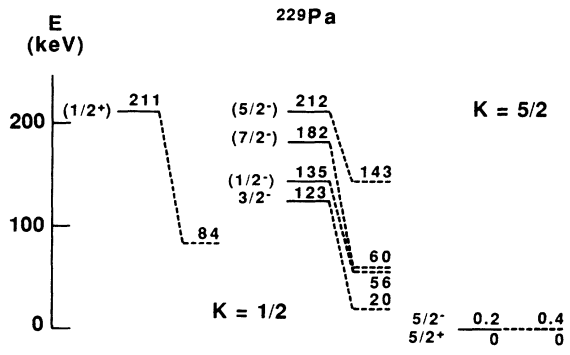

FIG. 9. Experimental levels and assignments in ^{229}Pa from Ref. 50, and the corresponding subset of calculated levels.

the head of the band based on the $\Omega = \frac{3}{2}$ orbital just below the $Z = 88$ gap in the single-particle scheme. The presence of two $\Omega = \frac{3}{2}$ single-particle orbitals (the other one in ^{227}Ac gives rise to the ground-state parity doublet band) was also discussed above in connection with ^{223,225}Fr (Sec. III C 1). In terms of the schematic four-level model of Ref. 8, such "sister" doublets are predicted because a basis space consisting of two opposite-parity single-particle orbitals, combined with parity doubling due to an octupole mode, always leads to two states of each parity, i.e., two doublets, with opposite signs of the parity splittings. The schematic model showed that for octupole vibrations or deformations of order $\beta_3 \approx 0.1$, the "sister" doublets could have fairly collective matrix elements to the ground-state doublet (the higher doublets were rediscovered in Ref. 12 due to this property). Unfortunately, in this case the collectivity of the $E3$ matrix elements from the ground state is not strong enough to make the second $K^p = \frac{3}{2}^+$ band readily observable in a Coulomb excitation experiment, and the intrinsic $E1$ moment of ^{227}Ac is known to be small (Sec. IV B 1), so competing $M1$ transitions are calculated to be the predominant γ-decay modes. These $M1$ transitions are the only ones observed so far. However, the $B(E1)$ transition rate from the $\frac{3}{2}^+$ "sister" band head to the ground state is predicted to be 50% larger than the known $B(E1)$ rate within the $\frac{3}{2}^\pm$ ground-state doublet, and if this property could be verified experimentally it would help to confirm the nature of the 537 keV level.

For the nucleus ^{229}Pa, the parameters that are used to reproduce the $K = \frac{5}{2}$ ground state and the near degenera-

cy of the ground-state doublet (Fig. 9) include a well-defined value of β_3 equal to 0.08, somewhat smaller than the value 0.1 used for most nuclei (Table II). This reduced β_3, necessary to fit the spectroscopic data, is qualitatively consistent with the location of ^{229}Pa at the boundary of the octupole-deformed region. The other odd-Z borderline nuclei are discussed in the following subsection.

3. *The transitional nuclei ^{219}Ac and ^{229}Ac*

These two nuclei would *a priori* be expected to lie at the limits of the range of validity of the reflection-asymmetric rotor model. Both doubly even neighbors of ^{219}Ac are calculated to have spherical ground-state equilibrium shapes, and the doubly even neighbors of ^{229}Ac have prolate equilibrium shapes at or very close to reflection symmetry.[17] The high-spin states of ^{219}Ac have been studied in heavy-ion fusion reactions,[53,54] while selected states of ^{229}Ac have been populated by the t,α reaction.[55] It turns out that the main features of the band structure of ^{219}Ac can be reproduced by the present model using a small quadrupole and octupole deformation, $\beta_2=\beta_3=0.05$, while the levels of ^{229}Ac are reproduced with an octupole deformation component $\beta_3=0.07$.

No model description of any kind has been published previously for ^{219}Ac. Experiment and the present calculation are compared in Fig. 10. There is an overall agreement, apart from the rotational stretching of the calculated spectrum at high spins (cf. Fig. 1). The deviant decay pattern of the experimental $\frac{17}{2}_2^+$ level might be explained by mixing between the near-lying pairs of levels observed for $\frac{17}{2}^+$, and predicted for $\frac{15}{2}^-$ and $\frac{13}{2}^+$. The calculation cannot be expected to reproduce such mixing quantitatively, if for no other reason because the energy spacings are not accurate enough. The calculated $\frac{9}{2}^-$ ground state is a spherical $h_{9/2}$ state: The wave function has nearly equal amplitudes of the five suborbitals from the $h_{9/2}$ shell and the spectroscopic quadrupole moment is zero (Table IX). The excited states are grouped into three parity doublet bands on the basis of their calculated structure. In the band to the left in Fig. 10, the dominant components of the wave functions are the $\Omega=\frac{1}{2}$, $\frac{3}{2}$, and $\frac{5}{2}$ $h_{9/2}$ suborbitals, so this band can be characterized as a $h_{9/2}$ hole configuration. The middle band, of which only two levels have been seen in experiment, has about equal and dominant amplitudes of the $\Omega=\frac{5}{2}$, $\frac{7}{2}$, and $\frac{9}{2}$ $h_{9/2}$ suborbitals and is thus a $h_{9/2}$ particle configuration. The parity-doublet band to the right is based mainly on the $\Omega=\frac{1}{2}$ orbital just above the Fermi level, obtained by octupole mixing of $f_{7/2}$ and $i_{13/2}$ orbitals.

The experimental and calculated levels in ^{229}Ac are shown in Fig. 11. The good agreement for the energies is specifically due to the inclusion of octupole deformation. In Ref. 55 fair agreement was obtained in a Coriolis coupling model without octupole deformation, but with a much larger quadrupole deformation than the equilibrium deformation of the model employed, namely $\epsilon_2=0.225$ versus the equilibrium value[29] $\epsilon_2\lesssim 0.18$. The level assignments in Fig. 11 are largely the same as those of Ref. 55. A qualitative comparison has been made between the present calculated structure factors and the ex-

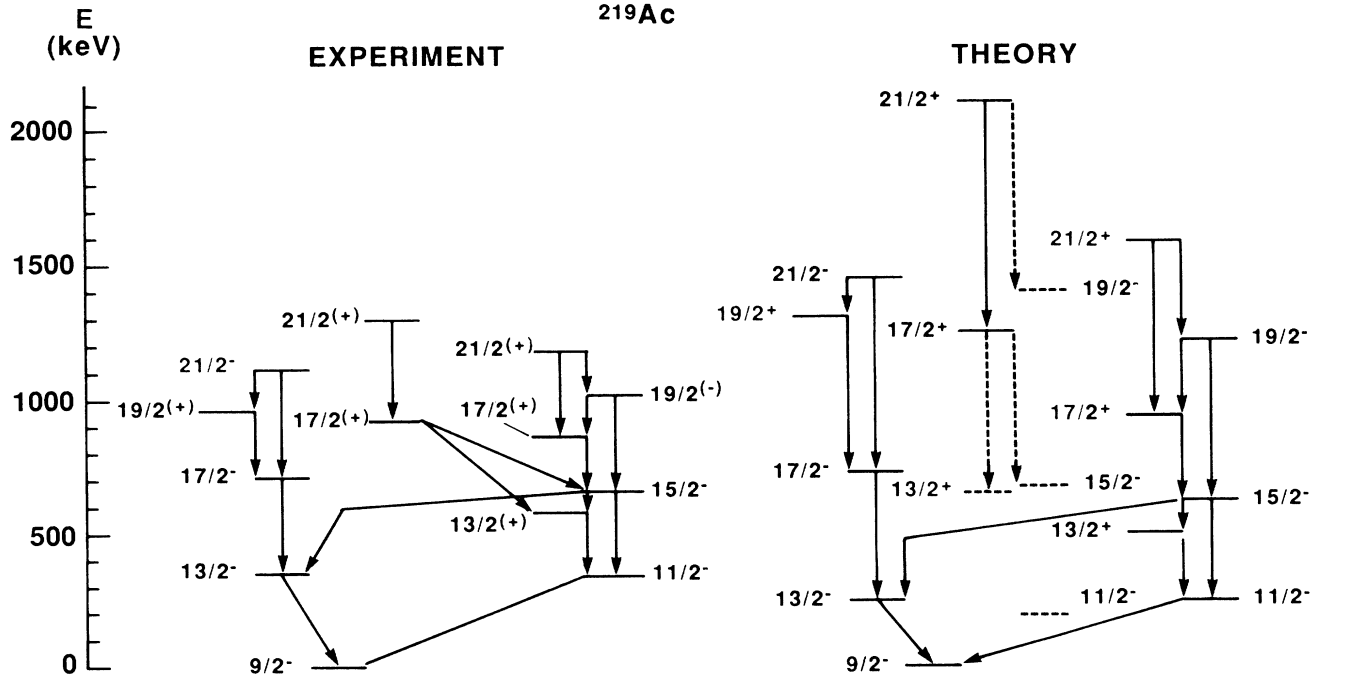

FIG. 10. Experimental levels (Refs. 53 and 54) in ^{219}Ac up to $I=\frac{21}{2}$, and the corresponding calculated levels. The levels at 926 and 1293 keV are reported only in Ref. 54. For the other experimental levels, the depopulating transitions reported in both Refs. 53 and 54 are shown. The calculated level scheme shows the levels that come lowest in energy for the relevant spin parities, and their dominant decay branches. Dashed levels and transitions were not observed in experiment.

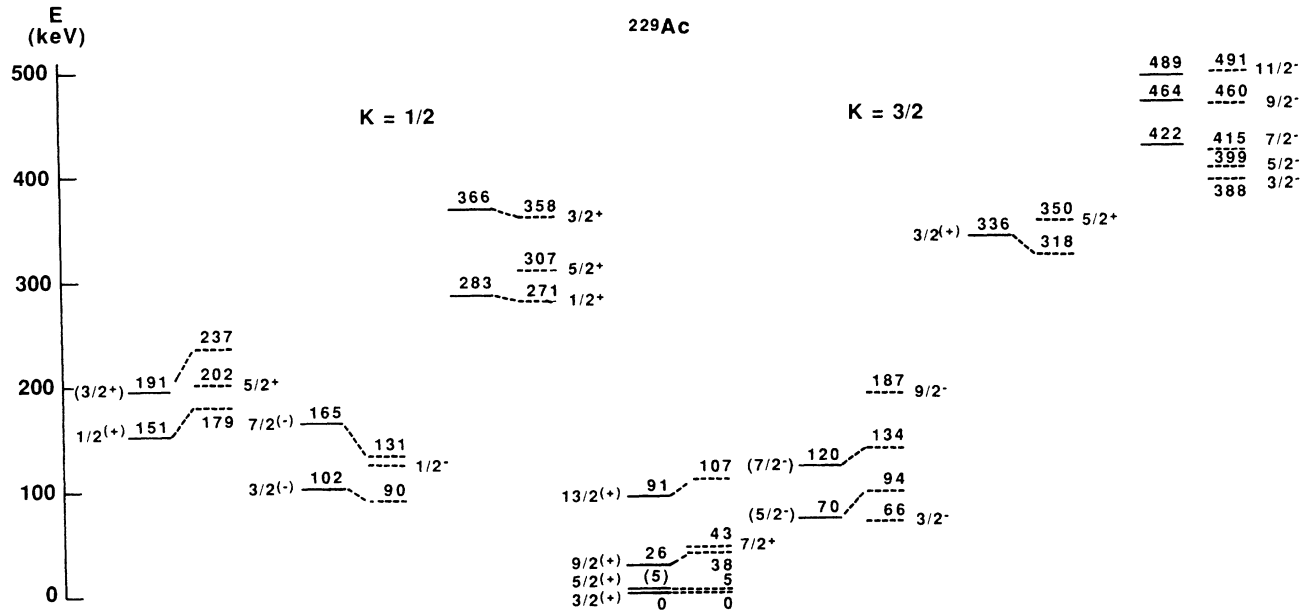

FIG. 11. Levels of ^{229}Ac below 500 keV observed in the (t,α) reaction (Ref. 55) (solid lines), and the lowest levels in each of the calculated bands below 500 keV (dashed lines). Tentative new assignments to second $K^p=\frac{1}{2}^+$ and $\frac{3}{2}^-$ bands are indicated by the placement of the experimental levels in the figure, without connecting dashed lines to the calculated levels.

perimental cross sections. No states with small calculated structure factors have been observed, and the only state with a large calculated structure factor that has not been observed is the $\frac{9}{2}^-$ member of the low-lying $K^p=\frac{3}{2}^-$ band. The explanation could be a near degeneracy between this state and the strongly populated 165 or 191 keV levels. The present calculation predicts additional bands. There is a second $\frac{1}{2}$[400]-like band based on the $\Omega=\frac{1}{2}$ orbital just below the 88 gap (Fig. 3), whose $\frac{1}{2}$ and $\frac{3}{2}$ members are tentatively identified with the previously unassigned 283 keV and unsatisfactorily assigned 366 keV experimental levels, respectively. A problem with these assignments, or at least with the model description of the wave functions, is that the calculated $\frac{1}{2}^+$ spectroscopic strength is rather evenly distributed between the two $K^p=\frac{1}{2}^+$ band heads, whereas the experimental cross section is much larger for the lower one. There is also a second calculated $K^p=\frac{3}{2}^-$ band below 500 keV, the parity doublet of the second $\frac{3}{2}^+$ band based on the $\Omega=\frac{3}{2}$ orbital just below the 88 gap. The $\frac{7}{2}^-$, $\frac{9}{2}^-$, and $\frac{11}{2}^-$ members of this band have calculated structure factors of order 0.1, and might thus be the three observed levels between 400 and 500 keV.

D. Odd-N nuclei

1. The $N=131$ isotones ^{219}Ra and ^{221}Th

These neutron-deficient nuclei, and their even-even neighbors, have been studied in heavy-ion fusion reactions.[56–59] The high-spin states populated by these reactions form parity doublet bands connected by collective $E2$ and $E1$ transitions. The α decay into and out of ^{219}Ra was also studied recently,[60] and suggested a ground-state spin-parity assignment of $\frac{7}{2}^+$. The present work provides the first theoretical interpretation of the ^{219}Ra and ^{221}Th spectra based on a $\frac{7}{2}^+$ ground state.

These two nuclei lie at the edge of the region where a reflection-asymmetric rotor core might be useful. The Strutinsky equilibrium shape is spherical for both even-even neighbors of ^{219}Ra, and for one neighbor of ^{221}Th, so a single calculation was carried out for both nuclei at an assumed dynamical deformation $\beta_2=\beta_3=0.1$. The $\Omega=\frac{1}{2}$ orbital at the $N=131$ Fermi level at this deformation in Fig. 4 is the main component of an $i_{11/2}$-like decoupled band that reproduces a $\frac{7}{2}^+$ ground state and the parity doubled yrast bands of ^{219}Ra and ^{221}Th (Fig. 12). A low-spin positive-parity state of ^{219}Ra is observed in the decay work[60] at an energy of 26 keV, which fits the calculated position of the $\frac{3}{2}^+$ member of this band (Fig. 12).

The $K=\frac{1}{2}$ and $\frac{3}{2}$ orbitals below the Fermi level, and the $K=\frac{5}{2}$ orbital just above it, Coriolis couple to form a second decoupled parity-doublet band, denoted $K=\frac{1}{2}'$ in Fig. 12, which has a $g_{9/2}$ and $j_{15/2}$-like character. It is unclear whether any of the levels participating in an observed[57] nonyrast gamma decay path in ^{219}Ra can be identified with this calculated band.

To the right in Fig. 12, some levels of ^{219}Ra are shown that are populated by the α decay of ^{223}Th, whose ground state has a main component of the $K=\frac{5}{2}$ orbital just above the Fermi level. The $\frac{5}{2}^+$ level in ^{219}Ra that corresponds to the ^{223}Th ground state is distinguished by a very low α hindrance factor. Two other levels with low α hindrance factors are marked by asterisks in Fig. 12, and should correspond to calculated levels designated $K=\frac{1}{2}'$ or $\frac{5}{2}$.

Octupole deformation $\beta_3\sim0.1$ is needed to reproduce

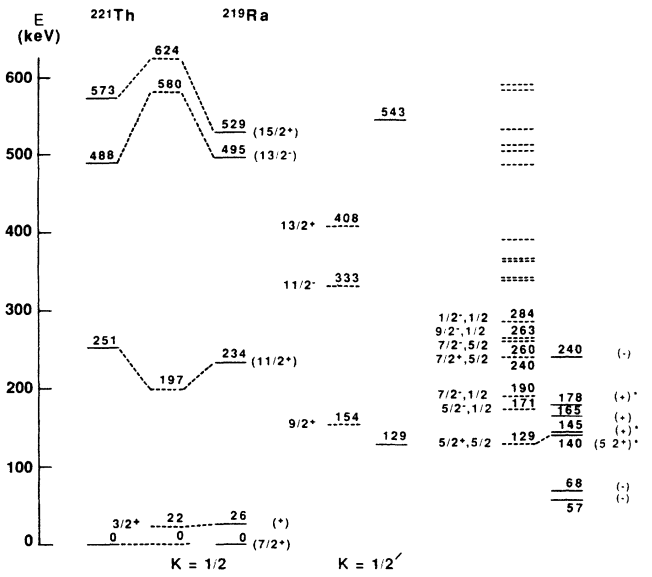

FIG. 12. Experimental levels (Ref. 58) in ^{221}Th (solid lines on left), experimental levels (Refs. 56, 57, and 60) in the isotone ^{219}Ra (all other solid lines), and calculated levels at an assumed dynamical deformation $\beta_2=\beta_3=0.1$ (dashed lines). The calculated ground-state parity-doublet band (to the left) matches the spin parities of the ^{219}Ra ground-state parity-doublet band, and corresponding assignments to the ground-state parity-doublet band of ^{221}Th are indicated by dashed lines on the basis of the similarity with ^{219}Ra. A second calculated decoupled band, and additional high-spin states observed in ^{219}Ra, are denoted $K=\frac{1}{2}'$. Other calculated and observed levels are shown to the right. The analog of the $\frac{5}{2}^+$ α-decay parent state has been assigned, and asterisks denote other experimental levels with low α hindrance factors that may correspond to the $K=\frac{1}{2}'$ and $\frac{5}{2}$ levels that are calculated at nearby energies.

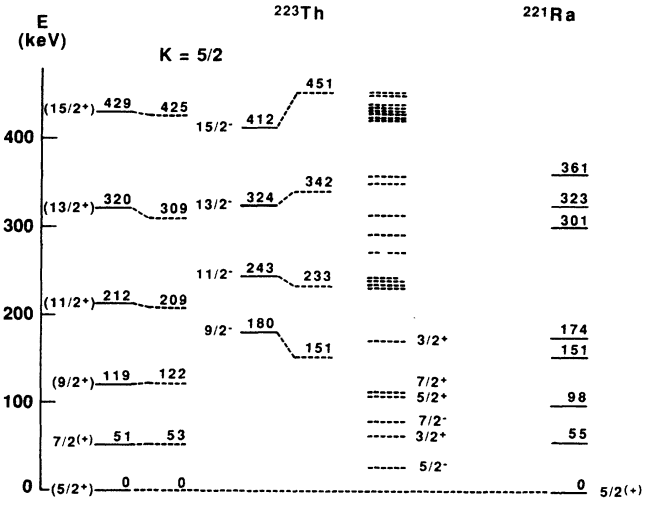

FIG. 13. Experimental levels (Ref. 59) in ^{223}Th (solid lines on the left side of the figure), calculated levels in ^{223}Th (dashed lines), and experimental levels (Ref. 34) in ^{221}Ra (solid lines on the right side of the figure), up to 500 keV excitation energy.

the parity doublet ground band and the low energy of the level favored by α decay. A remark that is generally valid for the treatment of nearly spherical nuclei in the present framework can be made, however, regarding the unassigned experimental levels. In soft nuclei, with purely dynamical deformation, "intruder" configurations with deformations quite different from the adopted one are to be anticipated.

2. *The $N=133$ isotones ^{219}Rn, ^{221}Ra, and ^{223}Th*

Experimental information comes from the α decay[61] of ^{223}Ra into ^{219}Rn, laser measurements[62,63] of the ground state spins and moments of ^{219}Rn and ^{221}Ra (Table X), and a heavy-ion fusion reaction[59] that populated high-spin states of ^{223}Th. The ground states of ^{219}Rn and ^{221}Ra have spin $\frac{5}{2}$ and large positive quadrupole moments, indicating strong coupling, and the ground band of ^{223}Th has the $\Delta I=1$ sequence characteristic of strong coupling (Fig. 13). A high-K orbital is most likely to support strong coupling at small deformation, and the obvious candidate for the ground state of all three nuclei is the $K=\frac{5}{2}$ orbital situated at the $N=133$ Fermi level in the right-hand part of Fig. 4, i.e., for shapes with β_2 and β_3 in the vicinity of 0.1. The present calculation reproduces the features discussed above, and also the measured magnetic moments of ^{219}Rn and ^{221}Ra. Both the measured and calculated values of μ and Q are smaller in ^{219}Rn than in ^{221}Ra, which in the calculation is due to a smaller deformation and accompanying enhancement of Coriolis decoupling. Experimental ground-state moments for ^{223}Th are not available, but the measured $E2/M1$ mixing ratio, $\delta^2=0.044\pm0.004$, for the transition between the two lowest states agrees with the calculated value, $\delta^2=0.043$. This value is actually three times larger than the mixing ratio calculated in pure strong coupling, which illustrates the well-known sensitivity of mixing ratios to nonadiabatic couplings.

In Fig. 13, the observed levels of ^{223}Th up to $I=\frac{15}{2}$ are identified with the calculated yrast states. The compression of the experimental negative-parity band may reflect the observed compression[66,67] of the negative-parity band in the even-even core, a feature that is not modeled by the present core. At high spins the calculated $K=\frac{5}{2}$ levels begin to interact with a $K=\frac{1}{2}$ band, which shows up in the $E1/E2$ branching ratios (Sec. IV B 1). Several additional states are calculated at low energy. Some of these may correspond to levels observed in α decay to ^{221}Ra (right part of Fig. 13), but specific assignments cannot be made from the limited data available on this decay.[34]

An interpretation of the level structure of ^{219}Rn based on a spin $\frac{5}{2}$ ground state has not been presented earlier. In Fig. 14, theoretical assignments are proposed for some of the low-lying levels populated by the α decay of ^{223}Ra. The experimental spin assignments in Fig. 14 are based on Ref. 61, and a reanalysis of the α,γ data[68] in light of the new ground-state spins that have been determined by laser measurements for both the parent and daughter nu-

clei. The spectrum of states with low α hindrance factors forms an irregular pattern that is explained by the calculation at the adopted octupole-deformed shape in terms of the $\Omega=\frac{1}{2}$ orbit just below the $N=133$ Fermi level, and the $\Omega=\frac{3}{2}$ orbit just above. These orbits Coriolis couple, and all the resulting states have significant amplitudes of the $\Omega=\frac{3}{2}$ orbit. The same $\Omega=\frac{3}{2}$ orbit is the dominant (90%) component of the ^{223}Ra ground state (Sec. III D 4). Its square amplitude is given for the theoretical states in Fig. 14, along with the experimental α hindrance factors. The proposed assignments lead to a correspondence between large theoretical amplitudes and small experimental hindrance factors, taking into account that the α transition to the $\frac{7}{2}^+$ level is suppressed by the higher spin. The experimental level with a hindrance factor of 5.9 at 447 keV, whose predominant gamma decay mode is an $E1$ transition to the 159 keV level, is tentatively assigned as the parity doublet of the $K^p=\frac{3}{2}^+$ band head. Favored α transitions to both parities of a doublet have been observed for other nuclei in the present mass region (e.g., Ref. 8). The levels observed at 4 and 14 keV, with very large α hindrance factors, are not explained by the present calculation.

3. *The nuclei ^{221,223,225}Rn*

Recent laser measurements[62] have provided the first solid spectroscopic information about these nuclei (Table X). The ground state spins are all $\frac{7}{2}\hbar$, and the electromagnetic moments indicate that each ground state has a complex structure, for which there exists no previous theoretical explanation. Within the present model, taking $\beta_3=0.1$, plausible explanations can be contrived for most of these ground-state properties.

TABLE X. Experimental versus calculated ground-state spins, parities, spectroscopic magnetic dipole moments, and electric quadrupole moments for the odd-N nuclei considered in this work. Experimental moments are from Ref. 62 for the Rn isotopes, Ref. 63 for ^{221,223,227}Ra, Ref. 64 for ^{225}Ra, and Refs. 42 and 65 for ^{229}Th.

	Experiment			Theory		
Nucleus	I^p ($\hbar$)	μ (μ_N)	Q (b)	I^p ($\hbar$)	μ (μ_N)	Q (b)
$N=131$						
^{219}Ra	$(\frac{7}{2}^+)$			$\frac{7}{2}^+$	0.66	−1.25
^{221}Th				$\frac{7}{2}^+$	0.66	−1.25
$N=133$						
^{219}Rn	$\frac{5}{2}^+$	−0.43	1.16	$\frac{5}{2}^+$	−0.44	1.30
^{221}Ra	$\frac{5}{2}$	−0.18	1.9	$\frac{5}{2}^+$	−0.28	1.52
^{223}Th	$(\frac{5}{2})$			$\frac{5}{2}^+$	−0.23	1.74
$N=135$						
^{221}Rn	$\frac{7}{2}$	−0.02	−0.47	$\frac{7}{2}^+$	0.62	−0.47
^{223}Ra	$\frac{3}{2}^+$	0.28	1.2	$\frac{3}{2}^+$	0.43	1.04
^{223}Ra*	$\frac{3}{2}^-$	0.43		$\frac{3}{2}^-$	0.42	1.05
^{225}Th				$\frac{3}{2}^+$	0.44	1.15
$N=137$						
^{223}Rn	$\frac{7}{2}$	−0.76[a]	0.99[a]	$\frac{7}{2}^-$[c]	−0.74[c]	1.01[c]
^{225}Ra	$\frac{1}{2}^+$	−0.73		$\frac{1}{2}^+$	−0.85	
^{227}Th	$(\frac{1}{2}^+)$			$\frac{1}{2}^+$	−0.93	
$N=139$						
^{225}Rn	$\frac{7}{2}$	−0.68[a]	1.03[a]	$\frac{7}{2}^-$[c]	−0.74[c]	1.12[c]
^{227}Ra	$\frac{3}{2}^+$	−0.41	1.5	$\frac{3}{2}^+$	−0.37	1.40
^{229}Th	$\frac{5}{2}^+$	0.45	3.1[b]	$\frac{5}{2}^+$	0.63	2.88

[a]Preliminary data.
[b]Deduced from Coulomb excitation data.
[c]Lowest calculated negative-parity state, located 8 keV above the lowest calculated positive-parity state in ^{223}Rn and 26 keV above in ^{225}Rn.

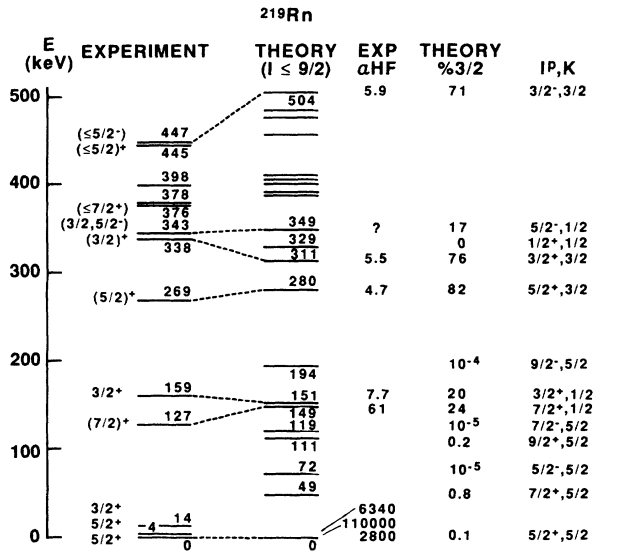

FIG. 14. Levels and proposed assignments in ^{219}Rn. The figure shows, from the left, experimental spins and parities (Refs. 61 and 68), experimental levels up to 500 keV from α decay, levels from the present calculation up to 504 keV and $I=\frac{9}{2}$, experimental α hindrance factors for some levels, the square amplitude in the calculated wave function of the $K=\frac{3}{2}$ component that is the dominant component of the ^{223}Ra parent nucleus ground state, and I^p and the predominant K of the calculated wave function.

Let us first consider the nucleus ^{225}Rn. At $\beta_2=0.155$ and $\beta_3=0.1$ in Fig. 4, an $\Omega=\frac{3}{2}$ and an $\Omega=\frac{7}{2}$ orbital are seen to lie near the Fermi level for $N=139$. A strong-coupled $K=\frac{7}{2}$ band head cannot *per se* account for the ground-state moments, because the strong-coupling formula (3.5) would give $Q\approx 3.0$ e b, which is much larger than the experimental value. Furthermore, the particular $\Omega=\frac{7}{2}$ orbital in Fig. 4 would give $\mu=-0.17$ μ_N in strong coupling, also in poor agreement with the data. However, mixing with another $\frac{7}{2}$ state, based on the $\Omega=\frac{3}{2}$ orbital, can reproduce the observed moments. After some adjustments of the quasiparticle energies (Table VII), in order to fine-tune the relative energies of the $\Omega=\frac{3}{2}$ and $\frac{7}{2}$ quasiparticle orbitals by 25 keV to get the right mixing, and to push away an extraneous $\Omega=\frac{5}{2}$ orbital just below the Fermi level (Fig. 4), the reflection-asymmetric rotor coupling calculation produces a $\frac{7}{2}^-$ state with the correct moments. The calculation also gives some positive-parity levels that are lower in energy by up to 26 keV, but it is possible to bring the $\frac{7}{2}^-$ level below them by minor perturbations of the parameters (we could achieve this by a small *ad hoc* adjustment of the deformation), so this $\frac{7}{2}^-$ level is a plausible candidate of the ^{225}Rn ground state.

The nucleus ^{223}Rn has the same spin and similar moments compared to ^{225}Rn. For $N=137$ and a smaller β_2 deformation, the $\Omega=\frac{7}{2}$ orbital is still near the Fermi level, but the $\Omega=\frac{3}{2}$ orbital is further away and its role is taken over by an $\Omega=\frac{1}{2}$ orbital (Fig. 4). Without any adjustments of the quasiparticle energies, but after a careful positioning of the Fermi level within the $N=138$ gap (Sec. III A 3), the coupling calculation again produces a $\frac{7}{2}^-$ state with the correct moments, due to mixing in this case of $\Omega=\frac{1}{2}$ and $\frac{7}{2}$. Again a positive-parity state is calculated to be lower in energy than the proposed $\frac{7}{2}^-$ ground state, but only by an insignificant 8 keV.

The spin $\frac{7}{2}$ ground state of ^{221}Rn has a negative Q, signaling decoupling, and a μ close to zero (Table X). A decoupled $\frac{7}{2}^+$ ground state results from a calculation with parameters given by the standard prescriptions of Sec. III A and a nonzero β_3 of about 0.1. It has the character of a decoupled $i_{11/2}$ state and arises from the $\Omega=\frac{3}{2}$ orbital at the $N=135$ Fermi level coupled to the $\Omega=\frac{1}{2}$ orbital below it. However, the calculated moments are $\mu=0.6$ μ_N and $Q=-0.8$ e b. The best candidate with which to mix in order to improve the moments, as in the two previous cases, would appear to be a low-lying $\frac{7}{2}^+$ level with negative μ and slightly positive Q that is based on the $\Omega=\frac{5}{2}$ orbital near the Fermi level. When this mixing is achieved by adjusting the quasiparticle energies (Table VII), Q but not μ can be made to agree with the data (Table X).

In summary, the odd radon ground states appear to have complex structures. The present calculations can only demonstrate the feasibility of obtaining such structures within the model, and excited-state spectroscopy is needed to establish any specific configurations. Regarding systematics, the following comments can be made. Although the spectroscopy of the ^{223,225,227}Ra isotones of ^{221,223,225}Rn has been studied extensively (Secs. III D 4 and III D 5), no kind of structure with a $\frac{7}{2}$ band head has been identified that might provide clues as to the nature of the $\frac{7}{2}$ ground states in the Rn nuclei. The calculated $\frac{7}{2}^+$ ground state of ^{221}Rn is, however, similar to the calculated $\frac{7}{2}^+$ ground state of ^{219}Ra (Sec. III D 1). The negative parity proposed here for the ^{223,225}Rn ground states is unusual for odd-N nuclei in the present mass region.

4. *The nuclei ^{223,225}Ra*

The experimental band structure of the nuclei ^{223,225}Ra (Figs. 15 and 16) has emerged from a series of experiments. The ground-state spins were established fairly recently by laser measurements.[63] On the basis of these spins and previous α- and β-decay studies,[34,71] all the observed levels below 500 keV in ^{223}Ra and most of the levels in ^{225}Ra could be assigned to $K=\frac{1}{2}$, $\frac{3}{2}$, and $\frac{5}{2}$ parity doublet bands.[68,69,74] In ^{225}Ra these bands have been extended by recent α-decay work,[72] and several high-spin states have been added through a study of the ^{3}He,α reaction.[73] Notably, the latter reaction produced a $\frac{15}{2}^-$ level at 538 keV, which is the only assigned member of the $K^p=\frac{5}{2}^-$ band in ^{225}Ra.

A corresponding trio of $\Omega=\frac{1}{2}$, $\frac{3}{2}$, and $\frac{5}{2}$ orbitals can be found in the $\beta_3=0.1$ single-particle diagram of Fig. 4, with $\Omega=\frac{3}{2}$ at the $N=137$ Fermi level and $\Omega=\frac{1}{2}$ at the $N=139$ Fermi level in agreement with the measured ground-state spins. The properties of these octupole-

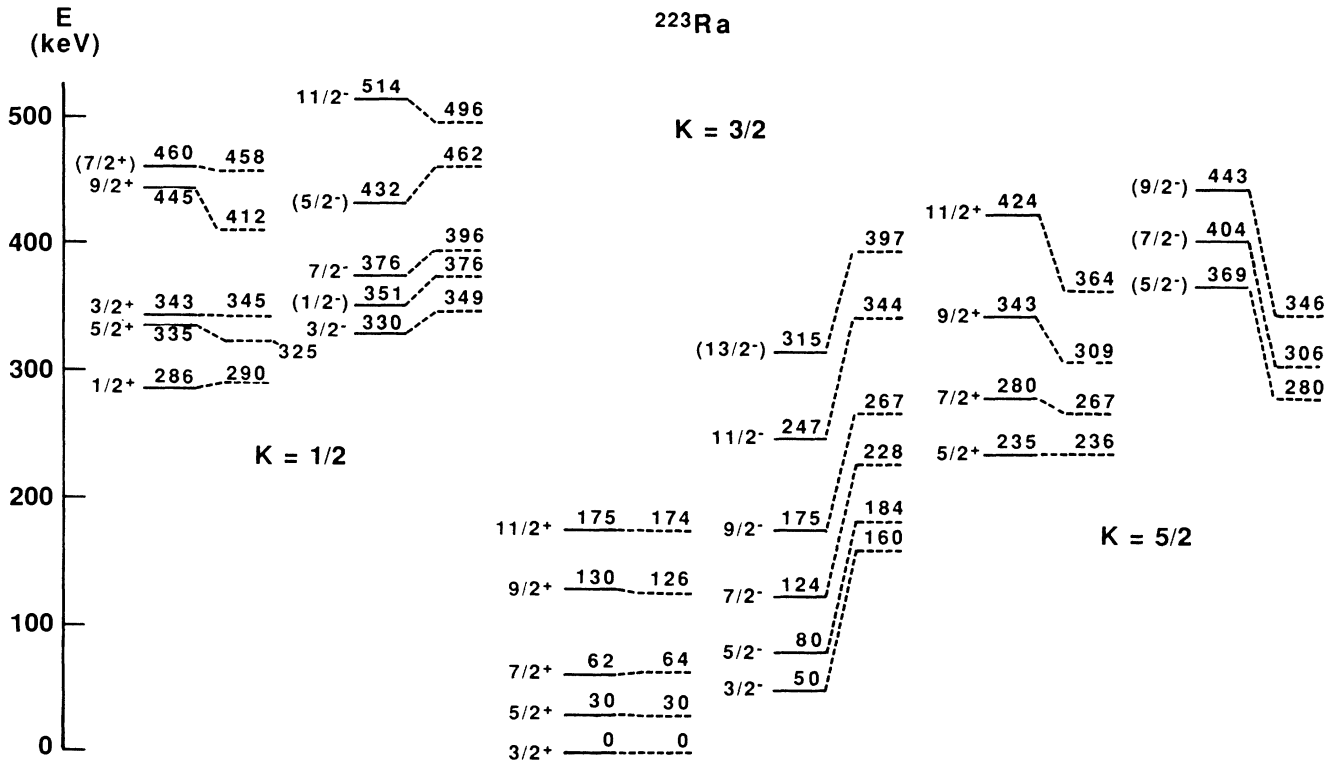

FIG. 15. Experimental levels (Ref. 34) up to 514 keV (solid lines) and calculated levels (dashed lines) in the nucleus ^{223}Ra. The experimental I^p,K assignments (Refs. 68 and 69) are valid for the calculated levels as indicated. The calculated bands are only shown up to the highest observed spin. There are no other calculated bands below 500 keV.

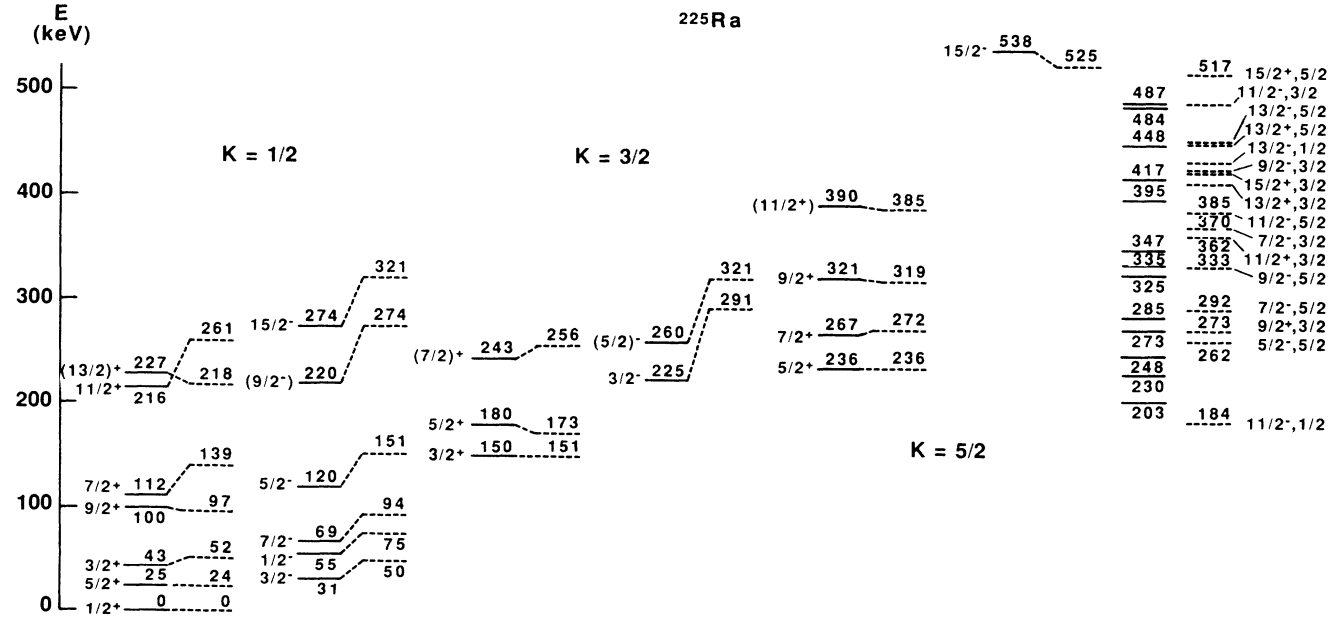

FIG. 16. Experimental levels (Refs. 70–73) (solid lines) and calculated levels up to $I=\frac{15}{2}$ (dashed lines) below 538 keV in the nucleus ^{225}Ra. The experimental I^p,K assignments (Refs. 72–74) are valid for the calculated levels as indicated. The additional calculated levels to the right also belong to the $K=\frac{1}{2}$, $\frac{3}{2}$, and $\frac{5}{2}$ parity-doublet bands. Several of the unassigned observed levels have recently been questioned on experimental grounds (Ref. 72).

deformed single-particle orbits have previously been considered in the framework of strong coupling.[6,8,74,75] The observed band heads, moments, decoupling parameters, and spectroscopic factors are clearly more consistent with octupole deformation than reflection symmetry. It has also been shown[76] that the data are more consistent with the octupole deformed equilibrium shapes obtained by mean field calculations than with the α-cluster-like potentials that might be inferred from the model proposed in Ref. 77.

The optimal β_3 depends on what quantities are considered. The large well-defined value $\beta_3=0.15$ is optimal for the wave function of the $\Omega=\frac{1}{2}$ orbital. Octupole deformation introduces a complicated mixing of several $\Omega=\frac{1}{2}$ orbitals that is sensitive to β_3, but also to details of the modeling. Thus, in the modified oscillator potential, an $\Omega=\frac{1}{2}$ wave function that matches the ^{225}Ra ground-state properties is not obtained at all for the $\Omega=\frac{1}{2}$ orbital closest to the Fermi level, but occurs for the next higher $\Omega=\frac{1}{2}$ orbital.[6] The folded Yukawa potential is similar to the present Woods-Saxon potential, with the appropriate $\Omega=\frac{1}{2}$ wave function occurring at the Fermi level but at a large octupole deformation,[8] $\epsilon_3\approx 0.11$, which corresponds to $\beta_3\approx 0.15$ according to (2.23) and (2.25). However, $\beta_3=0.1$ is more optimal for other spectroscopic properties of ^{223,225}Ra. For example, at $\epsilon_3=0.11$ or $\beta_3=0.15$ the models predict a low-lying $K=\frac{7}{2}$ parity-doublet band in both nuclei that has not been observed. Therefore, in the present core-particle calculations, $\beta_3=0.15$ is used for the $\Omega=\frac{1}{2}$ *wave functions*, and $\beta_3=0.1$ otherwise (Sec. III A 1). The value $\beta_3=0.15$ for the $\Omega=\frac{1}{2}$ wave functions gives about the right decoupling parameters for the $K^p=\frac{1}{2}^{\pm}$ bands of ^{223,225}Ra, the right magnetic moment for the $\frac{1}{2}^+$ ground state of ^{225}Ra (Table X), the right $B(M1)$ rate for the $I^p,K=\frac{7}{2}^+,\frac{1}{2}$ to $\frac{5}{2}^+,\frac{1}{2}$ transition (calculated value 0.013 μ_N^2 vs experimental value[72] 0.017 ± 0.003 μ_N^2, both small), and the right spectroscopic factors for $K^p=\frac{1}{2}^{\pm}$ (Sec. IV C). This large β_3 could be an artificial means to achieve the right mixing of $\Omega=\frac{1}{2}$ orbitals, mocking up deficiencies of the single-particle potential.

The results of the present calculation for ^{223}Ra have previously been compared with experiment in Ref. 69. There is a one-to-one correspondence between the observed and calculated levels below 500 keV (Fig. 15). Furthermore, it was noted that the presence of a second unobserved $K^p=\frac{1}{2}^+$ band is indicated by the sign of the signature splitting in the $K^p=\frac{3}{2}^+$ ground band, since Coriolis coupling to the observed $K^p=\frac{1}{2}^+$ band would give signature splitting in the opposite direction from that observed. In the calculation, the $\Omega=\frac{1}{2}$ orbital below the $N=137$ Fermi level at $\beta_3=0.1$ (Fig. 4) provides this second band above 500 keV with the desired effect on the signature splitting. In ^{225}Ra there is also correspondence between the observed and calculated levels below 500 keV to the extent that there exist experimental I^p,K assignments (Fig. 16).

Some comments can be made regarding the weak population of negative parity states in ^{225}Ra by α decay. Earlier work has shown that the parent nucleus ^{229}Th has a reflection-*symmetric* $I^p,K=\frac{5}{2}^+,\frac{5}{2}$ ground state.[8,11,42] By analogy with the systematics for α decay of reflection-symmetric even-even nuclei into the octupole-deformed region (see, e.g., Ref. 8), the decay into the parity doublet of the favored $K^p=\frac{5}{2}^+$ band in ^{225}Ra should be suppressed, and the $K^p=\frac{5}{2}^-$ band is in fact not observed (Fig. 16). Suppression of the α transitions to negative parity is also observed for the low-lying $K=\frac{1}{2}$ bands in ^{225}Ra, with the measured α hindrance factors of the $I^p=\frac{7}{2}^+$ and $\frac{7}{2}^-$ members differing by 2 orders of magnitude. The present coupling calculation accounts fully for this difference by giving a nonadiabatic admixture of the α-favored $K=\frac{5}{2}$ component into the $K=\frac{1}{2}$ bands that is larger for positive than for negative parity.

5. *The nuclei ^{225,227}Th*

The levels of ^{225}Th and ^{227}Th can be reassigned, relative to earlier interpretations,[34] in light of what is now known about their isotones ^{223,225}Ra. Six states of ^{225}Th have been seen in α decay. Five of them form a sequence with monotonically increasing α hindrance factors, and energy spacings that are quite close to the spacings of the first five levels in the ground band of the isotone ^{223}Ra. In Fig. 17, these states have been given the same assignments as in ^{223}Ra. The sixth observed state in ^{225}Th, at 102 keV, could be the $\frac{3}{2}^-$ member of the ground-state parity doublet, located at somewhat higher energy than in ^{223}Ra and somewhat lower energy than calculated. Another possibility is the $K^p=\frac{5}{2}^+$ band head, which would then lie lower than in ^{223}Ra but precisely at the energy calculated without corrections to the quasiparticle energies. In that case, the rather low α hindrance factor of 37 could be attributed to Coriolis mixing with the favored ground band.

Three states of ^{227}Th have been seen in β decay.[34] Assignments are proposed in Fig. 18 on the following experimental grounds. (i) The isotone ^{225}Ra has an $I^p=\frac{1}{2}^+$

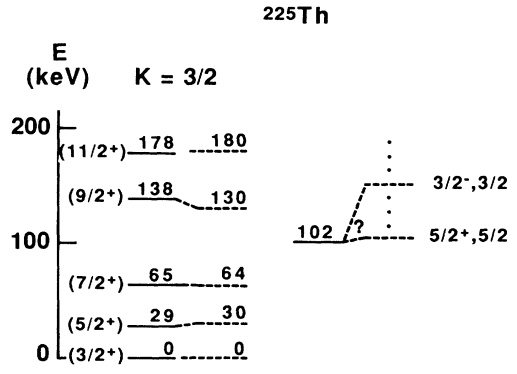

FIG. 17. Experimental (Ref. 34) (solid lines) and calculated (dashed lines) levels in ^{225}Th. Dots indicate that all calculated levels are not shown above 100 keV. I^p,K assignments are proposed for the experimental levels on the basis of similarity with ^{223}Ra.

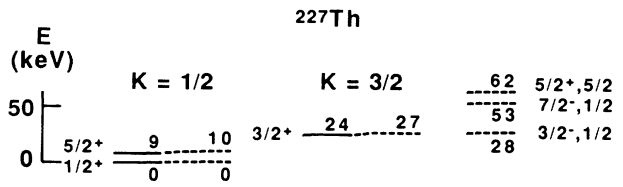

FIG. 18. Experimental levels (Ref. 34) (solid lines) and calculated levels up to 62 keV (dashed lines) in ^{227}Th. Assignments are discussed in the text.

ground state. (ii) The favored α-decay branch of the ^{227}Th ground state goes to a 286 keV level in ^{223}Ra (Ref. 34) that fits into the band structure of that nucleus with an assignment of[69] $I^p, K=\frac{1}{2}^+, \frac{1}{2}$. (iii) Tentative multipolarities of the electromagnetic transitions connecting the three levels of ^{227}Th have been obtained from the data.[34] Assuming a $\frac{1}{2}^+$ ground state, these multipolarities would strongly favor the spin-parity assignments of Fig. 18 for the excited states. (iv) The logft values of all three states in the β decay of the ^{227}Ac $\frac{3}{2}^-$ ground state are ~ 7, which indicates that the possible spins are indeed $\frac{1}{2}$, $\frac{3}{2}$, or $\frac{5}{2}$.

The spin-parity assignments in Fig. 18 are the same as for the first three levels in the $K^p=\frac{1}{2}^+$ ground band of ^{225}Ra, but differences in structure between the two isotones are indicated by the energy spacings. In the calculation for ^{227}Th, the compression of the $\frac{1}{2}^+$-$\frac{5}{2}^+$ spacing relative to ^{225}Ra was reproduced by using a slightly less enhanced β_3 deformation ($\beta_3=0.13$) for the $\Omega=\frac{1}{2}$ wave functions, which leads to a larger decoupling factor. The lower-lying $\frac{3}{2}^+$ level in ^{227}Th was reproduced with a smaller increase of the $\Omega=\frac{3}{2}$ quasiparticle energy relative to the $K=\frac{1}{2}$ quasiparticle energy than in ^{225}Ra (Table VII). A $K=\frac{1}{2}$ or $\frac{3}{2}$ assignment for this $\frac{3}{2}^+$ level of ^{227}Th would be equally compatible with the small $B(M1)$ branching ratio,

$$B(M1;\tfrac{3}{2}^+\rightarrow\tfrac{1}{2}^+)/B(M1;\tfrac{3}{2}^+\rightarrow\tfrac{5}{2}^+)=0.03\ ,$$

that can be deduced from the ^{227}Th data[61] since this ratio is a factor of 2 larger than the calculated $B(M1)$ ratio from the $\frac{3}{2}^+,\frac{3}{2}$ level, and a factor of 2 smaller than the measured $B(M1)$ ratio from the $\frac{3}{2}^+,\frac{1}{2}$ level in ^{225}Ra.

6. *The transitional N=139 isotones ^{227}Ra and ^{229}Th*

The states of ^{227}Ra were studied in β decay and the (n,γ), (d,p), and (t,d) reactions,[78] and all but one of the known levels below 300 keV have been assigned to the bands shown in Fig. 19. There has also been a laser measurement on the ground state,[63] and a later β-decay study[79] which supports the assignments in Fig. 19. Similar bands, and three additional $K=\frac{5}{2}$ bands, have been assigned in the spectrum of ^{229}Th (Fig. 20), following extensive studies of this nucleus by α-, β-, and electron-capture decay,[80] optical hyperfine spectroscopy on the ground state,[65] and partly unpublished but fruitful studies of the (d,t), (d,d'), and (α,α') reactions.[42,80,81]

The lowest-energy $K=\frac{1}{2}$, $\frac{3}{2}$, and $\frac{5}{2}$ bands can be ascribed to the $\Omega=\frac{1}{2}$, $\frac{3}{2}$, and $\frac{5}{2}$ orbitals above the $N=138$ gap at $\beta_3=0.1$ in Fig. 4, on the basis of magnetic moments (Table X) and decoupling factors.[6,8] It has been established experimentally that the high-energy $K^p=\frac{5}{2}^-$ band starting at 512 keV in ^{229}Th is the octupole doublet of the ground state band.[42,81] The presence of a second

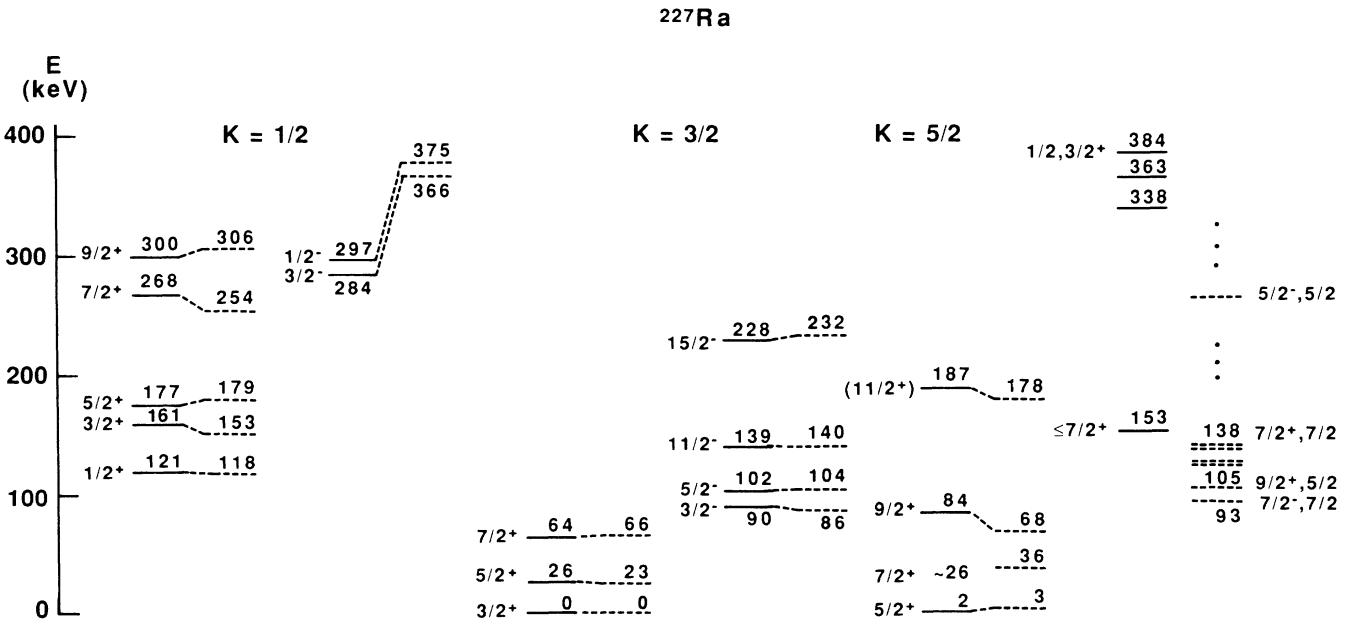

FIG. 19. Experimental (Ref. 78) (solid lines) and calculated (dashed lines) levels below 400 keV in ^{227}Ra. Dots indicate that all calculated levels are not shown.

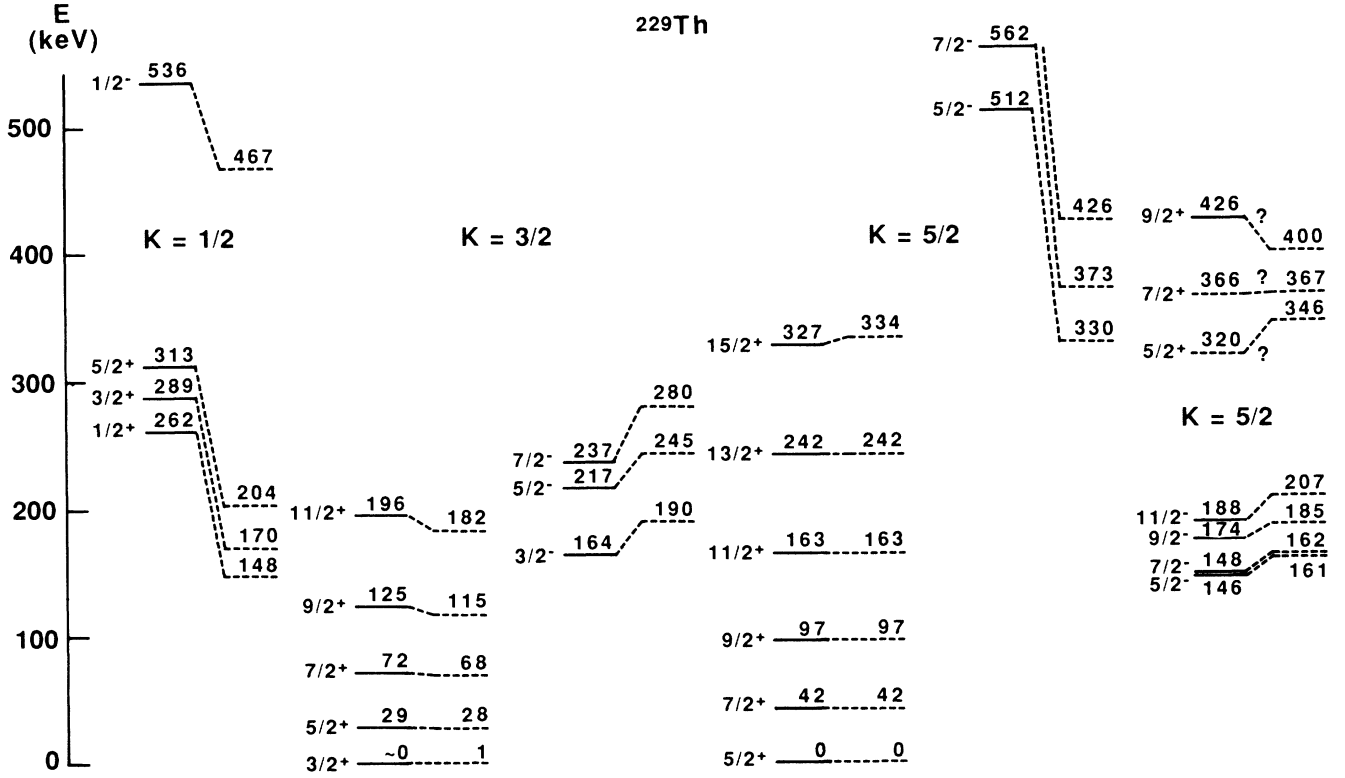

FIG. 20. Experimental (Refs. 42 and 80) levels up to 562 keV in ^{229}Th (solid lines) and the corresponding calculated levels (dashed lines).

$K=\frac{5}{2}$ parity doublet in ^{229}Th can be understood from the single-particle diagram at the somewhat reduced octupole deformation, $\beta_3=0.07$ (middle part of Fig. 4), that was adopted in the present core-particle calculation. The second $K^p=\frac{5}{2}^+$ band, which has been speculatively interpreted as a very low-lying β band in the literature, then emerges from the calculation as the parity doublet of the second $K^p=\frac{5}{2}^-$ band. The value $\beta_3=0.1$ was used in the calculation for ^{227}Ra, though the nonobservation of an $\Omega=\frac{7}{2}$ orbital may indicate that a somewhat reduced octupole deformation would have been appropriate for this nucleus too. Evidence for the $\Omega=\frac{7}{2}$ orbital does occur in the $N=139$ isotone ^{225}Rn, where it appears to play a role in the ground state (Sec. III D 2).

The octupole shape transitional nucleus ^{229}Th has previously attracted attention because it displays octupole shape coexistence, predicted by theory[8,11] and corroborated by data.[42,81,82] It is interesting to see how coexistent states are described in the present fixed-deformation model. According to the previous work, the $I^p,K=\frac{5}{2}^+,\frac{5}{2}$ ground band is reflection *symmetric*, and has a one-phonon octupole excitation built on it with about the same energy and collective strength as the octupole vibration in ^{230}Th. The $K=\frac{3}{2}$ bands, on the other hand, are described in Ref. 8 as condensates of dynamical octupole phonons which is suggestive of octupole deformation. The effective β_3 deformation, 0.07, in the present core-particle calculation is equal to the rms dynamical β_3 deformation of the $K^p=\frac{3}{2}^-$ band and should thus be able to describe the $K=\frac{3}{2}$ doublet but not necessarily the $K=\frac{5}{2}$ doublet. However, it turns out that the distribution of $B(E3)$ strength from the $\frac{5}{2}$ ground state is the same in the present fixed-deformation model as in experiment and the octupole-dynamical models: It goes almost entirely to the high-lying $K^p=\frac{5}{2}^-$ band. The main discrepancy in the fixed-deformation model is that the calculated energy splitting of the $K=\frac{5}{2}$ parity doublet, although large, is not large enough. A smaller β_3 for $K=\frac{5}{2}$ would also improve the calculated ground-state magnetic moment, which is slightly too large (Table X), and the calculated $B(M1;\frac{7}{2}^+\rightarrow\frac{5}{2}^+)$ rate which is correspondingly small (0.006 μ_N^2 vs experimentally 0.011 μ_N^2).

The calculated $K^p=\frac{1}{2}^+$ bands of ^{227}Ra and ^{229}Th have decoupling factors of positive sign due to the octupole deformation, in agreement with the data (Figs. 19 and 20). A negative sign is calculated, and observed in the data[83] for heavier nuclei, for the orbit $\frac{1}{2}[631]$ that would be assigned to these bands in a reflection symmetric scheme.

IV. EVALUATION

A. Energy spectra

1. *Parity splitting*

The reduced parity splitting is defined as the energy difference between the parity doublet band heads, divided by the energy of the virtual $R^p=0^-$ band head in the core,

$$\overline{\Delta E} = [E(I=K,p=-)-E(I=K,p=+)]/[E_{\text{core}}(1^-)-\hbar^2/J] \ , \tag{4.1}$$

where $\hbar^2/J$ is taken from Table III. The splittings of all except the most tentatively assigned doublets from Figs. 5–20 are compiled in Fig. 21. If there were perfect agreement between calculation and experiment, the doublets would lie on the dashed line. The doublets do in fact cluster along this line. There are no doublets in the second and fourth quadrants, which means that all the calculated parity splittings have the right sign.

In Fig. 21, squares are used for odd-proton doublets and circles for odd-neutron doublets. It is seen that eight out of nine odd-proton doublets have negative $\overline{\Delta E}$, and ten out of 11 odd-neutron doublets have positive $\overline{\Delta E}$. These statistics by themselves provide further evidence that the doublets are linked by octupole correlations. If the two opposite-parity members of each doublet originated from two reflection-symmetric Nilsson orbitals that happened to come close in energy, there would be an equal probability in each case for either of the two orbitals to lie closest to the Fermi level.

The nonadiabatic couplings can influence the parity splitting significantly. This effect improves the agreement with experiment in some cases, but not consistently, in the present calculations. An example is given in Fig. 22, which shows the parity splitting for an odd-proton $K=\frac{5}{2}$ orbital that has been observed in four nuclei spanning a wide range of β_2 deformations. The experimental reduced parity splitting is compared with the parity splitting from the strong coupling formula (2.8) and the nonadiabatic calculation. The experimental and calculated splittings all exhibit a trend from negative to positive values with increasing β_2. The nonadiabatic effects on the parity splitting are largest in ^{229}Pa. The deviation between theory and experiment is enlarged by the nonadiabatic effects in one case, ^{225}Ac, but the rms deviation for all four nuclei together is reduced by a factor of 2.

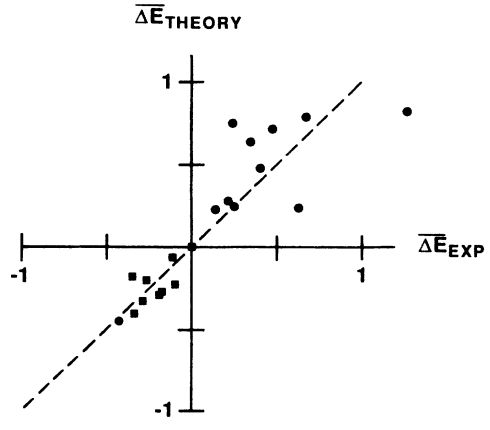

FIG. 21. Compilation of the reduced parity splittings (4.1) in the assigned parity-doublet bands. Filled squares are for doublets in odd-proton nuclei and filled circles for doublets in odd-neutron nuclei. Each symbol indicates both the observed and calculated splitting of the doublet.

2. *Decoupling factors*

The strong-coupling formula, Eq. (2.9), can be used to extract decoupling factors, a, from the energy levels of $K=\frac{1}{2}$ bands. If the experimental values are to be compared with the single-particle matrix elements (2.6) this procedure is both inaccurate, since off-diagonal couplings are neglected in extracting a from the data, and ambiguous, since the experimental levels do not conform perfectly to (2.9). These difficulties are avoided in the present comparisons because a is extracted by identical prescriptions from the experimental and calculated level spectra. Thus, "effective" decoupling factors are obtained by fitting a and $\hbar^2/2J$ in (2.9) to the spacings of the three lowest observed band members, and the corresponding calculated levels. For the $K^p=\frac{1}{2}^-$ band of ^{227}Ra, only two levels have been observed, and a is extracted using the same value of $\hbar^2/2J$ as for the $K^p=\frac{1}{2}^+$ band. Experimental decoupling factors for both parities can thus be obtained in five nuclei (Fig. 23). Experimental values for only one parity are obtained in the additional nuclei ^{229}Pa (the experimental value of a is -1.6 vs theory -2.9), ^{219}Ra (-6.4 vs -6.4), and ^{229}Th (0.04 vs 0.30).

Each symbol in Fig. 23 represents, by its two coordinates, the two different decoupling factors (times parity) of the opposite-parity bands of a $K=\frac{1}{2}$ doublet. In strong coupling to the octupole deformation the decoupling invariants, i.e., the decoupling factor times the parity, would be the same for both parities [Eq. (2.6)] and the points would lie on the diagonal of Fig. 23. The distance

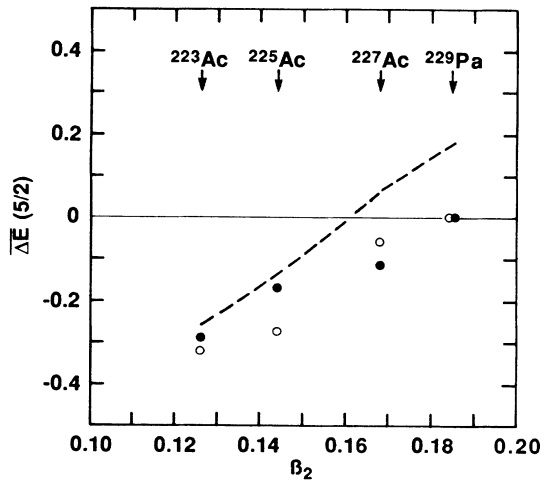

FIG. 22. Reduced parity splitting $\overline{\Delta E}$, defined by Eq. (4.1), of the $K=\frac{5}{2}$ parity doublet in ^{223,225,227}Ac and ^{229}Pa, plotted as a function of β_2 as given by Table I. Filled circles represent the experimental data, open circles the present nonadiabatic core-particle coupling results, and the dashed line shows the parity content $\langle \hat{\pi} \rangle$ of the $K=\frac{5}{2}$ single-particle orbital, which is equal to the reduced parity splitting $\overline{\Delta E}$ in the strong-coupling approximation.

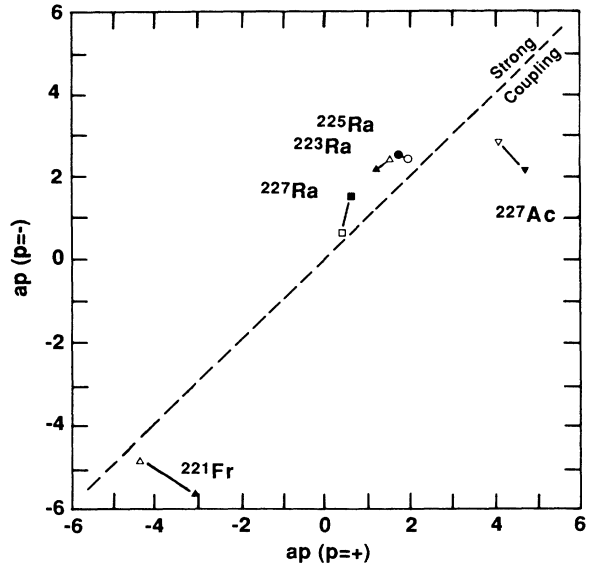

FIG. 23. The decoupling factor a times the total parity p for $K=\frac{1}{2}$ parity doublet bands. Filled symbols represent the measured data for the nuclei indicated in the plot, and open symbols with connecting lines to the filled ones show the corresponding results of the present nonadiabatic core-particle coupling calculation. The abscissa of each symbol gives the ap of the positive-parity band, and the ordinate that of the negative-parity band, in a $K=\frac{1}{2}$ doublet. In adiabatic (strong) coupling, the points would lie on the diagonal (dashed), with the same ap for both parities.

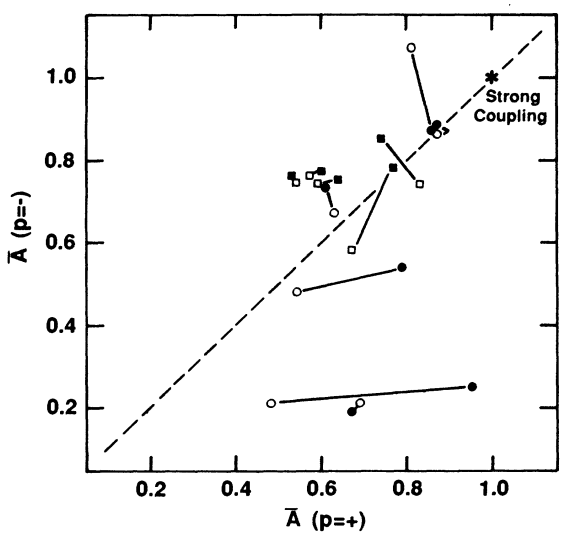

FIG. 24. Reduced moment of inertia $\bar{A}$, defined by (4.2), for $K>\frac{1}{2}$ parity doublet bands. The abscissa of each symbol gives the reduced moment of inertia of the positive-parity band, and the ordinate that of the negative-parity band, in a $K>\frac{1}{2}$ doublet. Squares represent doublets in odd-proton nuclei and circles represent doublets in odd-neutron nuclei. Filled symbols are obtained from the experimental data in Figs. 6–20, and open symbols with connecting lines to the filled ones show the corresponding results of the present nonadiabatic core-particle coupling calculation. An asterisk marks the adiabatic (strong) coupling approximation, in which $\bar{A}$ equals unity, and a dashed line marks the locus of the points in the absence of parity decoupling.

from the diagonal is a measure of the parity decoupling from the octupole deformation. This distance is about the same for the experimental point (solid triangle) and the theoretical point (open triangle) representing ^{223}Ra. For the other nuclei, the distance from the diagonal is larger to the experimental than the theoretical points. Thus the parity decoupling mechanism in the nonadiabatic reflection-asymmetric rotor-plus-particle model appears to account partly but not wholly for the difference between the parities in $K=\frac{1}{2}$ parity doublet bands.

Although the statistics in Fig. 23 are not as good as in Fig. 21, there is a discernible trend as to whether the points are located above or below the diagonal. A little piece of the high-j intruder strength is fragmented onto each orbital and tends to be enhanced by decoupling. Thus $j_{15/2}$-like decoupling has the largest magnitude in the odd-neutron doublets, and $i_{13/2}$- or $h_{9/2}$-like decoupling has the largest magnitude in the odd-proton doublets, although especially for the odd-neutron doublets this magnitude has a much smaller value than would ordinarily be associated with the high-j intruder.

3. Coriolis interaction

First, two familiar effects[21] of Coriolis coupling on $K>\frac{1}{2}$ bands in odd-A nuclei will be analyzed. They are the change in the moment of inertia, and the signature splitting. For this purpose it is useful to define a reduced inertial parameter,

$$\bar{A}(K^p)=\frac{E_\gamma(I=K+2\rightarrow K)}{(4K+6)\hbar^2/2J}\ , \tag{4.2}$$

where $\hbar^2/2J$ is the core inertial parameter from Table III, so that $\bar{A}$ is the dimensionless ratio between the odd-A and core moments of inertia, equal to unity for the model in the strong-coupling approximation. The signature effect will be measured by the dimensionless parameter

$$A_\sigma(K^p)=\frac{E_\gamma(I=K+2\rightarrow K)}{E_\gamma(I=K+1\rightarrow K)}\frac{(K+1)}{(2K+3)}\ , \tag{4.3}$$

which is unity if the band spacings are proportional to $I(I+1)$. These quantities are plotted in Figs. 24 and 25, respectively, for the known $K>\frac{1}{2}$ parity doublets.

Both the moment of inertia and the signature splitting are sensitive to the positions of bands lying just above the observed ones, which may be the main reason for the varying degree of agreement between theory and experiment for individual bands. Some interesting comparisons between theory and experiment can nevertheless be made on the basis of a statistical analysis. First of all it is clear that there is some correlation between the experimental and calculated points: In both Figs. 24 and 25 the average distance between the experimental and the corresponding calculated points is less than half the average

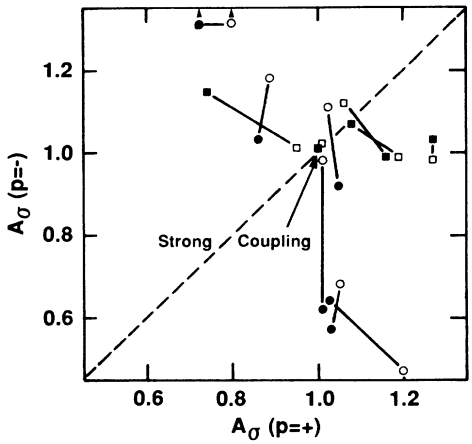

FIG. 25. Similar to Fig. 24, but for the signature splitting parameter A_σ defined by (4.3).

distance between the experimental points. Furthermore, certain average features are similar for the distribution of the experimental and the calculated points (Table XI). The average deviation from the strong-coupling limit, which corresponds to the points $\bar{A}=1$ and $A_\sigma=1$ in the diagrams, and the size of the fluctuations around the average, are equally large for theory and experiment. This suggests that the overall magnitude of the Coriolis couplings is correct. It may be remarked that all the $K>\frac{1}{2}$ bands in Figs. 24 and 25 were observed in deformed nuclei, for which a Coriolis attenuation power of $n=2.5$ or less was used in the calculation. Furthermore, the average distance from the diagonal in Figs. 24 and 25, and the size of the fluctuations around this average, are only slightly smaller for the theoretical than the experimental points. Thus, by these measures, almost the right amount of parity decoupling is obtained in the model.

Some remarks on Coriolis attenuation will conclude this section. It is well known that an *ad hoc* attenuation of the Coriolis couplings is generally needed in particle-rotor model descriptions of reflection-symmetric nuclei. The necessary attenuation in well-deformed nuclei can be obtained[25] by raising the BCS $uu+vv$ factors to a power of typically $n=3-5$. Table VIII shows that the present calculations required strong attenuation, $n=5$, for the near-spherical $N\leq 133$ nuclei, but little or no attenuation for larger N. Let us first mention some of the detailed observations underlying this statement. The stronger attenuation is needed for $N=130$ and 131 to suppress the complete decoupling of the high-j shells, and for $N=133$ to keep the $K=\frac{5}{2}$ ground-state band strong coupled. Fitting n to individual features of the spectra at larger N called for slight deviations from the gross trend to Table VIII only in three cases: (1) $n=1$ instead of 2 in ^{221}Rn because Coriolis attenuation would bring lower-spin states below the $I=\frac{7}{2}$ ground state; (2) $n=3$ instead of 2 in ^{225}Ra because the stronger Coriolis coupling for $n=2$ shifts too much particle-transfer strength from the higher-lying $K=\frac{5}{2}$, $I^P=\frac{11}{2}^+$ and $\frac{15}{2}^-$ states to the yrast states of the same spin and parity; (3) $n=2.5$ instead of 1 or 2 in ^{229}Th from a fit to the energies of the strongly Coriolis mixed $K^P=\frac{3}{2}^-$ and $\frac{5}{2}^-$ bands.

One reason that so little quenching is needed in the more deformed nuclei may be that the large off-diagonal Coriolis matrix elements are smaller in a well-deformed Woods-Saxon potential than in the more widely used deformed modified oscillator potential (see Fig. 7 of Ref. 84). It could also be connected with the substantial reduction of the large Coriolis matrix elements that is already brought about in the present case by octupole deformation.[3,8,85] It may be speculated that in nuclei without octupole deformation, the couplings to octupole vibrational modes are a contributing factor to Coriolis attenuation.

B. Electromagnetic properties

In the pure rotational model, which is frequently referred to below, the collective transition rates between the states (2.5) in a parity doublet band of given $K\neq\frac{1}{2}$ are

$$B(E\lambda;IK\rightarrow I'K)=\frac{(2\lambda+1)(1+3\delta_{\lambda 1})}{16\pi}Q_{\lambda 0}^2 \times\langle IK\lambda 0\,|\,I'K\rangle^2 . \quad (4.4)$$

This also holds true for $K=\frac{1}{2}$ if the multipolarity λ is odd.[28]

1. *E1 transitions*

The $E1$ transitions within parity doublet bands are modeled in strong coupling by a rotating electric dipole. The present model introduces the effects of band mixing and the odd-quasiparticle contribution.

First we examine whether the empirical electric dipole moments of odd-A nuclei are consistent with those of their doubly even neighbors. Experimental in-band $B(E1)$ rates have been deduced from lifetime measurements in several odd-mass nuclei.[50,69,86–88] The core dipole moments, Q_{10}, required to reproduce these $B(E1)$ rates in the present calculations are given in Table V. These Q_{10} values are similar to the ones that would be

TABLE XI. The average distance from relevant limits, and the rms fluctuation around the average, of the points representing $\bar{A}$ and A_σ for $K>\frac{1}{2}$ parity doublets in Figs. 24 and 25, respectively.

	$\bar{A}$		A_σ	
Distance from	Expt.	Theory	Expt.	Theory
$(x,y)=(1,1)$	0.46±0.21	0.52±0.23	0.24±0.14	0.21±0.16
$x=y$	0.14±0.14	0.12±0.09	0.19±0.13	0.17±0.15

obtained from the strong-coupling formula (4.4). In addition to Q_{10} values from lifetimes, Table V includes two values fitted to reproduce measured $E1/E2$ ratios: For ^{223}Th using data from Ref. 59, and a very crude estimate for ^{219}Ac. Table V also gives the Q_{10} values for the two doubly even neighbors, from the microscopic theoretical calculations of Ref. 28. These calculated values are reasonably consistent with the measured $E1/E2$ branching ratios for doubly even nuclei throughout the region. With the exception of ^{229}Pa, each odd-A nucleus is seen to have a Q_{10} value close to that of one of its doubly even neighbors, or intermediate between the two neighbors.

Next we consider whether all the $E1$ rates in a given nucleus are consistent with one common intrinsic $E1$ moment. The case of ^{223}Ra has already been analyzed in Ref. 69, where it is found that eight $K^p=\frac{3}{2}^-$ to $\frac{3}{2}^+$ rates and one $\frac{1}{2}^-$ to $\frac{1}{2}^+$ rate, with rather large uncertainties, are compatible with $Q_{10}\approx 0.13$ e fm, while one $K^p=\frac{5}{2}^-$ to $\frac{5}{2}^+$ rate is significantly slower. In ^{225}Ra, two $K^p=\frac{1}{2}^+$ to $\frac{1}{2}^-$ rates and one $\frac{1}{2}^-$ to $\frac{1}{2}^+$ rate have been measured rather accurately, and it was pointed out[89] that there is some deviation from the pure rotational model. One of these transitions, $I^p,K=\frac{7}{2}^+,\frac{1}{2}$ to $\frac{7}{2}^-,\frac{1}{2}$ is suppressed by a small Clebsch-Gordan coefficient and is therefore sensitive to nonadiabatic band mixing: The pure rotational model gives a $B(E1)$ rate in units of 10^{-3} e^2fm^2 that is 0.07, the present calculation with $Q_{10}=0.14$ e fm gives 0.004, and with $Q_{10}=-0.14$ e fm it gives 0.16. The experimental value is 0.12 ± 0.02. Generally, transition rates associated with small Clebsch-Gordan coefficients by (4.4) should thus not be expected to agree with the rotational model. The other two transitions in ^{225}Ra have larger Clebsch-Gordan coefficients, and the measured transition rates are an order of magnitude larger. They are consequently less sensitive to the modest amount of band mixing obtained in the present calculation. The experimental ratio of these large $B(E1)$ rates is 0.68 ± 0.16, which is significantly different from the pure rotational model ratio of $\frac{4}{3}$. This discrepancy in ^{225}Ra is certainly too large to be accounted for by calculated band mixing. Other available data are $E1$ branching ratios to final states of spin I vs $I-1$ in the $K=\frac{3}{2}$ parity doublet band of ^{229}Th. The $E1$ branching is affected by the strong mixing between the $K^p=\frac{3}{2}^-$ and $\frac{5}{2}^-$ bands, and actually comes closer to the rotational model in the data[82] than in the present calculation. In summary, the present model assumption of a constant collective $E1$ moment for in-band transitions $I,K,p\rightarrow I',K,-p$ appears to be moderately useful. The data suggest dependence on p in ^{225}Ra, and dependence on K in ^{223}Ra.

Large effects from band mixing are obtained in ^{223}Th, where some major deviations from the pure rotational model have been observed[59] and are reproduced by the present calculation up to $I=\frac{17}{2}$. The $B(E1)/B(E2)$ ratios in the $K=\frac{5}{2}$ parity doublet ground band are plotted in Fig. 26. Four of the measured branching ratios, including all three for simplex[90] $s=i$ (i.e., for initial states $I^p=\frac{13}{2}^+$, $\frac{15}{2}^-$, and $\frac{17}{2}^+$), are compatible with the pure rotational model. The corresponding ratios from the present calculation are very close to the rotational model.

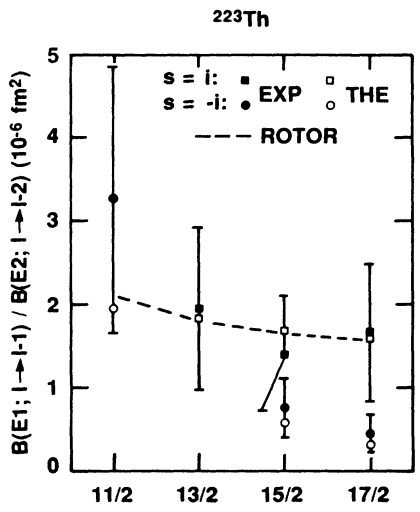

FIG. 26. $B(E1)/B(E2)$ ratios along the parity-doubled yrast band of ^{223}Th. Solid and open symbols are for experiment (Ref. 59) and the present calculation, respectively. Squares are for initial states of simplex $s=i$ ($I^p=\frac{11}{2}^-,\frac{13}{2}^+,\ldots,$), and circles for $s=-i$ ($I^p=\frac{11}{2}^+,\frac{13}{2}^-,\ldots,$). The dashed curve is from the rotational model formula (4.4) with $K=\frac{5}{2}$ and using the core dipole and quadrupole moments (Sec. III A 2). The measured branching ratios are assumed to have a 50% uncertainty.

For the $s=-i$ initial states with $I^p=\frac{15}{2}^+$ and $\frac{17}{2}^-$, however, both the measured and calculated ratios lie significantly below the rotational model values. In the calculation, this occurs because the favored $s=-i$ band based on a $K=\frac{1}{2}$ orbit just below the Fermi level approaches the yrast line and mixes with the $K=\frac{5}{2}$, $s=-i$ levels. This is the same $K=\frac{1}{2}$, $s=-i$ band that accounts for the yrast levels of ^{219}Ra and ^{221}Th (Sec. III C 1).

2. *E3 transitions*

The most direct proof that a $K=0$ parity doublet arises as a consequence of the octupole mode is the observation of a collectively enhanced $E3$ transition between two of its members. This holds true in general, and in particular for both the weak-coupled vibrational limit and the strong-coupled deformed limit of the $K=0$ octupole mode in odd-mass nuclei. Two odd-mass nuclei in the $A\sim 219$–229 region have half-lives that are long enough to measure the collective $E3$ matrix elements from their ground states by Coulomb excitation, namely ^{229}Th and ^{227}Ac.

The ^{229}Th case is known to represent the octupole vibrational limit,[42,81] with the dominant $E3$ matrix elements from the ground state going to a parity-doublet band just above 500 keV, the energy region where the octupole vibration is observed in neighboring ^{230}Th. It is interesting from the modeling point of view that the collective $E3$ rates obtained with the present deformed model are very similar to those obtained from the anharmonic octupole-vibrational model of Ref. 8 (Sec. III D 6), with the largest $E3$ matrix elements going from the ground

state to a higher-energy band as observed in experiment.

The ^{227}Ac is predicted to approach the strong-coupled octupole-deformed limit[11] with the dominant $E3$ matrix elements from the ground state going to the low-lying parity-doublet band that starts at 27 keV. The present octupole-deformed model can be used to predict the redistribution of $E3$ strength relative to the strong-coupled limit due to nonadiabatic effects. The results are shown in Fig. 27. Most of the $E3$ strength from the $\frac{3}{2}^-$ ground state is predicted to go to the low-energy $K^p=\frac{3}{2}^+$ parity doublet band, as in the calculation of Ref. 11. The Coulomb excitation of ^{227}Ac would thus appear to offer a unique opportunity to establish the existence of a near-degenerate parity doublet specifically due to the octupole mode. Figure 27 also shows that some deviations of the $E3$ strength function from the strong-coupled pattern are to be anticipated. Some of the rotational model $E3$ strength is fragmented from the $K^p=\frac{3}{2}^+$ parity-doublet band to higher-lying bands due to parity decoupling and Coriolis decoupling. The fraction of the strength that is lost from the $K^p=\frac{3}{2}^+$ band is seen to increase with increasing spin, so the relative $E3$ strengths in this band are not proportional to the squares of Clebsch-Gordan coefficients. Some $E3$ strength is predicted in the $K^p=\frac{5}{2}^+$ band starting at 305 keV, due to Coriolis mixing with the lower-lying $K^p=\frac{3}{2}^+$ band.

3. *M1 moments and transitions*

The ground-state magnetic moments are reproduced by the present calculation for all nuclei except ^{221}Rn (Tables IX and X). The agreement between theory and experiment could, of course, be fine-tuned by adjusting g_s and g_R within the physical range for each nucleus individually.

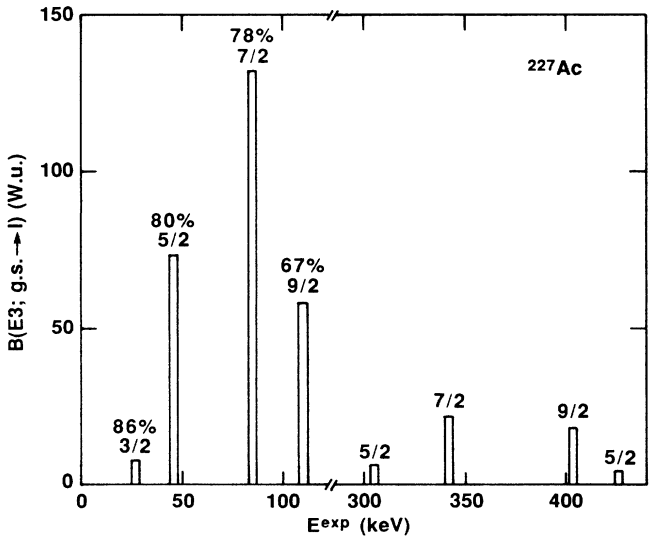

FIG. 27. Calculated $B(E3)$ transition rates from the $\frac{3}{2}^-$ ground state to excited states of ^{227}Ac are indicated in W.u. by the height of the bars placed at the experimental level energies. The spin of the excited state is shown above each bar (the parity is of course positive). For the lowest levels, the magnitude of the calculated $B(E3)$ value is also given in percent of the rotational model value (4.4).

An interesting prediction regarding magnetic moments from previous calculations of strong-coupled octupole-deformed orbitals is the "hybridization" of moments in certain odd-proton nuclei.[4,5,8] For these nuclei, the reflection-symmetric single-particle scheme has a positive-parity orbital with spin up and a negative-parity orbital with spin down near the proton Fermi level, both with Ω equal to the ground state K. If the ground-state parity doublet were attributed to these two reflection-symmetric orbitals, its opposite-parity members would have distinctive and widely different magnetic moments. Octupole deformation mixes the two reflection-symmetric orbitals, however, and a parity doublet based on one such mixed orbital should have hybridized magnetic moments corresponding to $\langle s_z \rangle \approx 0$, intermediate between the values for the reflection-symmetric orbitals and similar for both parities. The magnetic moment of the ^{227}Ac $\frac{3}{2}^-$ ground state does in fact assume the hybridized value.[5] A similar moment was predicted for the $\frac{3}{2}^+$ level, and a similar effect was predicted for the $K=\frac{5}{2}$ doublet that is ground in ^{223}Ac and ^{229}Pa (Ref. 4). In Sec. III C 1, it was noted that hybridization appears to occur in the $\frac{3}{2}^-$ ground states of ^{223,225}Fr.

The present nonadiabatic calculations lead to a partial revision of the predictions. The calculated magnetic moments of the relevant parity doublets are given in Table XII, along with the hybridized moment assuming $\langle s_z \rangle \equiv 0$,

$$\mu_0 = \frac{K}{K+1}(g_R + K) . \tag{4.5}$$

A salient feature of Table XII is that while the magnetic moments of the negative-parity states are close to the hybridized limit, the moments of the positive-parity proton levels are predicted to deviate significantly in several cases. The positive-parity proton valence shell is the high-j intruder $i_{13/2}$, and it appears to give the positive-parity states a greater propensity to decouple. Magnetic moments have not yet been measured for any of these

TABLE XII. The partial hybridization of magnetic moments in the ground-state parity doublets of some odd-proton nuclei. $I^p_{\text{g.s.}}$ is the spin parity of the member of the doublet that is ground state, μ_+ is the magnetic moment (in μ_N) of the positive-parity doublet member from the present calculation, μ_- is the calculated magnetic moment of the negative-parity member, and μ_0 is the magnetic moment obtained in strong coupling with $\langle s_z \rangle = 0$.

Nucleus	$I^p_{\text{g.s.}}$	μ_+	μ_-	μ_0
^{223}Fr	$\frac{3}{2}^-$	1.32	1.22	1.13
^{225}Fr	$\frac{3}{2}^-$	1.28	1.13	1.13
^{225}Ac	$\frac{3}{2}^-$	1.39	1.20	1.14
^{227}Ac	$\frac{3}{2}^-$	1.37	1.08	1.14
^{223}Ac	$\frac{5}{2}^-$	2.62	1.93	2.07
^{229}Pa	$\frac{5}{2}^+$	2.67	1.89	2.07

positive-parity states.

However, the branching ratios in the low-lying $\frac{3}{2}^-$ and $\frac{3}{2}^+$ bands of ^{227}Ac give evidence for the stronger effect of decoupling on the positive-parity band. This can be seen by using the experimental transition energies, E_γ, and cascade to crossover branching ratios,

$$x_I = \frac{T(E2;I\to I-1)+T(M1;I\to I-1)}{T(E2;I\to I-2)} , \tag{4.6}$$

to evaluate the quantity

$$\left|\frac{g_K-g_R}{Q_0}\right| = \frac{0.289[x_I E_\gamma^5(I\to I-2)\langle IK20\,|\,I-2K\rangle^2 - E_\gamma^5(I\to I-1)\langle IK20\,|\,I-1K\rangle^2]}{K^2 E_\gamma^3(I\to I-1)\langle IK10\,|\,I-1K\rangle^2} . \tag{4.7}$$

In strong coupling, this quantity would be a constant. The experimental values are shown in Fig. 28, along with values extracted in the same way from the results of the present nonadiabatic calculation. For positive parity there is a strong staggering, or signature splitting, which is a well-known characteristic of $M1$ transition matrix elements in the presence of rotational decoupling.[92] The calculated signature splitting in the negative-parity band is weaker and cannot be discerned in the data.

The neutron single-particle orbitals relevant to the $A\sim 219$–229 region that are mixed by octupole deformation generally have similar spins, so the opposite-parity states of a doublet are expected to have similar magnetic moments regardless of mixing. In the only case where the magnetic moments of both parity-doublet band heads have been measured, namely the $K^p=\frac{3}{2}^\pm$ ground-state doublet of ^{223}Ra, the difference between the two parities is rather small (Table X). An even smaller difference was obtained from the present model. A difference of the magnitude that is observed in ^{223}Ra is predicted by the model for the $\frac{3}{2}^\pm$ ground-state doublet of ^{227}Ra, where $\mu=-0.37\ \mu_N$ is calculated for the $\frac{3}{2}^+$ ground state, and $-0.49\ \mu_N$ for the $\frac{3}{2}^-$ level.

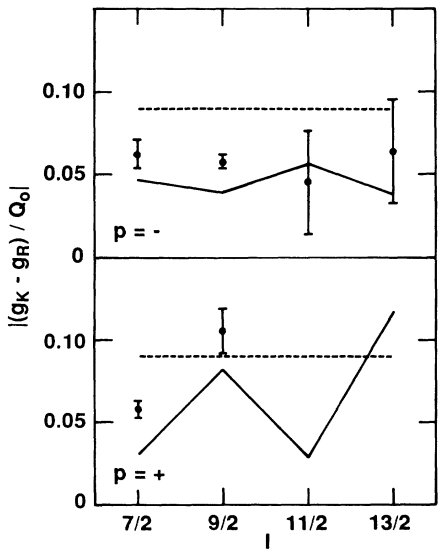

FIG. 28. The quantity $|(g_K-g_R)/Q_0|$ defined by (4.7) at spins $I=\frac{7}{2}$ to $\frac{13}{2}$ in the $K^p=\frac{3}{2}^-$ ground-state band of ^{227}Ac (upper panel) and the $K^p=\frac{3}{2}^+$ parity-doublet band (lower band). The filled circles with error bars are obtained from the experimental transition energies and branching ratios (Ref. 91). The solid lines connect the points obtained with the branching ratios from the present model calculation. The dashed lines indicate the value, independent of spin and parity, that is obtained in the strong-coupled rotational model.

4. *E2 moments and transitions*

The ground-state spectroscopic quadrupole moment, Q, is reproduced by the calculations for all the nuclei in which it has been measured (Tables IX and X). For the ten nuclei with positive values of Q, the discrepancies that do occur are rather systematically in the direction of smaller calculated than measured values, by an average of 8%. This is consistent with a likewise systematic small discrepancy between theory and experiment in the doubly even neighbor nuclei. Experimental intrinsic quadrupole moments, Q_{20}, deduced from the $B(E2;2^+\to 0^+)$ transition rates, are available for nine doubly even nuclei with mass numbers between 220 and 228.[38] When Q_{20} is calculated for these nuclei by the prescriptions used throughout this paper [β_2 from the Strutinsky equilibria of Ref. 17 but not less than 0.1, β_3 equal to 0.1, β_4 from (3.1), β_5 from (3.2), β_6 from (3.3), $\bar{\beta}_2$ from (2.26), and finally Q_{20} from (2.24)], the theoretical value is smaller than the experimental one for each nucleus by an average of 11%. An additional piece of information in line with the other data is the $E2$ transition rate from the $I^p=\frac{5}{2}^+$ first excited state of ^{225}Ra to the $\frac{1}{2}^+$ ground state, which has been determined directly by a lifetime measurement.[86] Comparison with the calculated rate suggests that the theoretical value of Q_{20} is 6 ± 2% too small. We refrain from speculating on the possible origins of this systematic discrepancy.

Another aspect of the collective quadrupole degrees of freedom is triaxiality. It has been proposed in the literature that certain bands, which differ by $\Delta K=2$ from the ground band, contain at any rate an admixture of the γ band built on the ground band.[10,42] These are the $K^p=-\frac{1}{2}^+$ and $-\frac{1}{2}^-$ bands of ^{223}Ra, whose ground band has $K=\frac{3}{2}$, the $K^p=-\frac{3}{2}^+$ and $\frac{5}{2}^+$ bands of ^{225}Ra, whose ground band has $K=\frac{1}{2}$, and the $K^p=\frac{1}{2}^+$ band of ^{229}Th, whose ground band has $K=\frac{5}{2}$. $E2$ transition rates from states in these bands to the ground band are ~ 0.5 (W.u.) Weisskopf units in ^{223,225}Ra, and ~ 4 W.u. in ^{229}Th, which is large enough to suggest a collective contribution. The present model does not include triaxiality, but nevertheless the calculated $E2$ rates from the $\frac{1}{2}^\pm$ bands in ^{223}Ra and the $\frac{3}{2}^+$ band in ^{225}Ra are even higher than the

measured rates. The reason is that $K=\pm\frac{1}{2}$ and $\pm\frac{3}{2}$ bands are $\Delta K=1$ as well as $\Delta K=2$ [both signs of K occur in the wave functions (2.5) after symmetrization], and are thus directly coupled by the Coriolis interaction in the present calculation. $K=\frac{1}{2}$ and $\frac{5}{2}$ bands are not directly coupled, and the present calculation is unable to account for the $E2$ matrix elements to the $K=\frac{5}{2}$ band in ^{225}Ra and the $K=\frac{1}{2}$ band in ^{229}Th, which thus remain as candidates for having a γ-band admixture. Considering the crucial influence of triaxiality in many other transitional regions, it is surprising that there is so little other evidence for it in the $A\sim219-229$ region and that the present axial model appears to account for so much of the data even in near-spherical cases.

C. One-particle transfer

Experimental nuclear structure factors are available in the literature for three nuclei in the $A\sim219-229$ region, namely ^{225,227}Ra and ^{227}Ac (Refs. 49, 71, 73, and 78). Comparison with the nuclear structure factors from the present calculation reveals two salient features. First, either the *absolute* magnitudes of the nuclear structure factors from the octupole-deformed rotor plus particle model are consistently too small, or else the coefficient N in Eq. (2.32), which relates the nuclear structure factors to absolute cross sections, is larger for the present reactions than expected from the standard phenomenology. Second, the *relative* magnitudes of the nuclear structure factors for different states are reproduced by the octupole-deformed rotor plus particle model.

1. Normalization

The experimental papers, Refs. 49, 71, 73, and 78, give estimates of N for the respective reactions. These estimates are expected to be accurate to within about 30%. Values of N that are instead consistent with the present theoretical nuclear structure factors are estimated as follows. For the reactions $(\alpha,t)^{227}$Ac and $(d,p)^{227}$Ra, N is fitted to the state with the dominant cross section in each nucleus, namely $\frac{13}{2}^+_1$ and $\frac{9}{2}^+_1$, respectively. These values of N are larger, by factors of 3 and 2.5, respectively, than the estimates in Refs. 49 and 78. The $(^3\mathrm{He},\alpha)^{225}$Ra reaction has large cross sections for several high-spin ($I>\frac{9}{2}$) final states. All of them, except for the $\frac{11}{2}^+_1$ state, are reproduced quite accurately with a value of N that is 2 times larger than that quoted in the experimental paper.[73] For the $(d,t)^{225}$Ra reaction there are no strong peaks at low energy, and in the construction of Fig. 30, where the experimental values for $I<\frac{7}{2}$ are obtained from this reaction, N is taken to be the same as in the experimental paper[71] for lack of any other evidence.

From the results above, the average discrepancy appears to be at least a factor of 2, significantly larger than the expected uncertainty of about 30% in the standard estimates. One possible reason why the average scaling between the actual and spherical DWBA cross sections might deviate from the systematics is that the target nucleus ^{226}Ra has a unique shape relative to all other target nuclei employed in one-particle transfer, with octupole and very large hexadecapole intrinsic deformations (Sec. III A 2). However, it has not been found previously, in other regions of nuclei, that the systematics are affected by different shapes. An alternative possibility is that the model wave functions might systematically underpredict the nuclear structure factors. It is instructive to consider the particle-core wave function $|I^p\rangle$ in a representation where the particle states $|j^\pi\rangle$ and core states $|R^P\rangle$ have good angular momentum,

$$|I^p\rangle=c_0\,|j^\pi=I^p\rangle\,|R^P=0^+\rangle + \sum_\nu c_\nu\,|(j^\pi)_\nu\rangle\,|(R^P)_\nu\neq0^+\rangle\ . \tag{4.8}$$

For simplicity, pure particle (or hole) states are assumed and quantum numbers other than spin parity have been dropped. The nuclear structure factor,

$$|c_0|^2=1-\sum_\nu |c_\nu|^2 \tag{4.9}$$

depends on the admixture of core states with $R^P\neq0^+$. The nuclear structure factor is thus enhanced by Coriolis decoupling, which reduces the $R>0$ admixture, and by parity decoupling, which reduces the $P=-$ admixture. If the present model systematically underestimates the parity decoupling, as discussed in Sec. IV A 2, this would account for some of the missing particle-transfer strength. However, a factor of 2 corresponds to the difference between the extremes of complete parity mixing in the model, which certainly does not occur, and complete parity decoupling in nature, which would conflict with the overwhelming evidence from other types of measurements that some form of octupole mixing does occur. Any enhancement of the parity decoupling relative to the present model, especially one that would be compatible with other data, could only enhance the particle-transfer strengths by a factor considerably less than 2. As for the Coriolis decoupling, it appears to be well adjusted to other data in the present calculations, especially in ^{225}Ra, where the Coriolis attenuation power n was fine-tuned to the relative nuclear structure factors.

2. Relative nuclear structure factors

Experimental nuclear structure factors for states in ^{227}Ac, ^{225}Ra, and ^{227}Ra, obtained with the normalization that fits cross sections in the present model, are compared with the calculated nuclear structure factors in Figs. 29–31. The rotational "signatures" or "fingerprints" are shown for parity-doublet bands, to the extent that data are available for both parities. A brief inspection of Figs. 29–31 leads to the main conclusion, namely that all the experimental fingerprints are recognizably reproduced by the model.

The remainder of this section contains some comments on details. First it should be emphasized that it is actually the square root of the nuclear structure factors that is represented by the bars in Figs. 29–31. This piece of plotsmanship reduces the difference between large and small bars, with the advantage that theory and experiment can be meaningfully compared for all relevant band members in the same graph, but it also reduces any

discrepancy between the theoretical and experimental bars and might thus exaggerate the quality of the agreement in the eyes of a viewer who is accustomed to the standard plots. The overall pattern of the fingerprints is of course unchanged.

The calculated rotational signature of the $K=\frac{3}{2}$ parity-doublet ground band of ^{227}Ac, shown in Fig. 29, was also presented in our previous paper, Ref. 15 (the experimental numbers, however, have been somewhat revised since then). There it was emphasized that both the Coriolis decoupling and the parity decoupling of the present nonadiabatic model *together* explain the large enhancement of the nuclear structure factor for $I^p=\frac{13}{2}$ relative to the other levels. It had previously been shown that the $i_{13/2}$ component is not so dominant in the relevant $\Omega=\frac{3}{2}$ adiabatic single-particle orbital for octupole-deformed shape, and that the inclusion of Coriolis coupling alone does not enhance the $\frac{13}{2}^+$ nuclear structure factor sufficiently.[93]

The comparison in Fig. 29 between theory and experiment for the higher-lying $K=\frac{1}{2}$ and $\frac{5}{2}$ bands of ^{227}Ac may be biased, on one hand, towards better agreement by the fact that the structure factors have been used to confirm some of the level assignments, and on the other hand towards poorer agreement by the fact that the details of the level energies have not been fine-tuned to the data. Several of the $K=\frac{5}{2}$ levels have been assigned in part on the basis of their nuclear structure factors.[49] Furthermore, the level at 515 keV with a tentative spin parity $\frac{3}{2}^+$ from β decay[34] is assigned as the $\frac{3}{2}^+$ member of the $K=\frac{1}{2}$ band on the basis of an appropriate structure

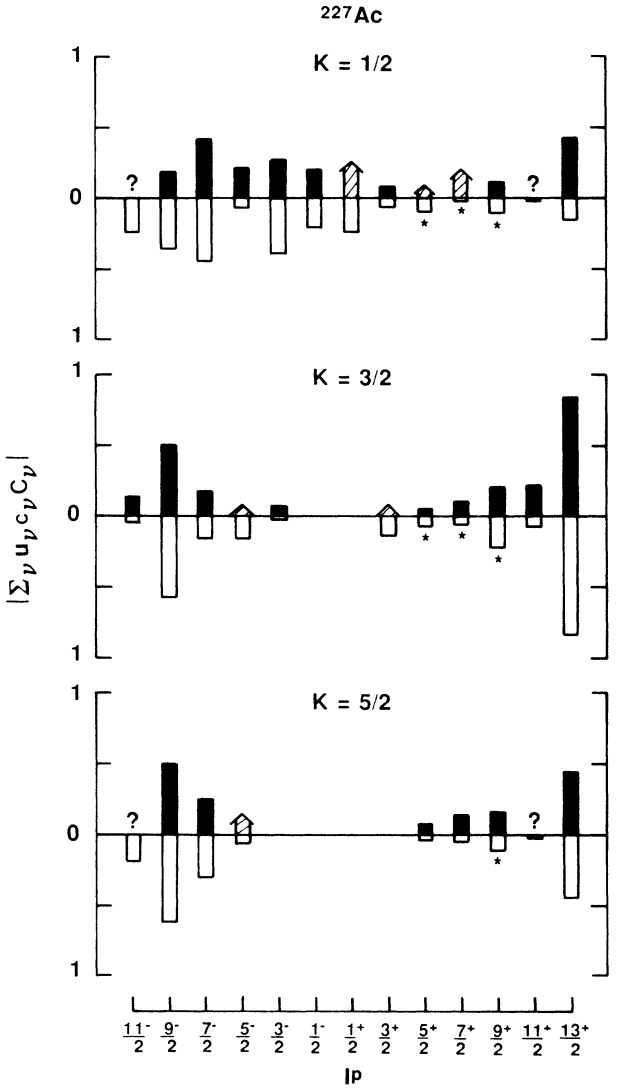

FIG. 29. Rotational signatures for the $K=\frac{1}{2}$, $\frac{3}{2}$, and $\frac{5}{2}$ parity doublet bands of ^{227}Ac. I^p is the spin-parity of the energy levels. The solid bars are obtained from (α,t) data (Ref. 49) as described in the text. The hatched arrows show the upper limits obtained for unresolved doublets, and a question mark indicates that the corresponding level was not observed. The open bars show the results of the present calculation. An asterisk indicates states that have sizable overlaps with more than one spherical *nlj* shell.

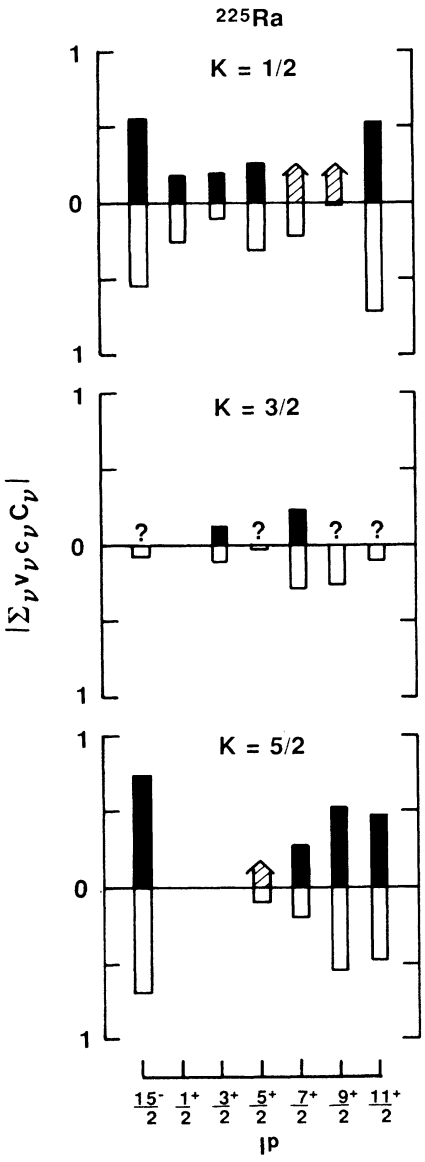

FIG. 30. Same as Fig. 29, but for ^{225}Ra. The solid bars are obtained from (d,t) data (Ref. 71) for $I\leq\frac{7}{2}$ and (^{3}He,α) data (Ref. 73) for $I\geq\frac{9}{2}$.

factor. The 537 keV level that previously had this assignment[5] has an order of magnitude larger structure factor,[49] and is tentatively reassigned as the $I^p=\frac{3}{2}^+$ band head of the parity-doublet band based on the $\Omega=\frac{3}{2}$ orbital just below the $Z=88$ gap, which has a correspondingly large calculated structure factor. The role that the detailed level energies may play is illustrated by the $I^p=\frac{13}{2}^+$ levels, which are calculated quite far apart in energy but experimentally lie so close that mixing is likely to occur (Fig. 8). The calculated nuclear structure factors for the two levels are quite different, while the experimental ones are nearly equal. The latter even distribution of the particle-transfer strength could be reproduced by a band-mixing calculation in which the level energies were fitted to experiment.[49] It may be remarked that no major conflict with experiment occurs for the states indicated by asterisks in Fig. 29, although the simple projection procedure described in Sec. II C was found to be ambiguous.

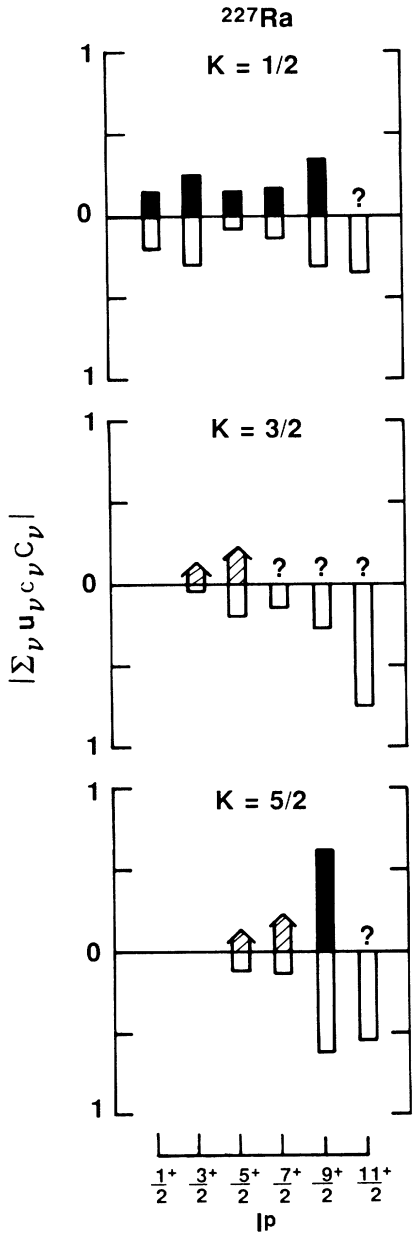

FIG. 31. Same as Fig. 29, but for ^{227}Ra. Experimental structure factors are from (d,p) data (Ref. 78), and are only available for positive parity states.

The $\frac{15}{2}^-$ structure factors in ^{225}Ra have previously been calculated for the adiabatic orbitals in the present octupole-deformed Woods-Saxon single-particle potential, and were found to reproduce the measured distribution of $\frac{15}{2}^-$ strength.[73,75] The present calculation also includes the positive-parity states. For these too, it turns out that the structure factors for strong coupling reproduce the data with only a few exceptions. Thus Coriolis coupling cannot be allowed to redistribute the strength in a major way. The minimum value of the Coriolis attenuation power that satisfies this requirement in the nonadiabatic calculation was found to be $n=3$ (Sec. IV A 3). With this value of n, the nonadiabatic effects in fact significantly improve the agreement with the data. For $I^p=\frac{7}{2}^+$, about the right amount of strength is shifted from the $K=\frac{3}{2}$ to the surrounding $K=\frac{1}{2}$ and $K=\frac{5}{2}$ levels—all three appear to be observed in the data with roughly equal structure factors (Fig. 30). For $I^p=\frac{11}{2}^+$, the experimentally unobserved $K=\frac{3}{2}$ level would have by far the largest structure factor in strong coupling, but the nonadiabatic calculation almost completely depletes the strength in this level and enhances the surrounding $K=\frac{1}{2}$ and $\frac{5}{2}$ levels, too much for $K=\frac{1}{2}$ and just right for $K=\frac{5}{2}$ (Fig. 30). For $I^p=\frac{15}{2}^-$, the strength is again depleted from the experimentally unobserved $K=\frac{3}{2}$ level, while the structure factor for $K=\frac{5}{2}$ remains larger than for the lower $K=\frac{1}{2}$ level, and is even slightly enhanced to perfect the agreement with the data (Fig. 30).

The structure factors of ^{227}Ra have previously been calculated for a reflection symmetric shape, both in strong coupling and with Coriolis coupling, which latter had to be attenuated drastically under the assumption of reflection symmetry.[78] The structure factors from the present nonadiabatic calculation for reflection asymmetric shape (Fig. 31) show some, though not very significant, improvement over the previous calculations. The only low-lying negative-parity state in ^{227}Ra with a measured cross section,[78] and the only one with a calculated structure factor in excess of 0.02, is the $\frac{15}{2}^-_1$ level with a calculated structure factor of 0.83. An experimental structure factor has not yet been calculated for this level, or for the many levels of ^{229}Ac and ^{229}Th populated[55,80] by pickup reactions on ^{230}Th. Also remaining to be completed is the evaluation of a proton pickup reaction[94] on ^{225}Ra, populating states of ^{225}Fr.

V. CONCLUSIONS

The purpose of this work has been to assess, by explicit calculations for all nuclei in which experimental data are available, to what extent the nonadiabatic rigid reflection-asymmetric rotor-plus-quasiparticle model describes the low-energy spectroscopic properties of odd-A nuclei in the $A\sim219$–229 region. Intrinsic equilibrium shapes with reflection-asymmetric octupole deformation

are obtained in this region from mean field theory. It was previously known that under the adiabatic (strong-coupling) approximation, the spectroscopy of these nuclei is often better explained by the reflection-*asymmetric* than the reflection-*symmetric* Nilsson scheme, but also that the data in many cases seem to correspond to an intermediate situation. The present model is based on the *asymmetric* levels, and the mechanism that can give rise to such intermediate situations in the model is nonadiabatic "parity decoupling" of the odd particle from the reflection asymmetry.

The description of experimental data was optimized for each nucleus with respect to β_3. The fact that this optimization invariably favored or allowed a nonzero β_3 leaves little doubt about the role of some sort of surface octupole mode in the $A \sim 219-229$ region. The main factors that might be expected to limit the success of the present model are the rigidity of the model core, the limited accuracy of the single-particle model, and the general feature of all particle-rotor models that they tend to overpredict Coriolis couplings.

The most important question is whether the rigidity of the core inhibits the proper description of those spectroscopic features that appear to be intermediate between the reflection symmetric and asymmetric limits, as would be the case if core softness was responsible for such features. The degree of "parity decoupling" from the asymmetric limit has been assessed quantitatively in several different ways: by the deviation of $K=\frac{1}{2}$ parity-doublet decoupling factors from $a(+)=-a(-)$, by the deviation of $K>\frac{1}{2}$ parity-doublet reduced moments of inertia from $\overline{A}(+)=\overline{A}(-)$, and by the deviation of $K>1/2$ parity-doublet reduced spin staggering from $A_\sigma(+)=A_\sigma(-)$. The latter measures indicated no major discrepancy between the parity decoupling in the present rigid model and the data, while the first measure, which may be more reliable since individual decoupling factors are better reproduced than individual moments of inertia or spin staggerings, implies that only about half of the observed parity decoupling is achieved in the present model. In summary, there is some evidence that the parity decoupling is only partly accounted for by the model, leaving room for the effects of core polarization.

The rigidity of the model core also leads to some obvious shortcomings. It gives an unrealistic spacing of the core yrast levels which, trivially, shows up in the level spacing of the calculated odd-A bands. Furthermore, the $E1$ transition rates are only moderately well reproduced under the assumption of a fixed intrinsic $E1$ moment for the core. On the other hand, there are some nontrivial successes despite the rigid model core. For example, the coexistence of a high-energy "vibrational-like" octupole mode on the ground state of ^{229}Th with low-energy "deformation-like" octupole modes on the quasiparticle excited states is reproduced by the present rigid model as a consequence of the odd-particle nonadiabaticity, with the same distribution of $E3$ strength as in shape dynamical models and the only shortcoming that the high-energy mode on the ground state does not come quite high enough. The $A=229$ isotopes of actinium, thorium, and protactinium are all shape transitional with respect to $K=0$ octupole deformation, but the present rigid model reproduces their energy spectra quite well with a fixed value of β_3 intermediate between 0 and 0.1 A certain measure of success is also obtained with the present model in the octupole and quadrupole shape transitional $A=219$, 221 nuclei with spherical or near-spherical potential-energy minima, using a fixed axially quadrupole-octupole deformed shape. Several previously unexplained ground states and the main features of the high-spin band structure are reproduced.

The viability of a static deformation model presumably has similar origins for the octupole β_3 mode as for the better studied case of the quadrupole triaxial γ mode. For the γ mode, the rigid triaxial rotor plus particle model,[95] which is the analog of the present rigid reflection-asymmetric rotor model, and the triaxial cranked shell model[96] have been widely and successfully applied despite shallow or nonexistent triaxial potential-energy minima. Interesting new light on this was shed by a recent proof that the solution of a γ-unstable model for realistic *finite* valence particle numbers is given very nearly, or in special cases even exactly, by a *rigidly* triaxial intrinsic state.[97] The physical manifestations of core softness are vibrations, which for the octupole mode in the $A \sim 220-228$ region are expected to be too high in energy to be of much practical significance,[98] and state-dependent shape polarization, which can be included in both the rotor and cranking static deformation models.[96,99] Thus, in the present model, the core potential energy and parameters could be established as functions of β_3, and the calculated energy of each level minimized with respect to β_3.

ACKNOWLEDGMENTS

We acknowledge the considerable efforts of M. J. Martin at the Nuclear Data Project in evaluating experimental data for the specific benefit of this study. We are grateful to I. Ahmad, C. W. Reich, R. K. Sheline, and G. L. Struble for providing their most recent data and discussing their implications during the course of this work. UNISOR is a consortium of universities, the State of Tennessee, Oak Ridge Associated Universities, and Oak Ridge National Laboratory and is partially supported by them and by the U. S. Department of Energy under Contract No. DE-AC05-OR00033 with Oak Ridge Associated Universities. The Joint Institute for Heavy Ion Research has as member universities the University of Tennessee, Vanderbilt University, and the Oak Ridge National Laboratory. It is supported by the members and by the Department of Energy through Contract No. DE-AS05-76ER04936 with the University of Tennessee.

*Permanent address: Institute of Atomic Energy, Beijing, China.

[1]K. Alder, A. Bohr, T. Huus, B. Mottelson, and A. Winther, Rev. Mod. Phys. **28**, 432 (1956), and R. F. Christy, quoted therein.

[2]F. Stephens, F. Asaro, and I. Perlman, Phys. Rev. **96**, 1568 (1954); **100**, 1543 (1955).

[3]G. A. Leander, in *Nuclear Structure 1985,* edited by R. A. Broglia, G. B. Hagemann, and B. Herskind (North-Holland, Amsterdam, 1985), p. 249.

[4]G. A. Leander, in *Lasers in Nuclear Physics,* edited by C. E. Bemis and H. K. Carter (Harwood, New York, 1982), p. 487.

[5]R. K. Sheline and G. A. Leander, Phys. Rev. Lett. **51**, 359 (1983).

[6]I. Ragnarsson, Phys. Lett. **130B**, 353 (1983).

[7]R. K. Sheline, D. Decman, K. Nybø, T. F. Thorsteinsen, G. Løvhøiden, E. R. Flynn, J. A. Cizewski, D. K. Burke, G. Sletten, P. Hill, N. Kaffrell, W. Kurcewicz, G. Nyman, and G. Leander, Phys. Lett. **133B**, 13 (1983).

[8]G. A. Leander and R. K. Sheline, Nucl. Phys. **A413**, 375 (1984).

[9]R. Piepenbring, J. Phys. Lett. (Paris) **45**, L1023 (1984).

[10]R. R. Chasman, Phys. Lett. B **175**, 254 (1986).

[11]R. R. Chasman, Phys. Lett. **96B**, 7 (1980).

[12]R. Piepenbring, Z. Phys. A **323**, 341 (1986).

[13]J. Engel, A. Frank, and S. Pittel, Phys. Rev. C **35**, 1973 (1987).

[14]H. J. Krappe and U. Wille, Nucl. Phys. **A124**, 641 (1969).

[15]G. A. Leander and Y. S. Chen, Phys. Rev. C **35**, 1145 (1987).

[16]G. A. Leander, R. K. Sheline, P. Möller, P. Olanders, I. Ragnarsson, and A. J. Sierk, Nucl. Phys. **A388**, 452 (1982).

[17]W. Nazarewicz, P. Olanders, I. Ragnarsson, J. Dudek, G. A. Leander, P. Möller, and E. Ruchowska, Nucl. Phys. **A429**, 269 (1984).

[18]P. Bonche, P. H. Heenen, H. Flocard, and D. Vautherin, Phys. Lett. B **175**, 387 (1986).

[19]W. Nazarewicz, G. A. Leander, and J. Dudek, Nucl. Phys. **A467**, 437 (1987).

[20]R. K. Sheline, Phys. Lett. B **197**, 500 (1987).

[21]A. Bohr and B. R. Mottelson, *Nuclear Structure* (Benjamin, New York, 1975), Vol. 2.

[22]S. G. Rohoziński and W. Greiner, Phys. Lett. **128B**, 1 (1983).

[23]S. Cwiok, J. Dudek, W. Nazarewicz, J. Skalski, and T. Werner, Comput. Phys. Commun. **46**, 379 (1987).

[24]J. Dudek, Z. Szymański, and T. Werner, Phys. Rev. C **23**, 920 (1981).

[25]J. P. Boisson and R. Piepenbring, Nucl. Phys. **A168**, 385 (1971).

[26]F. S. Stephens, P. Kleinheinz, R. K. Sheline, and R. S. Simon, Nucl. Phys. **A222**, 235 (1974).

[27]E. Osnes, J. Rekstad, and O. K. Gjötterud, Nucl. Phys. **A253**, 45 (1975).

[28]G. A. Leander, W. Nazarewicz, G. F. Bertsch, and J. Dudek, Nucl. Phys. **A453**, 58 (1986).

[29]S. G. Nilsson, C. F. Tsang, A. Sobiczewski, Z. Szymański, S. Wycech, C. Gustafson, I.-L. Lamm, P. Möller, and B. Nilsson, Nucl. Phys. **A131**, 1 (1969).

[30]G. R. Satchler, Ann. Phys. (N.Y.) **3**, 275 (1958).

[31]E. Rost, Phys. Rev. **154**, 994 (1967).

[32]A. S. Broad, D. A. Lewis, W. S. Gray, P. J. Ellis, and A. Dudek-Ellis, Nucl. Phys. **A273**, 69 (1976).

[33]F. Menas, Ph.D. thesis, Strasbourg University, 1987.

[34]*Table of Isotopes,* 7th ed., edited by C. M. Lederer and V. S. Shirley (Wiley, New York, 1978).

[35]J. Fernandez-Niello, H. Puchta, F. Riess, and W. Trautmann, Nucl. Phys. **A391**, 221 (1982).

[36]M. Gai, J. F. Ennis, M. Ruscev, E. C. Schloemer, B. Shivakumar, S. M. Sterbenz, N. Tsoupas, and D. A. Bromley, Phys. Rev. Lett. **51**, 646 (1983).

[37]W. Bonin, H. Backe, M. Dahlinger, S. Glienke, D. Habs, E. Hanelt, E. Kankeleit, and B. Schwartz, Z. Phys. A **322**, 59 (1985).

[38]S. Raman, C. H. Malarkey, W. T. Milner, C. W. Nestor, and P. H. Stelson, At. Data Nucl. Data Tables **36**, 1 (1987).

[39]W. Kurcewicz, N. Kaffrell, N. Trautmann, A. Plochocki, J. Zylicz, M. Matul, and K. Stryczniewicz, Nucl. Phys. **A289**, 1 (1977).

[40]C. Fleischmann, J. de Boer, E. Hauber, K. Kaiser, C. Lauterbach, W. Mayer, H. Müller, and C. Schandera, University of Munich Annual Report, 1985, p. 56, and as quoted in Ref. 41.

[41]H. J. Wollersheim, H. Emling, H. Grein, R. Kulessa, R. S. Simon, C. Fleischmann, J. de Boer, E. Hauber, C. Lauterbach, C. Schandera, and P. Butler, in *Proceedings of the International Conference on Nuclear Structure through Static and Dynamic Moments,* Melbourne, 1987, edited by H. H. Bolotin (Conference Proceedings Press, Melbourne, 1987), Vol. II, p. 88.

[42]C. E. Bemis, F. K. McGowan, J. L. C. Ford, W. T. Milner, R. L. Robinson, P. H. Stelson, C. W. Reich, and G. A. Leander, Phys. Scr. (in press).

[43]W. Nazarewicz and P. Rozmej, Nucl. Phys. **A369**, 396 (1981).

[44]S. G. Nilsson and O. Prior, K. Dan. Vidensk. Selsk. Mat. Fys. Medd. **32**, no. 16 (1961).

[45]P. Möller, S. G. Nilsson, and J. R. Nix, Nucl. Phys. **A229**, 292 (1974).

[46]A. Coc, C. Thibault, F. Touchard, H. T. Duong, P. Juncar, S. Liberman, J. Pinard, J. Lermé, J. L. Vialle, S. Büttgenbach, A. C. Mueller, and A. Pesnelle, Phys. Lett. **163B**, 66 (1985).

[47]R. K. Sheline, submitted to Phys. Lett. B.

[48]R. Eder, E. Hagn, and E. Zech, Z. Phys. A **323**, 185 (1986).

[49]H. E. Martz, R. K. Sheline, R. G. Lanier, R. W. Hoff, G. L. Struble, D. J. Decman, D. G. Burke, R. R. Chasman, and R. Naumann, Phys. Rev. C **37**, 1407 (1988).

[50]I. Ahmad, J. E. Gindler, R. R. Betts, R. R. Chasman, and A. M. Friedman, Phys. Rev. Lett. **49**, 1758 (1982).

[51]C. Maples, Nucl. Data Sheets **22**, 243 (1977).

[52]V. B. Subrahmanyam, Ph.D. thesis, University of California Report UCRL-11082, 1963.

[53]S. Khazrouni, A. Chevallier, J. Chevallier, O. Helene, G. Ramanantsizehena, and N. Schulz, Z. Phys. A **320**, 535 (1985).

[54]M. W. Drigert and J. A. Cizewski, Phys. Rev. C **33**, 1344 (1986).

[55]R. C. Thompson, W. Wilcke, J. R. Huizenga, W. K. Hensley, and D. G. Perry, Phys. Rev. C **15**, 2019 (1977).

[56]C. Mittag, C. Lauterbach, H. Puchta, F. Riess, A. Celler, C. Briancon, A. Lefebvre, J. Fernandez-Niello, J. Zylicz, and R. Kulessa, Technical University of Munich Annual Report, 1983, p. 49.

[57]P. D. Cottle, M. Gai, J. F. Ennis, J. F. Shriner, D. A. Bromley, C. W. Beausang, L. Hildingsson, W. F. Piel, D. B. Fossan, J. W. Olness, and E. K. Warburton, Phys. Rev. C **33**, 1855 (1986); **36**, 2286 (1987).

[58]M. Dahlinger, E. Hanelt, E. Kankeleit, B. Schwartz, D. Schwalm, D. Habs, R. S. Simon, and H. Backe, Z. Phys. A **321**, 535 (1985).

[59]M. Dahlinger, Ph.D. thesis, Technical University of Darmstadt, 1987.

[60]A. M. Y. El-Lawindy, J. D. Burrows, P. A. Butler, J. R. Cresswell, V. Holliday, G. D. Jones, R. Tanner, R. Wadsworth, D. L. Watson, K. A. Connell, J. Simpson, C. Lauterbach, and J. R. Mines, J. Phys. G **13**, 93 (1987).
[61]C. Maples, Nucl. Data Sheets **22**, 223 (1977).
[62]W. Borchers, R. Neugart, E. W. Otten, H. T. Duong, G. Ulm, and K. Wendt, Hyp. Int. **34**, 25 (1987); and private communication.
[63]S. A. Ahmad, W. Klempt, R. Neugart, E. W. Otten, K. Wendt, and C. Ekström, Phys. Lett. **133B**, 47 (1983).
[64]E. Arnold, W. Borchers, M. Carre, H. T. Duong, P. Juncar, J. Lerme, S. Liberman, W. Neu, R. Neugart, E. W. Otten, M. Pellarin, J. Pinard, G. Ulm, J. L. Vialle, and K. Wendt, Phys. Rev. Lett. **59**, 771 (1987).
[65]S. Gerstenkorn, P. Luc, J. Verges, D. W. Englekemeir, J. E. Gindler, and F. S. Tomkins, J. Phys. (Paris) **35**, 483 (1974).
[66]D. Ward, G. D. Dracoulis, J. R. Leigh, R. J. Charity, D. J. Hinde, and J. O. Newton, Nucl. Phys. **A406**, 591 (1983).
[67]W. Bonin, H. Backe, M. Dahlinger, S. Glienke, D. Habs, E. Hanelt, E. Kankeleit, and B. Schwartz, Z. Phys. A **322**, 59 (1985).
[68]R. K. Sheline, Phys. Lett. **166B**, 269 (1986).
[69]R. K. Sheline, Y. S. Chen, and G. A. Leander, submitted to Nucl. Phys.
[70]S. A. Baranov, V. M. Shatinskii, V. M. Kulakov, and Yu. F. Rodionov, Yad. Fiz. **11**, 925 (1970) [Sov. J. Nucl. Phys. **11**, 515 (1970)].
[71]K. Nybø, T. F. Thorsteinsen, G. Løvhøiden, E. R. Flynn, J. A. Cizewski, R. K. Sheline, D. Decman, D. G. Burke, G. Sletten, P. Hill, N. Kaffrell, W. Kurcewicz, and G. Nyman, Nucl. Phys. **A408**, 127 (1983).
[72]R. G. Helmer, M. A. Lee, C. W. Reich, and I. Ahmad, Nucl. Phys. **A474**, 77 (1987).
[73]G. Løvhøiden, T. F. Thorsteinsen, K. Nybø, and D. G. Burke, Nucl. Phys. **A452**, 30 (1986).
[74]R. K. Sheline, D. Decman, K. Nybø, T. F. Thorsteinsen, G. Løvhøiden, E. R. Flynn, J. A. Cizewski, D. G. Burke, G. Sletten, P. Hill, N. Kaffrell, W. Kurcewicz, G. Nyman, and G. Leander, Phys. Lett. **133B**, 13 (1983).
[75]W. Nazarewicz, in *Nuclear Structure 1985,* edited by R. A. Broglia, G. B. Hagemann, and B. Herskind (North-Holland, Amsterdam, 1985), p. 263.
[76]G. A. Leander, in *Interacting Boson-Boson and Boson-Fermion Systems,* edited by O. Scholten (World-Scientific, Singapore, 1985), p. 167.
[77]F. Iachello and A. D. Jackson, Phys. Lett. **108B**, 151 (1982).
[78]T. von Egidy, G. Barreau, H. G. Börner, W. F. Davidson, J. Larysz, D. D. Warner, P. H. M. van Assche, K. Nybø, T. F. Thorsteinsen, G. Løvhøiden, E. R. Flynn, J. A. Cizewski, R. K. Sheline, D. Decman, D. G. Burke, G. Sletten, N. Kaffrell, W. Kurcewicz, T. Björnstad, and G. Nyman, Nucl. Phys. **A365**, 26 (1981).
[79]M. J. G. Borge, D. G. Burke, H. Gietz, P. Hill, N. Kaffrell, W. Kurcewicz, G. Løvhøiden, S. Mattson, R. A. Naumann, K. Nybø, G. Nyman, and T. F. Thorsteinsen, Nucl. Phys. **A464**, 189 (1987).
[80]K. S. Toth, Nucl. Data Sheets **24**, 263 (1978).
[81]I. Ahmad, A. M. Friedman, R. R. Chasman, R. R. Betts, J. E. Gindler, and H. C. Griffin, Bull. Am. Phys. Soc. **26**, 1118 (1981).
[82]L. A. Kroger and C. W. Reich, Nucl. Phys. **A259**, 29 (1976).
[83]R. R. Chasman, I. Ahmad, A. M. Friedman, and J. R. Erskine, Rev. Mod. Phys. **49**, 833 (1977).
[84]Th. Lindblad, H. Ryde, and D. Barneoud, Nucl. Phys. **A193**, 155 (1972).
[85]I. Ahmad, R. R. Chasman, J. E. Gindler, and A. M. Friedman, Phys. Rev. Lett. **52**, 503 (1984).
[86]T. Ishii, I. Ahmad, J. E. Gindler, A. M. Friedman, R. R. Chasman, and S. B. Kaufman, Nucl. Phys. **A444**, 237 (1985).
[87]I. Ahmad, J. E. Gindler, A. M. Friedman, R. R. Chasman, and T. Ishii, Nucl. Phys. **A472**, 285 (1987).
[88]I. Ahmad, R. Holzmann, R. V. F. Janssens, M. Huyse, and P. Dendooven, Bull. Am. Phys. Soc. **32**, 1545 (1987).
[89]C. W. Reich, I. Ahmad, and G. A. Leander, Phys. Lett. **169B**, 148 (1986).
[90]W. Nazarewicz, P. Olanders, I. Ragnarsson, J. Dudek, and G. A. Leander, Phys. Rev. Lett. **52**, 1272; (E) **53**, 2060 (1984).
[91]W. Teoh and R. D. Connor, Nucl. Phys. **A319**, 122 (1979).
[92]I. Hamamoto, Phys. Lett. **106B**, 281 (1981).
[93]R. R. Chasman, Phys. Rev. C **30**, 1753 (1984); and private communication.
[94]M. J. G. Borge, D. G. Burke, H. Gietz, N. Kaffrell, J. Rogowski, W. Kurcewicz, G. Løvhøiden, K. Nybø, T. F. Thorsteinsen, G. Nyman, and R. Naumann, Bull. Am. Phys. Soc. **32**, 1546 (1987).
[95]J. Meyer-ter-Vehn, Nucl. Phys. **A249**, 111 (1975); **A249**, 141 (1975).
[96]S. Frauendorf and F. May, Phys. Lett. **125B**, 245 (1983).
[97]T. Otsuka and M. Sugita, Phys. Rev. Lett. **59**, 1541 (1987).
[98]J. Engel and F. Iachello, Nucl. Phys. **A472**, 61 (1987).
[99]I. Ragnarsson, in *Future Directions in Studies of Nuclei Far from Stability,* edited by J. H. Hamilton, E. H. Spejewski, C. R. Bingham, and E. F. Zganjar (North-Holland, Amsterdam, 1980), p. 367.